DEVELOPMENT AND CHARACTERIZATION OF NON-ENZYMATIC CARBON BASED ELECTROANALYTICAL METHODS FOR MITIGATING DIABETES MELLITUS

BY

NURUDEEN ADEWALE ODEWUNMI

A Dissertation Presented to the

DEANSHIP OF GRADUATE STUDIES

KING FAHD UNIVERSITY OF PETROLEUM & MINERALS

DHAHRAN, SAUDI ARABIA

In Partial Fulfillment of the
Requirements for the Degree of

DOCTOR OF PHILOSOPHY

In

CHEMISTRY

DECEMBER 2018

KING FAHD UNIVERSITY OF PETROLEUM & MINERALS

DHAHRAN- 31261, SAUDI ARABIA

DEANSHIP OF GRADUATE STUDIES

This thesis, written by **NURUDEEN ADEWALE ODEWUNMI** under the direction of his thesis advisor and approved by his thesis committee, has been presented and accepted by the Dean of Graduate Studies, in partial fulfillment of the requirements for the degree of **DOCTOR OF PHILOSOPHY IN CHEMISTRY.**

Dr. Abdel-Nasser Kawde
(Advisor)

Dr. Khalid R. Alhooshani
Department Chairman

Dr. Basheer Chanbasha
(Member)

Dr. Salam A. Zummo
Dean of Graduate Studies

Dr. Mohamed Ali Morsy
(Member)

30/12/18
Date

Dr. Anvarhusein A. Isab
(Member)

Dr. Abdalla M. Abulkibash
(Member)

Dedicated to my immediate and extended family

ACKNOWLEDGMENTS

All praises and adorations are due to Allah, most compassionate and most merciful, for his favor on me from the beginning to the successful completion of my Ph.D. program. May His peace and blessing be unto Prophet Muhammad (ﷺ). I pray to Allah to make this work beneficial to the entire world and accept it as an act of worship.

I will like to appreciate my thesis advisor, prof. Abdel-Nasser Kawde for his support, advice, and encouragement during my research and coursework. Great thanks to my thesis committee members Dr. Basheer Chanbasha, Dr. Mohamed Ali Morsy, Dr. Anvarhusein I. Isab and Dr. Abdalla Mahmoud Abulkibash for their contributions.

My unique and sincere appreciation goes to my wife for her patience and sacrifice during my study and my children for enduring with me. My friends, colleagues, seniors, juniors from different countries in the chemistry department and KFUPM at large are all acknowledged for their support. However, Nigerian community that makes Saudi Arabia home away from home for my family are well appreciated.

Finally, I will like to remember the entire faculty that taught me in chemistry and other departments, the chemistry department that accepted me for both my master and Ph. D programs. I commend the chemistry department chairman for his wisdom in coordinating the department which enables me to benefit maximally from their facilities.

Thank you all for being there for me: more blessing and abundant reward from Allah to you all.

TABLE OF CONTENTS

LIST OF TABLES

LIST OF FIGURES

LIST OF ABBREVIATIONS

AA	:	Ascorbic Acid
AD	:	Alzheimer's disease
ATP	:	Adenosine Triphosphate
BET	:	Brunayer, Emmet and Teller
BGCE	:	Bare Glassy Carbon Electrode
BGPE	:	Bare Graphite Pencil Electrode
BJH	:	Barrett, Joyner and Halenda
CCD	:	Charge Couple Device
CV	:	Cyclic Voltammetry
CVs	:	Cyclic Voltammograms
CSLSV	:	Cathodic Sweep Linear Scan Voltammetry
CLSVs	:	Cathodic Sweep Linear Scan Voltammograms
DB-M	:	Diabetes Mellitus
DGLPE	:	Disposable Graphite Lead Pencil Electrode
DGPE	:	Disposable Graphite Electrode
DLM	:	Dextrorotation and Laevorotation Methionine

EDX	:	Energy Dispersive X-ray Spectroscopy
FE-SEM	:	Flame emission Scanning Electron Microscopy
GD-M	:	Gestational Diabetes
HXA	:	Hypoxanthine
IHOAM	:	Incipient Hydrous Oxide Adatom Mediator
PDPD	:	Protein Deficiency Pancreatic Diabetes
PDXL	:	Integrated X-ray Powder Diffraction Software
ROS	:	Reactive Oxygen Species
SWV	:	Square Wave Voltammetry
SWVs	:	Square Wave Voltammograms
UA	:	Uric Acid
XA	:	Xanthine
XRD	:	X-ray Diffraction
XPS	:	X-ray Photoelectrons Spectroscopy

ABSTRACT

Full Name : [Nurudeen Adewale Odewunmi]

Thesis Title : [Development and Characterization of Non Enzymatic Carbon Based Electroanalytical Methods For Mitigating Diabetes Mellitus]

Major Field : [Chemistry]

Date of Degree : [December 2018]

Growing in the prevalence of diabetes is a great concern that necessitates investigation of potent compounds that can be used to support glucose levels monitoring in diagnoses and mitigating diabetes mellitus. Analytes that will serve as corrective and preventive measures are required to manage the deadly disease that is found to be originated from a systematic and metabolic disorder in a human. Methionine, Ascorbic acid (AA) and some reactive oxygen species (ROS) such as Uric acid (UA), Xanthine (XA) and Hypoxanthine (HXA) are identified as essential compounds for mitigating diabetes mellitus. Proficient, cost-effective and prompt electrochemical methods were developed with graphite pencil electrode (GPE) for all these compound of interest and characterized accordingly with flame emission – scanning electron microscope (FE-SEM/EDX), X-ray photoelectron spectroscopy (XPS), Raman spectroscopy and N_2 adsorption-desorption instruments. Electrocatalytic property of copper was explored to enhance secondary oxidation peak of glucose for the development of electrochemical methods for a glucose sensor in NaOH and simultaneous determination of UA, XA and HXA in phosphate buffer solution. Silver (II) oxide (AgO) was also utilized to initiate secondary oxidation peak of methionine on bare GPE for the first time and use to development electrochemical method for methionine detection. Selective and simultaneous determinations of AA, UA, XA, and

HXA were also achieved on a bare GPE without any electrode surface modifications in phosphate buffer. Performance of all developed electrochemical methods was impressive with wide linear ranges of detections, low limit of detection and outstanding real-life application in some biological samples (urine and serum) with impressive percentage recovery in the presence of potential interferences.

ملخص الرسالة

الاسم الكامل: نورالدين أدولي أودميني

عنوان الرسالة: تطوير وتوصيف طرق كربونية الأساس غير انزيمية كهروكيميائية لضبط داء السكري

التخصص: كيمياء

تاريخ الدرجة العلمية: ديسمبر، 2018

يعتبر إنتشار داء السكري مصدر قلق كبير و يتطلب الإستقصاء عن مركبات فعالة للمساعدة في تشخيص ومراقبة مستويات الجلوكوز لضبط داء السكري. المواد التي تعمل كتدابير تصحيحية ووقائية مطلوبة للتعامل مع مرض مميت ناتج من خلل نظامي او إستقلابي في جسم الإنسان، مركبات مثل الميثيونين، حمض الأسكوربك و بعض مركبات الأوكسجينية النشطة مثل حمض اليويريك، الزانسين و الهايبوزانسين تصنف كمركبات مهمة لضبط مرض السكر. تم تطوير طرق كهروكيميائية فعالة، منخفضة التكلفة وسريعة بإستخدام قطب قلم الجرافيت لكل المركبات المذكورة وتم توصيف (FE-SEM/EDX) بإستخدام إنبعاث اللهب، المجهر الماسح الضوئي والمطيافية الإلكتروضوئية للأشعة (XPS)السينية ، مطيافية رامان و جهاز ادمصاص-إنحلال النيتروجين. تم إختبار التحفيز الكهربي للنحاس لتعزيز الإشاره الثانوية الناتجة من أكسدة الجلوكوز، لتطوير طريقة كهروكيميائية لحساس جلوكوز في هيدروكسيد في محلول الفوسفات المنظم. تم أيضا لأول مرة إستخدام أوكسيد HXA و UA, XA الصوديوم والكشف الآني ل الفضة لبدء إشارة الأكسدة الثانوية للمثيونين على قطب قلم الجرافيت الخالي وتم تطوير طريقة كهروكيميائية لكشف بإستخدام قطب قلم الجرافيت الخالي في HXA و AA, UA, XAالميثيونين. تم تطوير طريقة إنتقائية وآنية لكشف محلول الفوسفات المنظم بدون أي تعديل على سطح القطب. ولقد اظهرت الأقطاب المطورة اداء كهروكيميائيا مبهرا ونطاق كشف خطي واسع و حد كشف وتطبيق عملي ممتازفي عينيات بيولوجية (عينات بول ومصل دم)، و نسبة

CHAPTER 1

INTRODUCTION

Glucose level monitoring have been the fundamental diagnostic tool to ascertain diabetic status of individuals which seems not enough to be an indicator to suggest a corrective and preventive measures for diabetes mellitus (DB-M) and its severe complications such as kidney and liver failures, nerve, eye, skin, foot, Alzheimer's and cardiovascular diseases including stroke [1-3]. A comprehensive investigation on the cause of insulin resistance is necessary to be able to identify an analyte and or group of compounds that can serve as an indicator for controlling DB-M along with glucose monitoring.

1.1 Prevalence of Diabetes Mellitus

Diabetes prevalence has been attributed to the cause of economic stress and increasing deteriorating health conditions as a result of changed lifestyle due to technological advancement in developed nations and poor health system in underdeveloped countries [4]. Despite a huge development in the nutritional values of the food consumption in some part of the world, about 171 million people have been estimated to be affected by diabetes as at the year 2000 with a projection of more than twice of the figure to be affected by the year 2030 [5]. However, in 2013, 382 million people had diabetes; this number is expected to rise to 592 million by 2035 [4]. These numbers have increased to

415 million people in the world and more than 35.4 million people in the middle east region; by 2040, it will rise to 72.1 million with 3.4 million cases of diabetes in Saudi Arabia with the highest prevalence in the middle east [6]. Top 30 countries with the highest national prevalence (%) of DB-M in adults (18 – 99 years) and their economic implications in 2017 [7] are listed in Table 1-1.

Table 1-1: Top 30 countries with the highest national prevalence (%) of Diabetes Mellitus and their economic implication in 2017

#	Country	IDF Region	National adult [18-99 yrs] prevalence (%)	Mean Expenditure in USD per person
1	Marshall Islands	Western Pacific	31.38	761
2	Tuvalu	Western Pacific	27.66	757
3	Tokelau	Western Pacific	25.01	-
4	Niue	Western Pacific	24.52	-
5	New Caledonia	Western Pacific	24.24	-
6	Mauritius	South East Asia	23.97	548
7	Nauru	Western Pacific	22.89	691
8	Guam	Western Pacific	22.30	-
9	Réunion	Africa	18.42	-
10	Saudi Arabia	Middle East & North Africa	18.22	1,524
11	Barbados	North American & Caribbean	17.70	1,439
12	Martinique	North American &Caribbean	17.65	-
13	Palau	Western Pacific	17.26	1,653

#	Country	IDF Region	National adult [18-99 yrs] prevalence (%)	Mean Expenditure in USD per person
14	US Virgin Islands	North American &Caribbean	16.52	-
15	Malaysia	Western Pacific	16.41	641
16	Guadeloupe	North American &Caribbean	16.17	-
17	Bahrain	Middle East & North Africa	15.93	1,685
18	Curaçao	North American &Caribbean	15.83	-
19	UAE	Middle East & North Africa	15.36	1,679
20	Papua New Guinea	Western Pacific	15.34	138
21	Bermuda	North American &Caribbean	15.27	-
22	Portugal	Europe	14.90	2,420
23	Kuwait	Middle East & North Africa	14.77	1,834
24	Lebanon	Middle East & North Africa	14.60	787
25	Aruba	North American &Caribbean	14.25	-
26	Mexico	North American &Caribbean	14.15	992

#	Country	IDF Region	National adult [18-99 yrs] prevalence (%)	Mean Expenditure in USD per person
27	Belize	North American &Caribbean	13.98	449
28	Qatar	Middle East & North Africa	13.85	2,678
29	The British Virgin Islands	North American &Caribbean	13.85	-
30	Malta	Europe	13.81	2,966

Data obtained from International Diabetes Federation (IDF) Diabetes Atlas 8th- Edition Brussels Belgium Resource (http://diabetesatlas.org/resources/2017-atlas.html)

1.2 Significance of Methionine and Some Reactive Oxygen Species Such as Uric Acid, Xanthine, and Hypoxanthine in Mitigating Diabetes Mellitus

Emphasis on the role of methionine nutritional intake management for healthy lifestyle, extension of lifespan by slowing aging metabolic processes [8] and improvement of insulin resistance health-related conditions [9, 10] could be an eye-opener for recognition of plasma methionine monitoring for social economic values of individuals and groups to prevent and manage severe consequences of DB-M. Besides, uric acid (UA), xanthine (XA) and hypoxanthine (HXA) are coexisting purines molecules in the animal metabolic system. UA is the terminal product of the purine degradation while XA and HXA are intermediates products resulting from purine transformation by xanthine oxidase enzymatic reaction. The ratio of the reduced and oxidized forms of these ROS are possible potential biomarkers of oxidative stress in human [11] leading to many chronic diseases (cancer, diabetes and so on) and cardiovascular diseases. Coronary heart diseases have been associated with UA level in the body metabolic system. High risk of hypertension, stroke, heart failure and all symptoms leading to cardiovascular death issue were linked with elevated UA concentration [12].

1.3 Graphite Pencil Electrode and Other Carbon based Solid Electrodes

Carbon paste, graphite, glassy carbon, diamond, carbon fiber, carbon nanotubes, and fullerene are forms of carbon materials utilizing in the development of different solid

electrodes such as glassy carbon electrode (GCE), GPE, diamond electrodes and screen print electrodes for industrial and laboratory applications. They are very important in electroanalytical chemistry applications due to their lower background current, wide potential window for redox reaction, inertness to chemicals, low cost and ease of chemical modifications to suit various clinical and environmental applications [13-16].

However, the peculiarity of GPE due to some exceptional features as highlighted below when compared with other solid electrode has made it an interesting solid electrode for electrochemical sensing applications [17].

- Commercial availability and cost-effective of graphite pencil lead of different sizes in the local market compared with other solid electrodes with higher market values. Pencils are produced in large quantity for writing purpose and can easily be used as an electrode for sensing application.
- Adjustable exposed or contact surface area that can improve the sensitivity of target compound or molecule compared with others that have specific exposed surface area irrespective of the amount of detecting medium.
- Surface polishing before electrochemical testing that can increase chances of impurity in the detecting medium is not mandatory with GPE. It can be easily extruded from its mechanical compartment and electrochemically pretreated as required.
- It can be a single-use or disposable electrode like screen print electrode with minimal cost implication.

- Porosity and adsorption capabilities of pure graphite pencil can improve ease of surface modification for enhancing the sensitivity of target atom or molecule.

1.4 Research Objectives and Methodology

This research focused mainly on emphasizing that glucose monitoring is not enough to diagnose DB-M, corrective measures are required along with glucose detection for effective mitigation of the deadly disease that originated from systematic and metabolic disorders in human. Identification of essential analytes apart from glucose for corrective and protective measures of DB-M is the ultimate aim of this research. Methionine is a very important essential amino acid whose understanding and the knowledge obtained from its various metabolic reactions will be required to answer some very important analytical questions as highlighted below:

- What is the most critical analyte to be considered for mitigation of DB-M?
- Despite the importance of methionine as essential amino acid and its role in many detoxification processes and cell growth, why is it important for the control of DB-M?
- How is methionine detection going to be achieved electrochemically despite its non electroactive properties?
- Can other analytes such as UA, XA, and HXA be considered for mitigating DB-M?

Answers to these questions through a comprehensive literature review are the guidelines for the use of GPE to achieve the following specific objectives;

- Development of non-enzymatic cost effective electroanalytical methods for glucose detection to address the lack of selectivity of previously developed sensors.
- Development of an electroanalytical method for sensitive and selective determination of methionine as a corrective and protective measure for DB-M.
- Development of an electroanalytical method for sensitive simultaneous detections of UA, XA, and HXA.
- Development of electroanalytical methods for sensitive and selective simultaneous detections of Ascorbic acid (AA), UA, XA, and HXA.

CHAPTER 2

LITERATURE REVIEW

2.1 Evolution of Enzymatic Glucose Sensors

Glucose oxidase (Gox) is regarded as an ideal enzyme for glucose oxidation based on its superior electron acceptor, sensitivity, selectivity, and biocompatibility properties when compared with quinoprotein glucose dehydrogenases and glucose dehydrogenases [18]. The active redox center of Gox, flavin adenine dinucleotide (FAD) interacts with glucose to form gluconolactone as the initial oxidation reactions of glucose as shown in equation 1.1. However, classification of the enzymatic glucose biosensor into the first, second and third generations are depended on the mechanism of regeneration of the reduced FAD ($FADH_2$) directly on the electrode surface in the present or absent of oxygen or organic compound (mediator) as shown for the first generation that requires oxygen in equation 1.2.

$$\mathbf{Glucose} + \mathbf{Gox(FAD)} \rightarrow \mathbf{Gluconolactone} + \mathbf{Gox(FADH_2)} \qquad (\mathbf{1.1})$$

$$\mathbf{Gox(FADH_2)} + \mathbf{O_2} \rightarrow \mathbf{Gox(FAD)} + \mathbf{H_2O_2} \qquad (\mathbf{1.2})$$

2.1.1 Interaction of Glucose with Glucose Oxidase in the Presence of Oxygen

The first generation glucose biosensor is based on the interaction of glucose with FAD in GOD catalyzed by oxygen for the regeneration of FAD from $FADH_2$ to produce hydrogen peroxide (H_2O_2) (equation 1.1 & 1.2). Quantification of glucose was first based on the monitoring of the amount of oxygen consumed [19, 20] which was challenged with high background due to oxygen potential that requires that needs optimization for stable potential. An improvement on glucose sensor for the elimination of the oxygen background was achieved by measuring produced H_2O_2 instead of the fluctuating oxygen as the first amperometric glucose sensor [21].

High dependence of the first generation glucose sensor on oxygen along with fouling effect of the platinum electrode by the adsorbed chlorine and blood protein is a great challenge. To overcome these challenges, a complicated design was introduced with 2-D cylindrical electrodes [22] that altered the ratio of oxygen to glucose input and films[23] for diffusion control along with electrode rich of oxygen for a continuous internal source of oxygen [24, 25].

2.1.2 Indirect Interaction of Glucose with Glucose Oxidase in the Presence of Organic or Inorganic Mediators

The dependency of the first generation of glucose sensor on oxygen comes along with high interferences on glucose determination due to its high potential requirement for oxygen reduction and hydrogen peroxide oxidation. Alternative electroactive molecules such as quinonic materials [26, 27], imidazolic complexes [28], organic salts (ferricyanide and ferrocenes) [29-31] and polymeric materials [32] were investigated and successfully utilized as a mediator in glucose oxidation with Gox. Due to successful replacement oxygen with mediators, the interaction of glucose with Gox in the presence of a mediator is considered to be the second generation of glucose biosensor.

Accessibility of glucose and mediator to the redox center embedded in the 3-D network of Gox can only be achieved by diffusion. This is a major obstacle to achieving direct electron transfer for oxidation of glucose on a perfect solid electrode. Furthermore, mediators are found to be highly reactive, thereby competing with dissolved oxygen which is detrimental to the performance of many fabricated and commercialized glucose detection devices in term of durability, reproducibility, and biotoxicity.

2.1.3 Direct Interaction of Glucose on Modified Glucose Oxidase and Electrode Surface

Generally, the performance of Gox despite its comparatively high stability with other enzymes is limited to immediate surrounding humidity, lower temperature, and pH between 2 and 8 due to its intrinsic protein nature and smaller dynamic range from the first two glucose sensing generations [18]. There is a need to preserve the stability of Gox at the same time solve accessibility challenge to its redox center. Attention on the improvement of enzymatic glucose sensors was focused on the electrode of different porous materials (mesoporous, microporous and nanoporous) that possess high surface area and porosity for entrapment of Gox [33-36]. This approach can avoid complications presented by mediators and dependency of dissolved oxygen for direct electron transfer, but the competition between the electrode and the dissolved oxygen in the regeneration of enzymes is still a significant source of interference of the redox species.

Modification of the Gox for accessibility of its redox center for ease electron transfer reaction with an electrode for direct glucose oxidation. Efforts such as entrapment of enzymes as sol-gel [37], cross-linkage of enzymes [38], wiring of Gox electrochemically for reconciliation a polymer chain [39], incorporation of enzymes within a polymer via electro-polymerization [36] have been reported to preserve the stability of enzymatic glucose sensor and successfully utilized for direct oxidation of glucose without the involvement of oxygen or mediator. Direct oxidation of glucose with a modified Gox is the third generation of enzymatic biosensor but could only achieve a non-reusable device due to their inability to withstand modifications resulting from chemical and physical

processes involved in the fabrication procedures. Summary of the 3 generations of enzymatic glucose sensors is shown in Figure 2-1.

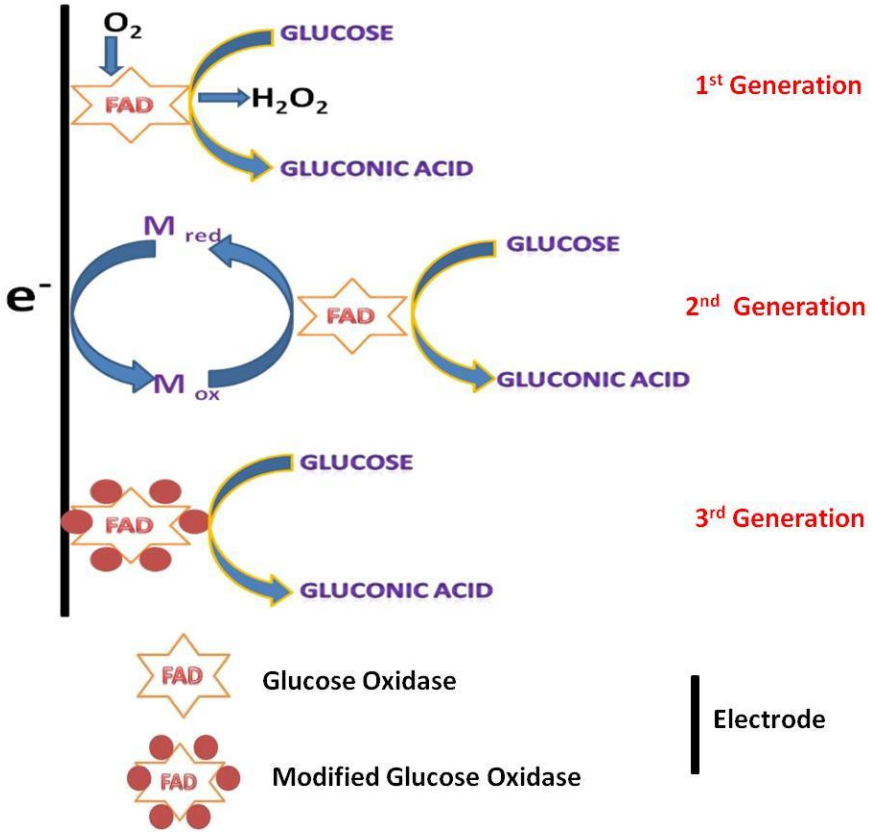

Figure 2-1: Schematic Diagram for the Evolution of the 3 Generations of Enzymatic Glucose Biosensor

2.1.4 Potential Forth Generation Glucose Biosensor (Non Enzymatic Glucose biosensor)

Challenges encountered by the first three generations of the enzymatic glucose biosensor are justification for tremendous research on enzyme's free glucose biosensor which involves electro-catalysis of glucose reduction-oxidation (redox) reactions as a potential fourth generation glucose biosensor. Two models have been proposed as a mechanism of enzyme's free biosensor. The first been reported by Pletcher [40] as chemisorptions model which involve simultaneous adsorption of glucose on the surface containing metal electro-catalyst and removal of the hemiacetalic hydrogen atom which is the rate determining step for electro-oxidation of glucose. Burke [41] proposed "Incipient Hydrous Oxide Adatom Mediator (IHOAM)" as the second model where the mediation of a pre-monolayer oxidation step that will form an incipient hydrous oxide (OH) of hydroxide adsorption (OH_{ads}) by an active metal surface atom for electro-oxidation of glucose and any other organic molecule. IHOAM explains the importance of the electrocatalytic performance of metals without a change in oxidation state.

Unique properties of transition metals that exhibit different oxidation numbers and their tunable physical, optical, conductivity, electrical and chemical properties in nano-scale and composite forms [42-48] have made them possible to be utilized for a non-enzymatic glucose sensor [49, 50] due to their improved electro-catalytic properties. Several transition metals in a nanoscale level that have been reported to be a good electrocatalyst for non-enzymatic detection of glucose include gold [51-54], platinum [55-61], nickel [62-64] and so on. However, copper is one of the most studied of these transition metals

as an enzymeless biosensor of glucose. Electrodes composed of copper nanoparticles modified with a graphene sheet (CuNPs/GS) [65], copper-porous silicon nano-composite (Cu/PSi) [66], hollow copper oxide (CuO) polyhedron [67], disposable pencil graphite copper nano-particle (PGE-CuNPs) [68], CuNPs functionalized with phosphorus and molybdenum on GC (CuNPs-P-M-GC) [69], copper nano-flower (CuNF) modified reduced graphene oxide on a flexible paper (CuNF-RGO-FP) [70] and so many other forms of copper have been reported to be a reliable amperometric biosensor of glucose.

Surprisingly, despite decades of research development on non-enzymatic glucose sensor, its practical application is still prevented by numerous challenges. Electrode fouling by the biological sample constituents, bared electrode slow kinetic property, incompatibility of the system with prevailing body pH (physiological pH) and lack of selectivity of the electrode between glucose peak and active component of the catalyst. Development of non-enzymatic glucose sensor had been based on a fixed applied potential amperometric method for quantification of glucose level in physiological applications.

2.2 Pancreas, Digestive System and Types of Diabetes Mellitus

The pancreas plays an essential role in human digestive systems through endocrine and exocrine glands for a healthy life. Any form of abnormality in the pancreas system has a direct relationship with malnutrition, metabolic disorder and organs (liver, kidney, intestine, stomach, heart) malfunctions [71] that have been responsible for the cause of DB-M and related complicated diseases.

2.2.1 Endocrine Pancreatic Disorder and Diabetes Mellitus (Insufficient Insulin)

DB-M has been associated initially with protein deficiency in the human as a result of malnutrition from consumption of foods that contain cyanide (cassava related foods) in some geographical locations (Oceanic, North American, and Europe) [72]. The argument on this is based on detoxification of free cyanide content from low protein foods that requires sulfur principally from amino acid for its conversion to thiocyanate (S-CN) otherwise; possess adverse effects on human pancreas endocrine activities. Lack of detoxification process of ingested cyanide has been reported as the main cause of unpopular acute pancreatic DB-M termed as J Type or Protein Deficiency Pancreatic Diabetes (PDPD) as a result of longtime exposure to food with high content of cyanide without detoxification process due to malnutrition [73-75]. An aggressive adverse condition of the pancreas as a result of external factors such as excessive smoking,

extreme alcoholism, and others have been attributed to the chronic pancreas condition of the exocrine gland that leads to hyperglycemia and generally referred to as Type 3c diabetes. This type of DB-M is characterized by cystic fibrosis, hemochromatosis (iron content overload), pancreatic cancer (pancreatic ductal adenocarcinomal) and others after surgery effects of the pancreas [76].

However, the primary function of the islet of beta (β) cell located in the pancreas is to store and release insulin (the hormone responsible for the blood sugar regulation) for regulating blood sugar concentration. This is achieved by converting glucose to the required energy for body metabolic reactions in the blood. Ineffective state of the pancreas will affect this process and lead to the inability of β-cell to secrete insulin. Recent classifications of diabetes into Type I and Type II have been insulin related. The inability of insulin secretion has been linked with Type I diabetes. Several potential cure and treatment for Type I diabetes have been proposed for possible treatment of the pancreas. Attempts include stem cell transplant, islet transplant, pancreas transplant, genetic manipulation of the cell and artificial devices but all are very risky and still on experimental stages [77].

Lack of effective treatment for type I diabetes have to lead to an advanced stage of diabetes usually referred to as Type II diabetes [78] due to prevalence metabolic disorder caused by alpha (α) and β- cells endocrine dysfunction [79, 80] of the pancreas and inability of the body to utilize insulin as an effect of a long time or excess supply of the body with insulin in an attempt to cure Type I diabetes.

Another form of DB-M that can only be found in women is gestational diabetes mellitus (GDB-M). Sustenance of pregnancy requires secretion of human chorionic gonadotropin (hCG) for the production of progesterone and estrogen by the placenta which makes a human system to be more resistant to insulin and apply pressure on the pancreas to produce excess insulin to overcome the resistance. The inability of the pancreas to cope with this task increases glucose level in the blood and thereby resulting in GDB-M in the mid or final stage of pregnancy [81-83] with high-risk symptoms of GDB-M developing to Type II DB-M [84]. Prematurity, stillbirth, shoulder dystocia and macrosomia are the adverse prenatal effect of GDB-M with hyperglycemia as a neonatal outcome [85, 86]. Children of a GDB-M patient are likely to have a high body mass index (BMI), high fasting glucose and high risk of progression to Type II diabetes [87, 88].

2.2.2 Exocrine Pancreatic Disorder and Diabetes Mellitus (Insulin Resistance)

Apart from the inability of the pancreas to cope with insulin requirement for the regulation of glucose level in the blood, insulin resistance DB-M can develop gradually as a function of certain disorder in body metabolism that makes body cell fail to respond to insulin despite abundant availability of insulin. This is a phenomenon generally referred to as exocrine pancreatic insufficiency (EPI), where the body cannot properly digest carbohydrate, protein, and fats in the food we eat [89] and thereby; leads to gastrointestinal with symptoms such as bloating, gallbladder disorder, peptic ulcer,

diarrhea, constipation, and other irritable abdominal complications. Obesity has been diagnosing to be associated with EPI base on stool test/fecal elastase 1 (EPL 1) [90], dementia otherwise called Alzheimer's disease (memory decline syndrome) which recently classified as Type 3 DB-M [91] have also been related to EPI in obese adult and drastic loss in weight in old age [92-94]. EPI has been found to be responsible for numerous complicated health conditions in older aged people that requires enzymes supplement therapy for their well being [95].

Amylase, protease, and lipase are essential digestive enzymes of carbohydrates, proteins, and lipids respectively produce in the pancreas by an exocrine gland which will be drastically affected by EPI. Lipids (cholesterol, phospholipids, triglycerides) are an essential part of cell membrane structure which is insoluble in water needs to combine with water-soluble protein to form lipoprotein for transportation to the blood. Any form disorder in the lipoprotein and lipid metabolism as a result of EPI will adversely affect the synthesis of some hormonal lipids from the liver and lipase hydrolysis of lipoprotein will distort uptakes and receptor of various forms of lipids in the liver and some essential organ in the body [96]. Carbohydrate metabolisms such as glucogenesis (glucose conversion to glycogen for storage in the liver), glycogenolysis (glycogen break down to glucose in the liver), gluconeogenesis (fatty acid conversion to energy) defects base on EPI will initiate different forms of DB-M due to lack of glucose level regulation [97]. Metabolic and systematic disorder originated from some natural phenomena such as genetic shared (inheritance/family history) [98-102], pre and postnatal nutritional environments [103-106], stress, excessive diet, obesity and aging [107-112] and many other risk factors including alcoholism [113, 114] and cigarette smoking [115, 116] are

likely responsible for gene alteration and protein expression that leads to insulin resistance as factor responsible for the onset of Type II DB-M by glucolipotoxicity [117, 118] or progression of Type I to Type II DB-M [119]. A chart summarizing the relationship among pancreas, digestive systems and different types of DB-M is shown in Figure 2-2.

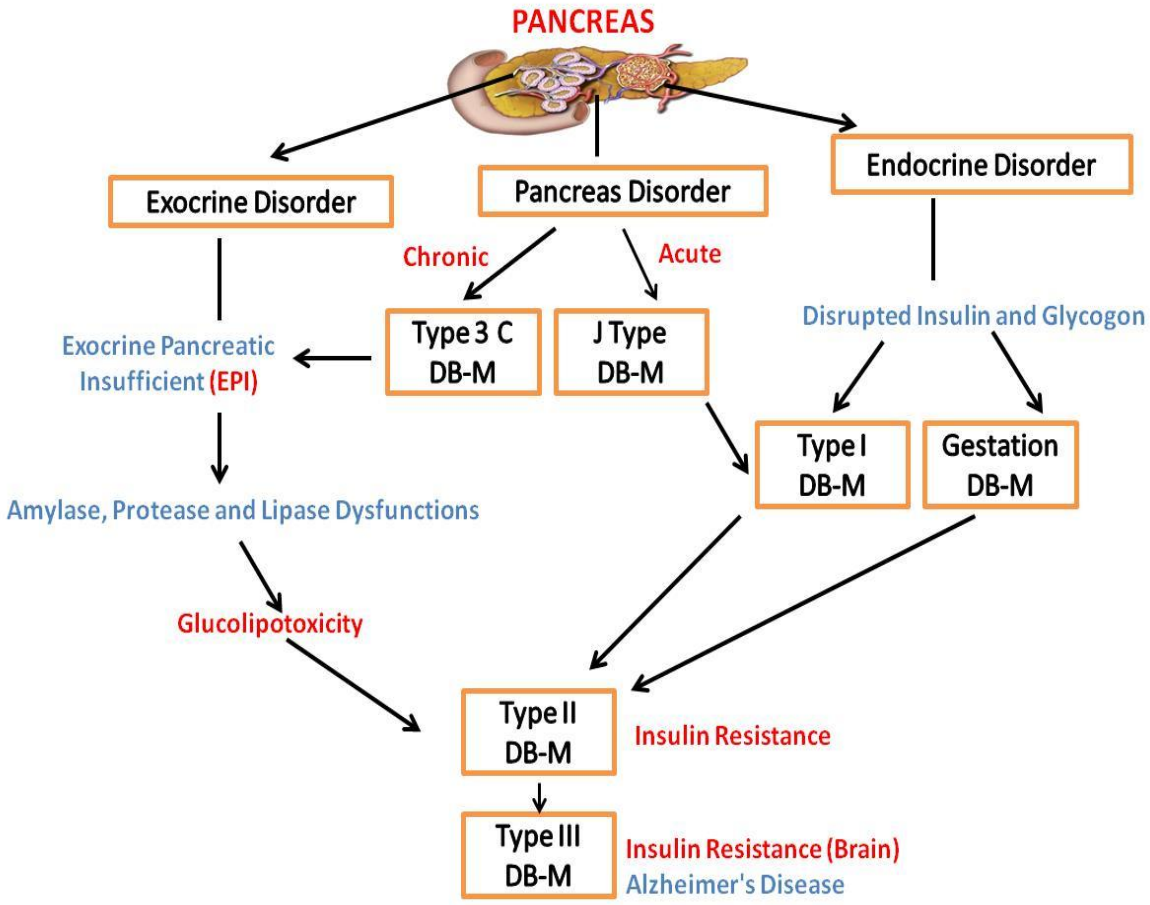

Figure 2-2: Chart showing the relationship between digestive, pancreas systems and types of Diabetes Mellitus (DB-M).

2.2.3 Importance and Consequences of Serum Methionine on Metabolic System

Sulfur is an essential element required for proper, healthy and effective metabolism in human. Essential amino acids such as methionine that generates sulfur are not naturally produced in the body but available in almost all human consumptions such as nuts, meat, chicken, cheese, fish, egg, dairy, beans, vegetables, etc. Methionine is an essential amino acid has been attributed to involved in many detoxifying processes, protection of cells from pollutants, slows cell aging, absorption and bioavailability of some macronutrient and prevents excess fat buildup. All these properties are credited to methionine because it serves as a precursor to many essential amino acids [120] and uses as an additive in most pharmaceutical products due to the presence of sulfur in its side chain that makes it help in improving growth of cell [121].

High level of serum methionine have found not to possess any adverse effect on human, but its role in elevating homocysteine level is a significant concern as a result of metabolic disorder reactions [122]. There are some groups of heterocyclic nitrogenous compounds (pyrimidines) generally refers to as purines which are utilizes by body cells for specific biological and enzymatic reaction in the body. Purines consist of adenosine triphosphate (ATP), flavin aniline dinucleotide (FAD), nicotinamide aniline dinucleotide (NAD), guanosine triphosphate (GNP) and many other vital molecules which are the backbone for ribonucleic acid (RNA) and deoxyribonucleic acid (DNA) formations that aid central nervous system [123].

Transformation of methionine to homocysteine is activated by ATP attack of the sulfur on methionine structure to form S-adenosyl methionine (SAM), follow by the removal of the terminal methyl group (CH_3) to yield S-adenosyl homocysteine (SAH) which then converted to homocysteine. An elevated level of homocysteine as a result of ATP-methionine metabolic disorder has been linking to much non insulin dependence DB-M including related kidney disease and cardiovascular diseases such as stroke and heart attack [124-126]. The possibility of reverting excess homocysteine to methionine with the aid of methyltransferase enzymatic reaction aided by folic acid, vitamin $B_{12,}$ and B_6 have been reported for the study for the treatment of heart-related disease [127].

Hypoxanthine (HXA), xanthine (XA) and uric acid (UA) are by-products in purine-methionine metabolism. Although, UA is produced in the body in different pathway but the dominant route seem through the action of xanthine oxidase on hypoxanthine or xanthine which could be formed from xanthylic acid or guanine and can be supported by the reason why xanthine to hypoxanthine ratio is higher in the urine sample of a patient diagnosed with xanthinuria (absent of xanthine oxidase) [128]. Metabolites pathway include the transformation of HXA to XA and XA to UA by of xanthine oxidase form of uric acid in urine are as shown in Figure 2- 3.

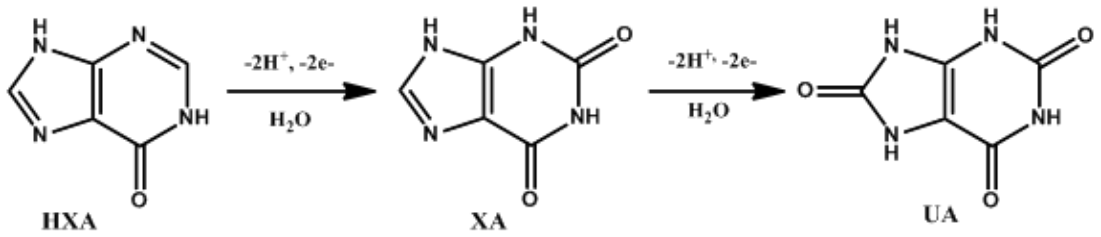

Figure 2-3: Metabolite Pathway of Purine By-Products by Xanthine Oxidase

Many clinical disorders such as DB-M, high cholesterol, obesity, gout, kidney diseases, hypertension and heart disease have been attributed to abnormal UA level in the body as a result of altered purine metabolic reactions [129-132] which affect the normal physiological range of UA level in blood (120 µM - 450 µM) and urine (2000 µM). UA concentration levels in human have been reported to be between 120 and 380 µM with a slight variation base on gender. UA concentration greater than 360 µM for women and greater than 386 µM or 420 µM for men are considered to be hyperuricemia (high concentration of UA) and have been linked with gout, renal, hypertension and many cardiovascular diseases [131, 133, 134] while UA concentration of about 120 µM or less are regarded as hypouricemia (low concentration of UA) which is also linked with eyes pain, Parkinson's and Alzheimer's diseases [135]. The ratio of intermediates products of purine by-products (HXA and XA) are also very important bio-markers in genetic purine metabolism disease [128]. HXA and XA are formed during ATP and adenine nucleotide purine degradation respectively, and their ratio is markers for a much clinical disorder such as gout, kidney failure, respiratory distress, tumor and so on [136].

Residual methionine in the blood can be easily oxidized into methionine sulphoxide due to the presence of sulfur in its structure. Methionine sulphoxide can enhance neurotoxicity properties of some peptides molecule in the body by initiating oxidative stress with some peptide and thereby causing them to function abnormally. Amyloid β-peptide (1-42) [Aβ-(1-42)] is a major 42-amino acid form that can develop into Alzheimer's disease (AD). If a single methionine residue is attached into one of the 42 sequences of amino acid in [Aβ-(1-42)], it will cause a defect that will lead to neurotoxicity and oxidative stress of the peptide that are characteristic AD. Contributions

of methionine residue in AD have been reported by initiation of oxidative stress of [Aβ-(1-42)] by attachment of single methionine residue the 35^{th} position of its amino acid sequence [137-139].

Parkinson's disease (PD) is another chronic disease that can be initiated by methionine sulphoxide. PD affects body movements progressively as a result of tremor, muscle rigidity caused by the inability of nerve cell in the brain to produce dopamine. Distortion of synchronization between heartbeat and pulse (fibrillation) caused by irregular contraction of muscle fibers is symptoms of Parkinson's disease. The presence of residual methionine can oxidize α-synuclein as a result of methionine residue have been reported as a contributing factor to the level of Parkinson disease disorder [140, 141]. Consequences of high-level serum methionine in distorted methionine metabolic reactions are summarized in Figure 2-4.

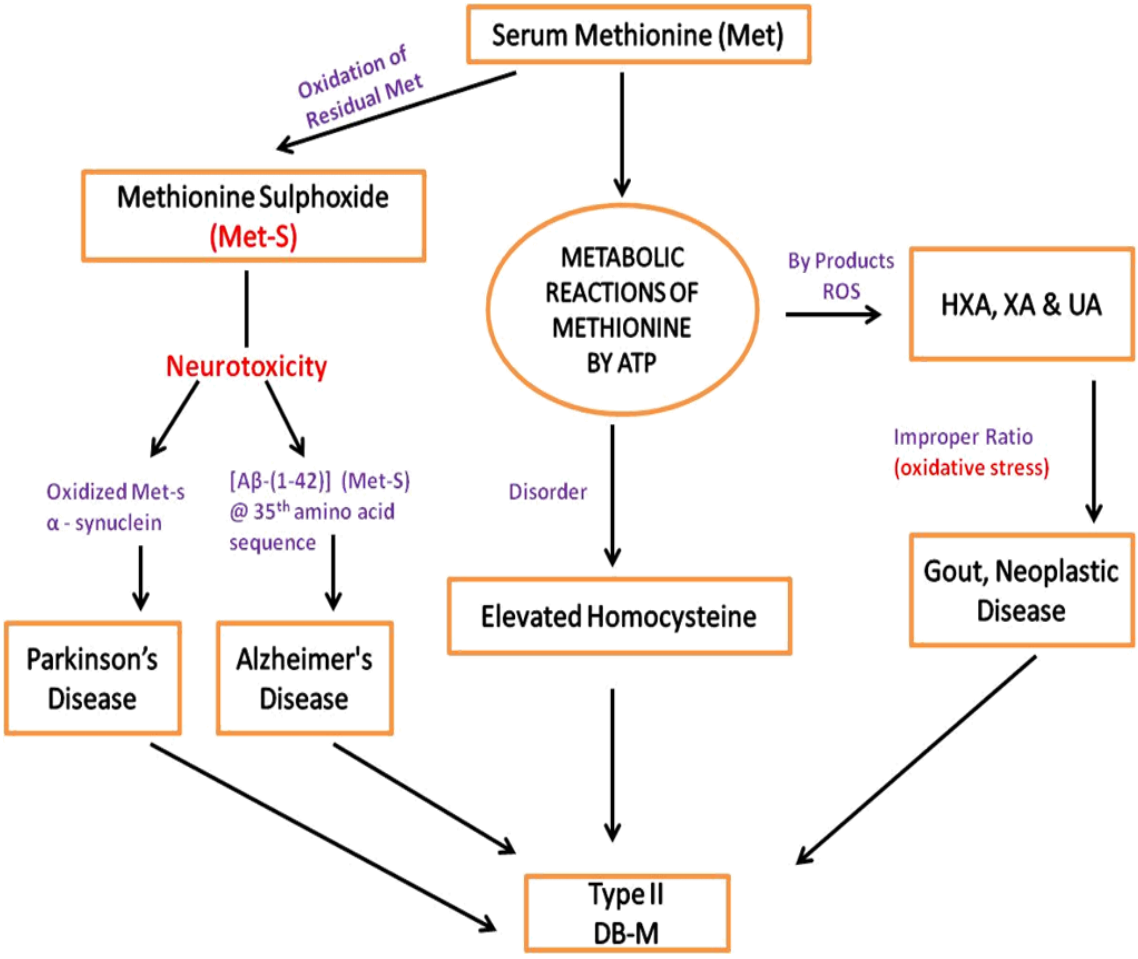

Figure 2-4: Proposed metabolism of serum methionine pathways to Type II DB-M

2.2.4 Regulation of Methionine Dietary by Serum Methionine Level Monitoring for Diabetes Mellitus Mitigation

An effective way of controlling DB-M is to find suitable answers to the following questions;

- Why can glucose level in the blood no longer be regulated?
- Why can the insulin requirement no longer be met?
- Why are the body physiological systems experiencing insulin resistance?

Answers to these questions have a direct relationship with the functionality of the pancreas and the digestive system [71] as a result of malnutrition, metabolic disorder and organs malfunctions base on aging, inactivity, excess diet, family history, obesity, and several other risk factors including nutritional environments. Understanding the important of pancreas in secretion of insulin and glucagon for glucose regulation in the blood and its enzymes secretion for proper breaking down of lipids, protein and carbohydrates in our food will help us to maintain a healthy lifestyle rather than attempt to distort normal body system with the use of drugs (although necessary in some situations) such as metformin that has some effect on cardiovascular system [142] to manage DB-M symptoms and other risk factors of complicated DB-M. Modifications of lifestyle regarding diet management and regular physical activities have been proven to be effective management of DB-M and its complications by reducing pressure on pancreas system for a proper digestive system [143, 144].

Despite several advantages of methionine to human metabolism, some individuals need to restrict it due to the presence of a specific disorder (endocrine and exocrine systems) that distorts methionine metabolic reactions. Monitoring of serum methionine seems a better option to regulate free radicals in the blood by slowing down the rate of reactive oxygen species (UA, XA, HXA, and others) production which will help to reduce aging of the cell and prevent disease vulnerability. Residual methionine oxidation to methionine sulphoxide due to high-level serum methionine can increase chances of developing neurodegenerative diseases (Parkinson and Alzheimer). Methionine restricted diets (MRD) which are primarily plant-based food (vegetables, fruits, grains, nuts, and beans) are necessary prevent some chronic health conditions including cancer [145, 146], depression, hyperuricemia, hypouricemia, gout, and other diabetic related diseases. MRD has been reported to improve renal insulin in aged kidney, improve glucose tolerance and decrease fasting glucose [9], remodeling of white adipose tissue and reverse of malfunction liver in mice [10]. Table 2-1 highlighted the methionine content of some raw and prepared foods as reported in the United States Department of Agriculture (USDA) food composition database.

Table 2-1: Methionine contents of some raw and prepared foods as reported by the United States Department of Agriculture (USDA) food composition database.

NDB #	Description of Food	Amount Measured (g)	Methionine content (g)
15225	Fish, yellowtail, mixed species, cooked, dry heat	146	1.282
05044	Chicken, broilers or fryers, dark meat, meat only, cooked, fried	140	1.119
05190	Turkey, all classes, back, meat and skin, cooked, roasted	140	1.023
05070	Chicken, broilers or fryers, drumstick, meat, and skin, cooked, stewed	140	0.952
01044	Cheese, pasteurized process, swiss	140	0.896
15189	Fish, bluefish, cooked, dry heat	117	0.889
23260	Beef, loin, top sirloin petite roast, boneless, separable lean only, trimmed to 0" fat, select, cooked, roasted	85	0.788
17333	Game meat, bison, chuck, shoulder clod, separable lean only, cooked, braised	85	0.777
13923	Beef, tenderloin, steak, separable lean and fat, trimmed to 1/8" fat, select, raw	149	0.751
13950	Beef, brisket, flat half, separable lean and fat, trimmed to 0" fat, select, cooked, braised	85	0.744
12084	Nuts, butternuts, dried	120	0.733
15029	Fish, flatfish (flounder and sole species), cooked, dry heat	127	0.711
12516	Seeds, pumpkin and squash seed kernels, roasted, with salt added	118	0.702

NDB #	Description of Food	Amount Measured (g)	Methionine content (g)
05038	Chicken, broilers or fryers, dark meat, meat, and skin, cooked, stewed	110	0.685
05666	Ground turkey, 93% lean, 7% fat, pan-broiled crumbles	85	0.677
17316	Lamb, Australian, imported, fresh, rib chop/rack roast, frenched, bone-in, separable lean only, trimmed to 1/8" fat, raw	114	0.663
15228	Crustaceans, spiny lobster, mixed species, cooked, moist heat	85	0.685
17272	Veal, breast, whole, boneless, separable lean and fat, cooked, braised	85	0.535
12039	Seeds, sunflower seed kernels, toasted, without salt	134	0.501
05152	Guinea hen, meat only, raw	85	0.485
13905	Beef, short loin, porterhouse steak, separable lean and fat, trimmed to 1/8" fat, choice, raw	85	0.466
16390	Peanuts, all types, dry-roasted, without salt	146	0.425
21003	Fast foods, biscuit, with egg and bacon	150	0.422
15164	Mollusks, mussel, blue, raw	150	0.402
01109	Milk, sheep, fluid	245	0.380
14067	Beverages, Protein powder soy based	45	0.325
20444	Rice, white, long-grain, regular, raw, unenriched	185	0.311
01091	Milk, dry, nonfat, regular, without added vitamin A and vitamin D	30	0.272

NDB #	Description of Food	Amount Measured (g)	Methionine content (g)
01081	Milk, reduced fat, fluid, 2% milkfat, protein fortified, with added vitamin A and vitamin D	246	0.244
20112	Noodles, egg, spinach, enriched, cooked	160	0.149
20410	Noodles, egg, unenriched, cooked, without added salt	160	0.138
11323	Peas and carrots, frozen, cooked, boiled, drained, without salt	278	0.125
11032	Lima beans, immature seeds, cooked, boiled, drained, without salt	170	0.116
18101	Cake, chocolate, prepared from recipe without frosting	95	0.110
11893	Turnip greens and turnips, frozen, cooked, boiled, drained, with salt	163	0.106
08091	Cereals, corn grits, white, regular and quick, enriched, cooked with water, without salt	257	0.095
08161	Cereals, corn grits, white, regular and quick, enriched, cooked with water, with salt	257	0.095
11459	Spinach, canned, regular pack, solids and liquids	234	0.091
12109	Nuts, coconut meat, dried (desiccated), sweetened, flaked, packaged	85	0.051
01130	Egg, whole, cooked, omelet	15	0.048
18963	Garlic bread, frozen	43	0.045
11869	Squash, winter, hubbard, cooked, boiled, mashed, with salt	236	0.042
11488	Squash, winter, butternut, frozen, cooked, boiled, without salt	240	0.036

NDB #	Description of Food	Amount Measured (g)	Methionine content (g)
11259	Mountain yam, Hawaii, cooked, steamed, without salt	145	0.033
18163	Cookies, chocolate chip, refrigerated dough biscuits, mixed grain, refrigerated dough	33	0.029
09030	Apricots, dehydrated (low-moisture), sulfured, uncooked	119	0.029
09260	Pears, dried, sulfured, stewed, without added sugar	255	0.028
11124	Carrots, raw	128	0.026
09277	Plantains, raw	148	0.025
11352	Potatoes, flesh, and skin, raw	75	0.024
11013	Asparagus, canned, regular pack, solids and liquids	122	0.021
11531	Tomatoes, red, ripe, canned, packed in tomato juice	240	0.019
01055	Cream, sour, reduced fat, cultured	15	0.011
14054	Beverages, almond milk, chocolate, ready-to-drink	240	0.010
09090	Figs, canned, water pack, solids, and liquids	248	0.007
11119	Cabbage, chinese (pe-tsai), raw	76	0.005
11447	Sesbania flower, raw	3	0.000
04027	Salad dressing, mayonnaise, imitation, soybean	15	0.000

Data obtained from USDA National Nutrient Database (https://ndb.nal.usda.gov/ndb)

NDB #: USDA Database code number

Complex nature of methionine is a huge challenge in different analytical methods for its selective determination from the matrix of other sulfur-containing derivatives such as cysteine and homocysteine. Sustainability of various analytical methods including chromatography [147-149], colorimetric [150], flow analysis [151] and several electrochemical techniques involving complicated electrode systems [152-156] have been challenged with low sensitivity, time-consuming analysis and relatively high-cost analysis for its routine determination. Comparison of the existing rugged chromatographic and spectroscopic analytical detection methods for methionine is listed in Table 2-2.

However, development of simple and effective method for methionine detection in biological fluid for monitoring the progress of a diabetic patient especially on MRD should be considered as potential treatment to improve many clinical conditions of a diabetes patient in conformity with several literatures that have regarded MRD as a mechanism of improving insulin sensitivity for effective mitigation of DB-M [157-159]. There should be a strategy to balance the consequence of excess serum methionine that can lead to DB-M base of certain metabolic disorder and insufficient methionine and its derivatives which are linked to blood poisoning, paralysis of muscles, depression, growth retardation and even death [160, 161] base on lack of some important process attributed to methionine when the required amount is not available. This is necessary because cases of DB-M cannot be generalized but requires special attention for specific prescription of some class of MRD as highlighted in Table 2-1 for proper regulation of methionine by methionine monitoring for the prevention and corrective measures of DB-M.

Table 2-2: Comparison of the existing chromatographic and spectroscopic analytical methods for the detection of methionine

#	Methods	Systems	LOD (µM)	Linear Range (µM)	Ref.
1	Colorimetry	Gold nanoparticle aggregation in melanine	0.025	0 – 1.00	[162]
		Bio dot gold nanoparticle aggregation	0.003	0.025– 0.50	[150]
2	Flow–Injection Chemiluminescence (FI-CL)	Lumino-KIO_4 thioglycolic acid-capped CdTe quantum dots	0.044	0.067 - 67	[151]
		methionine-sodium hydroxide-luminol	5.00	0.20 - 20	[163]
3	Fluorescence	L-tryptophan-Cu (II) fluorescent probe	1.40	4.8 - 30	[164]
		Rhodamine derivative fluorescent probe	0.005	0 - 40	[165]
4	Capillaries Electrophoresis	Electrophoresis – UV assay	0.50	-	[166]
5	Chromatography	Isotopical internal standard liquid chromatography/tandem mass spectrometry	0.20	5 - 600	[167]
		Reverse phase liquid chromatography/tandem mass spectrometry	0.04	0.5 - 400	[148]
		o-phtaldialdehyde on- column derivatization HPLC assay	-	2 - 60	[147]
		achiral column reverse phase HPLC with electrochemical detection	0.003	0.004 – 0.20	[149]
		Gas chromatography – mass spectroscopy	0.020	-	[168]

CHAPTER 3

Copper (I) Oxide Enhancement of Secondary Oxidation Peak of Glucose on a Bare Graphite Pencil Electrode for the Development of a Disposable Non-Enzymatic Voltammetric Glucose Sensor

3.1 Introduction

Diabetes is a famous clinical ailment that is responsible for several disabilities and death worldwide as a result of the alteration of gene and expression of the protein in human metabolism [119]. Increasing deteriorating health conditions as a result of changed lifestyle due to technological advancement in developed nations and poor health system in underdeveloped countries have been linked to diabetes [4] and necessitate regular monitoring of glucose level in blood. Dominance of enzymes based glucose biosensor in global market is due to superiority of glucose oxidase (GOD) in terms of its essential stability, immobilization property, biocompatibility, lower operating potential [169-171], but its performance is still limited to immediate surrounding humidity, lower temperature, and pH between 2 and 8 due to its intrinsic protein nature and smaller dynamic range compared with the first two glucose sensing generations. Efforts such as entrapment of enzymes as sol-gel, cross-linkage of an enzymes, wiring of GOD electrochemically for reconciliation a polymer chain and incorporation of enzymes within a polymer via electro-polymerization have been reported to preserve the stability of enzymatic glucose sensor but could only achieve a non-reusable device due to their inability to withstand modifications resulting from chemical and physical processes involved in the fabrication procedures of sensors [36-39].

Several transition metals in the nanoscale level have been reported to be an effective electrocatalyst for non-enzymatic detection of glucose include gold [51-54, 172-174], platinum [55-58], nickel [62-64] and copper to overcome the challenges of enzymes in sensor fabrication. However, copper is one of the most studied of these transition metals

as an enzymeless biosensor of glucose. Electrodes composed of copper nanoparticles modified with a graphene sheet (CuNPs/GS) [65], copper-porous silicon nano-composite (Cu/PSi) [66], hollow copper (II) oxide (CuO) polyhedron [67], disposable pencil graphite copper nano-particle (PGE-CuNPs) [175], CuNPs functionalized with phosphorus and molybdenum on GC (CuNPs-P-M-GC) [69], copper nano-flower (CuNF) modified reduced graphene oxide on a flexible paper (CuNF-RGO-FP) [70], carbon clothes composites of different forms (nanowire, nanoparticles and nanosheet) of copper oxides and other copper nanostructures [176, 177] have been reported to be a reliable biosensor of glucose.

Surprisingly, most of these biosensors are based on amperometric technique due to close or similar electro decomposition potentials of the immobilized compounds (metallic and non-metallic) and oxidation potential of glucose in other voltammetric methods. This challenge always resulted in multiple, broad and unresolved peaks and got complicated based on the complexity of the immobilized compounds on the transducer. Hence, might be responsible for the adoption or adaptation of amperometric technique in real life sensor applications for quantification of a glucose level which does not distinguish among glucose, potential interferences and immobilized compounds currents once a potential is applied.

GPE has been reported to be a fascinating electrochemical transducer for various environmental and clinical applications based on its cost-effectiveness, availability, flexibility, and renewability [17, 178-182]. Besides, enhancement of its catalytic properties for redox reaction of some species such as glucose is very important for the detection of such analyte at lower detection limits. This research is focusing on

integrating GPE attractive qualities with copper aqueous solution to develop very easy, facile, fast and affordable voltammetric technique to aid glucose sensor fabrications without synthesis and immobilization of any electro-catalyst, and ensure a well defined single peak of glucose devoid of oxidized or reduced copper peak for an effective quantification and qualification of glucose in real life application.

3.2 Experimental

3.2.1 Chemicals

Cu AAS specification standard solution (1000 ppm ± 4.0) prepared with nitric acid (HNO_3), and sodium phosphate monobasic anhydrous (NaH_2PO_4) were collected from Fluka. Sodium phosphate dibasic anhydrous (Na_2HPO_4), sodium hydroxide pellet, D-glucose, uric acid (UA), D-fructose, L-ascorbic acid (AA) and L-alanine were all used as purchased from Sigma-Aldrich. All solutions were prepared with double distilled water obtained from Aquatron water still A4000D water purification system.

3.2.2 Electrochemical Cell and Procedure

Three electrode systems comprise of a pencil with a graphite lead that can be propelled or extruded mechanically made in Korea as a working electrode, Ag\Agcl saturated KCl as reference electrode and counter electrode with a platinum wire were connected with CHI potentiostat workstation (CHI1232A, CH Instruments Inc, Austin, TX, USA) for all

electrochemical experiments and measurements with 0.10 M NaOH solution as supporting electrolyte were utilize for the investigation. Descriptions, fabrication and working principle of the mechanical pencil have been reported in the literature [183]. About 7.00 mm length of graphite lead of 0.50 mm diameter propelled out of the vertically fixed pencil with an electrical contact achieved by soldering of copper on its metallic part were made to be in contact with the electrolyte solution corresponding to the surface area of about 11.39 mm^2.

Cyclic voltammetry(CV) measurement was done in the potential window of -0.20 V and 0.80 V with a scan rate of 100 mV \ s. Cathodic sweep linear scan voltammetry (LSV) techniques were employed as the electrochemical technique for glucose determination between 1.00 V and -0.20 V potential range. Measurements were taken at room temperature, and accumulation steps were done under stirring conditions before cathodic sweeping at quiescent condition after 5 s quiet time.

3.2.3 Surface Characterization of Graphite Pencil Electrode

Image of GPE was recorded with FE-SEM and EDX instruments by TESCAN LYRA 3 from the Center of Research Excellence in Nanotechnology, King Fahd University of Petroleum and Minerals (KFUPM), Kingdom of Saudi Arabia (KSA). X-ray photon Spectroscopy (XPS) investigation was performed with Thermos-Scientific, an ESCALAB-250Xi instrument with monochromatic Al Kα radiation, hν = 1486.6 eV

installed in Physics Department, KFUPM, KSA. Data obtained from XPS was processed with Thermo Avantage 5.51 version, Surface Chemical Analysis software.

3.2.4 Serum Sample Collection and Preparation

Collection of the serum was achieved with the assistant of Imam Abdulrahman Teaching Hospital blood bank section from a healthy patient. Serum which was stored in the refrigerator, defrosted and an aliquot of 450 µL was taken and treated with methanol (900 µL) in ratio 1:2 to separate protein from the serum sample. Separation of the precipitated protein was achieved with a clear supernatant of the serum sample after centrifugation of the mixture for 20 minutes at 2000 rpm and subsequently filtered with a Millipore filter of 0.45 µm.

3.3 Results and Discussion

3.3.1 Redox Reactions of Glucose in the Presence of $Cu(NO_3)_2$ on Graphite Pencil Electrode

In the absence of $Cu(NO_3)_2$ as shown in Figure 3- 1Ab and 3- 1Ac, a secondary oxidation peak for 2.00 mM and 4.00 mM glucose respectively can be observed at about 0.63 V on a bared GPE in 0.10 M Na OH. This is due to the graphitic nature of GPE as compared to other solid electrodes that could not show similar response without any surface

modifications. However, enhanced peaks of glucose were observed in Figure 3- 1Bb and 3- 1Bc for the same glucose concentrations as in Figure 3- 1A due to the presence of 5.00 ppm $Cu(NO_3)_2$ solution but no redox peaks of Cu could be noticed in Figure 3-1Ba despite the presence of the 5.00 ppm $Cu(NO_3)_2$ solution. Oxidation peaks could not be observed either due to the presence of $Cu(NO_3)_2$ in the form of Cu^{2+} in the medium which could no longer be oxidized at a lower concentration of $Cu(NO_3)_2$ accumulated on GPE which might be below the detection limit. Besides, there is a possibility of reduction of Cu^{2+} to Cu^{+} which is also not noticed in the cathodic region of the cyclic voltammogram in Figure 3- 1Ba. This can be attributed to instability of Cu^{+} species in aqueous solution. Besides, reduction peak of Cu^{2+} to Cu^{+} have been successfully reported with the aid of selected ligand as a chelating agent in the electrochemical investigations of Cu on Cu electrodes [184, 185]. Surprisingly, secondary oxidation peak of glucose observed in Figure 3- 1Ab and 3- 1Ac got enhanced as a result of the presence of Cu in the medium. Reduction peak of Cu^{2+} to Cu^{+} on the surface of GPE is likely to be responsible for the enhancement of glucose peaks observed in Figure 3-1Bb and 3-1Bc.

Electrochemical redox reaction of $Cu(NO_3)_2$ on the surface of GPE, was studied by multiple cycles CV to probe reduction peak of Cu^{2+} to Cu^{+} in 0.1 M NaOH solution. Figure 3-2A and 3-2B represent 25 cycles of GPE in NaOH in the absence and presence of 10.00 ppm $Cu(NO_3)_2$ solution respectively. A broad accumulation reduction peak of Cu^{2+} to Cu^{+} can be observed in Figure 3-2B in the cathodic region of the multiple CV sweeps.

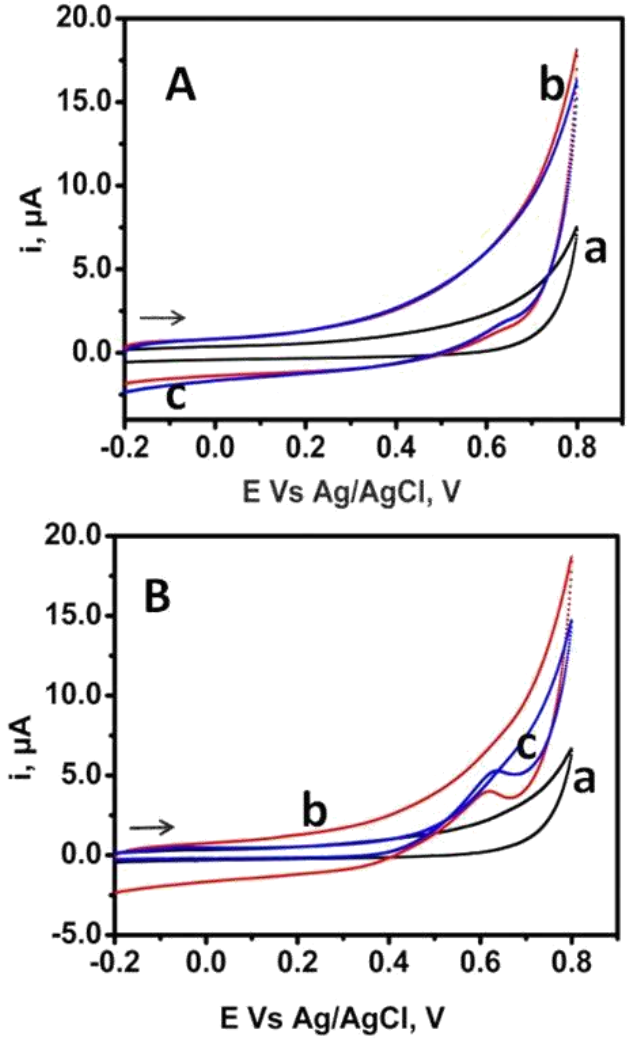

Figure 3-1: CVs in 0.10 M NaOH different concentration of glucose in the absence of 5.00 ppm $Cu(NO_3)_2$ (A) and glucose in the Presence of 5 ppm $Cu(NO_3)_2$ (B). (a) blank, (b) 2mM and (c) 4 mM.

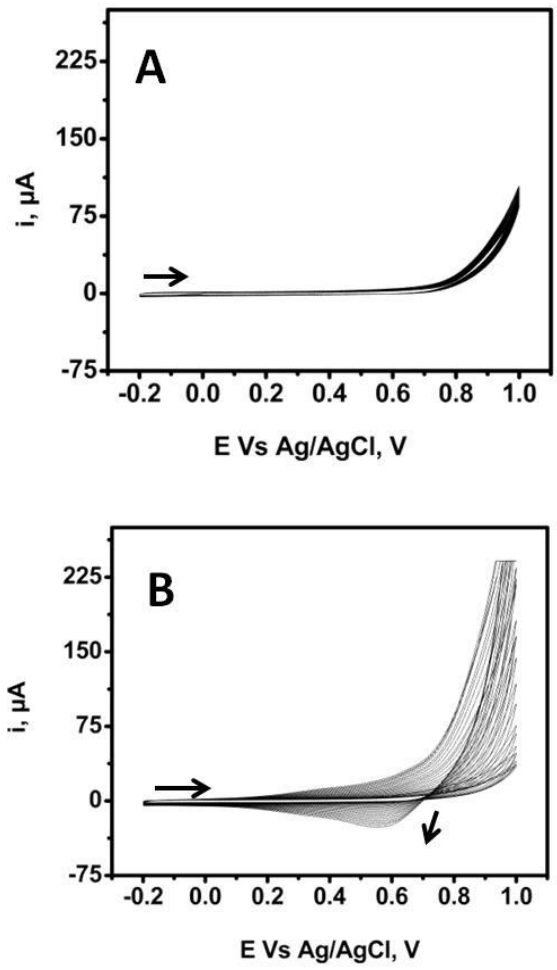

Figure 3-2: 25 cycles of CVs in 0.10 M NaOH pH 13.70 ± 0.20 solution (A) absence of $Cu(NO_3)_2$ solution and (B) presence of 10 ppm $Cu(NO_3)_2$ solution.

3.3.2 Characterization of Graphite Pencil Electrode Surface in the Presence of $Cu(NO_3)_2$

Effects of the reduction of Cu^{2+} to Cu^{+} on the surface of GPE shown in Figure 3-2 were investigated by FE-SEM / EDX analysis after 25 cycles CV. Figures 3-3A and 3-3B show the image of bare GPE and GPE in 0.10 M NaOH in the absence of 10.00 ppm $Cu(NO_3)_2$ solution. Formation of the irregular shape of Cu oxides can be observed on GPE surface containing 10.00 ppm $Cu(NO_3)_2$ solution in 0.10 M NaOH (Figure 3-3C). Elemental composition of the surface of GPE by EDX spectra reveal an average weight percent of 5 spot analyses of 96.02, 0.42 and 3.56 for C, Si, and Cu respectively confirming the presence of Cu on the GPE surface.

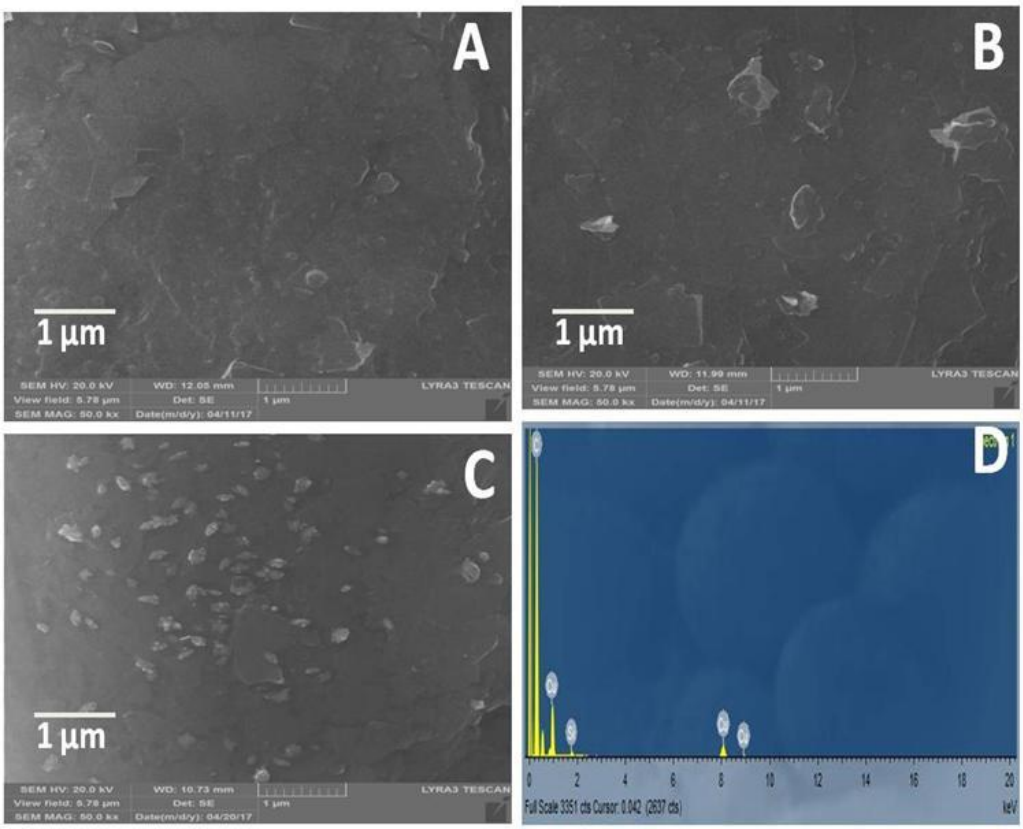

Figure 3-3: FESEM images of 25 cycles CVs of (A) bare GPE, (B) GPE in 0.10 M NaOH, (C) GPE of 10.00 ppm $Cu(NO_3)_2$ in 0.10 M NaOH and (D) EDX elemental composition of C.

The chemical state of elemental Cu reveals by the EDX elemental analysis shown in Figure 3-3D was investigated with XPS Cu2p and 01s spectra in Figure 3-4. Characteristic peaks of $Cu2p_{1/2}$ and $Cu2p_{3/2}$ at about 953 eV and 933 eV respectively attributed to Cu_2O/CuO [186, 187] can be observed in Figure 3-4A. Analysis of Figure 3-4A reveals the presence of CuO on the GPE by a strong Cu^{2+} satellite peak with binding energy (BE) of 943.31 eV as shown in Figure 3- 4A[l]. This peak is expected to be weak if it is a pure Cu_2O but the weak intensity of the second satellite peak of Cu^{2+} at 960.06 eV leverage the influence of CuO. An obvious higher ratio peak further confirmed the dominance of Cu_2O on the GPE surface with BE of 933.36 eV (10 : 1) compared with its counterpart with BE of 937.36 eV which is regarded as a footprint of Cu_2O and confirmation of Cu_2O as the significant species of Cu on GPE-surface [188]. A similar observation regarding the presence of Cu_2O can be seen from the O1s spectra at about 532 eV in Figure 3-4B. The presence of Cu_2O (532.08 eV) along with O=C (532.16 eV) that can be attributed to the adsorption of Cu_2O to GPE can be observed in Figure 3- 4B[l]. Detail compositions of peaks obtained in the XPS analysis are enumerated in Table 3-1.

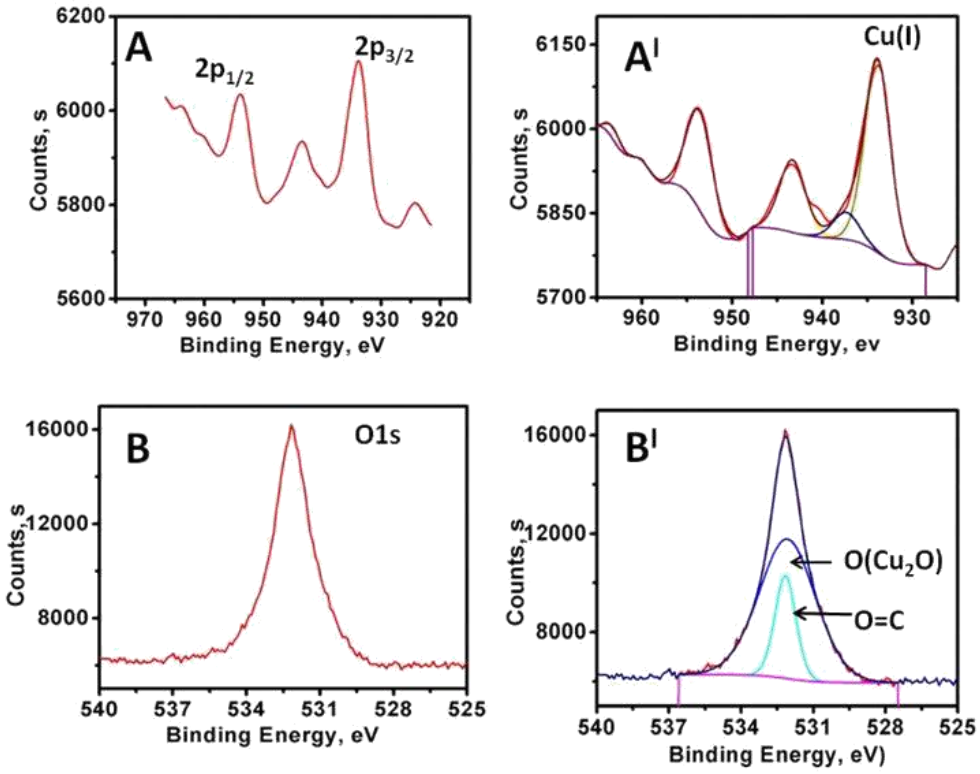

Figure 3-4: XPS analysis of (A) Cu2p and (B) O 1s on GPE surface after 25 cycles of cyclic Voltammograms in 10.00 ppm $Cu(NO_3)_2$ in 0.10 M NaOH pH 13.70 ± 0.20. (A^I) Deconvolution peaks of A and (B^I) Deconvolution peaks of B.

Table 3- 1: XPS of Cu2p and O1s Spectra Peak Analysis on GPE Surface

Spectra	Peak's Name	BE(eV)	FWHM (eV)	Peak Area (CPS.eV)	Atomic %
	2p A	963.13	1.77	41.15	0.93
	2p B	960.06	0.63	0.99	0.02
Cu2p	$2p_{1/2}$ C	953.57	3.37	645.51	42.55
	2p D	943.31	3.37	470.10	10.50
	2p E	937.36	3.37	176.78	3.94
	$2p_{3/2}$ F	933.86	3.37	1247.05	42.06
O1s	O1s A	532.08	2.75	16863.63	78.23
	O1s B	532.16	1.04	4692.74	21.77

3.3.3 Proposed Glucose Redox Reactions Mechanism on Graphite Pencil Electrode

Oxidations of different forms of copper immobilized on solid electrodes to +1, +2 and +3 oxidation states for glucose detection have been reported with mechanisms supporting copper peroxide (CuOOH) which have often referred to as Cu^{3+} as the species responsible for electrocatalysis of glucose in basic medium [66, 67, 69, 70, 175] and have been represented as shown in equation 3.1 – 3.3. This mechanism is valid for oxidation of glucose based on the abstraction of hydrogen from the β-OH group of the hemiacetal carbon center (carbon with ether and alcohol groups) by Cu^{3+} species and can be supported by a comprehensive study of Cu^{3+} complex for hydrogen atom abstraction from hydrocarbon [189]. However, Cu^{2+} species complex has also been reported to be an active hydrogen atom abstraction from organic molecules [190].

$$Cu^0 + 2OH^- \rightarrow CuO + H_2O + 2e^- \quad \boldsymbol{or}$$

$$Cu^0 + 2OH^- \rightarrow Cu(OH)_2 + H_2O + 2e^- \qquad (\mathbf{3.1})$$

$$CuO + OH^- \rightarrow CuOOH + e^- \quad \boldsymbol{or}$$

$$CuO + H_2O + 2OH^- \rightarrow Cu(OH)_4^- + e^- \qquad (\mathbf{3.2})$$

$$Cu^{3+} + Glucose + e^- \rightarrow Gluconolantone + Cu^{2+} \qquad (\mathbf{3.3})$$

It is worthy of mentioning that none of the equations 3.1, 3.2 and 3.3 represents redox reaction of Cu (either metallic or Cu^{2+}) to +1 oxidation state. Besides, a misrepresentation

of the oxidation state of Cu in $CuOOH$ as has shown in equation 3.2 needs a special consideration. Oxidation state of Cu in $CuOOH$ is +1 in contrast to +3 because oxygen oxidation number is always -1 in peroxides. So, equation 3.2 can also be possible electrochemically by reduction the reaction of Cu^{2+} to Cu^{+} by gaining of an electrons shown in Figure 3-2B.

The proposed mechanism of the glucose secondary oxidation peak on GPE as represented by equations 3.4 – 3.6 and as shown in Figure 3-5 is possible to base on coincidental reduction peaks of Cu^{2+} to Cu^{+} between 0.50 and 0.60 V (Figure 3- 2A) and a secondary oxidation peak of glucose on GPE (Figure 3-1A). This is in agreement with the model predicted by Pletcher, 1984 [40]. It involves simultaneous adsorption of glucose on the surface containing metal electro-catalyst (Cu^{+}) and removal of the hemiacetal hydrogen atom which is the rate determining step for electro-oxidation of glucose.

$$Cu(OH)_2 + OH^- + e^- \rightarrow CuOOH + H_2O \text{ (Red)} \quad \textbf{(3.4)}$$

$$CuOOH(Cu^+) + Glucose \rightarrow Gluconolactone + Cu(OH)_2 + e^- \ (Ox.) \quad \textbf{(3.5)}$$

$$Gluconolactone + H_2O \rightarrow Gluconic\ acid \ (Hydrolysis) \quad (\mathbf{3.6})$$

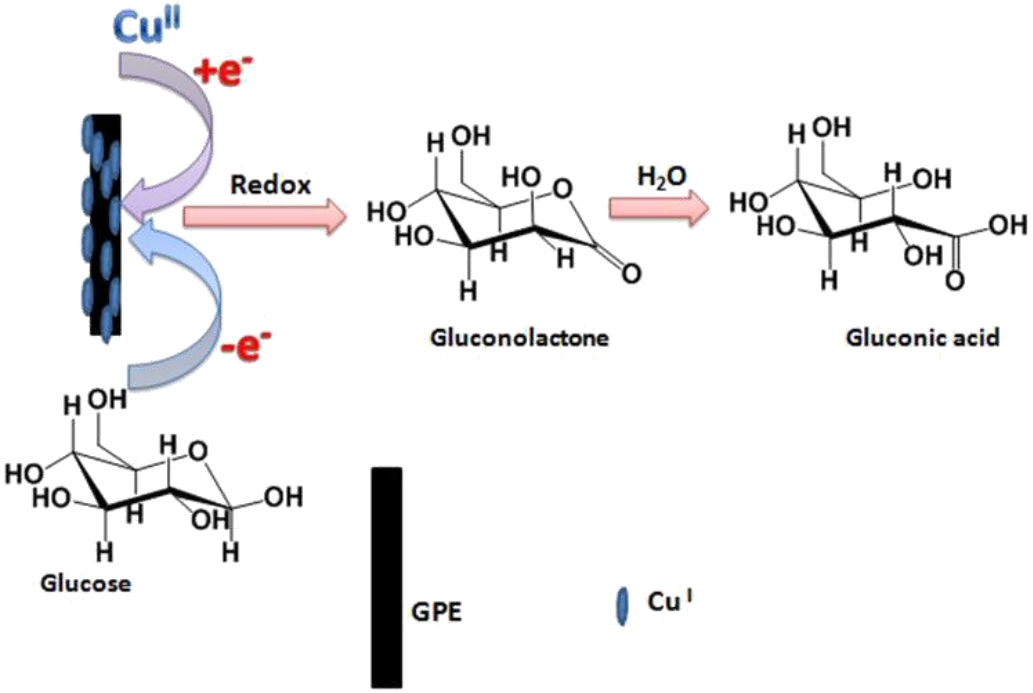

Figure 3-5: Proposed Redox Reaction Scheme of Glucose on GPE in the Presence of $Cu(NO_3)_2$ in 0.10 M NaOH.

3.3.4 Effect of $Cu(NO_3)_2$ Concentration on Glucose Oxidation

Cathodic sweep linear sweep voltammetry (CSLSV) was used for subsequent electrochemical investigations since all the reaction involving glucose detection are on the cathodic segment of CVs presented in Figure 3-1. To obtain the optimal concentration of $Cu(NO_3)_2$ required for glucose enhancement, series of concentrations of $Cu(NO_3)_2$ were tested by measuring the current-peak of 2.00 mM glucose in 0.10 M NaOH solution by CSLSV represented in Figure 3-6. Measurement began with zero (0.00 ppm) concentration of $Cu(NO_3)_2$ (Figure 3-6Aa), subsequently with the addition of 0.20 ppm – 5.00 ppm Cu to the 2.00 mM glucose as presented in Figure 3-6Ab to 3-6Ah and corresponding current-peaks were represented with a bar chart (Figure 3-6B). Electro-catalytic effect of Cu can be observed by the enhancement of current-peak of 2.00 mM glucose with 0.00 ppm concentration of $Cu(NO_3)_2$ compared with the current-peak in the presence of $Cu(NO_3)_2$. Current-peak of glucose was found to increase with the continuous addition of Cu from 0.20 to 2.00 ppm (Figure 3-6Ab to 3-6Af). However, no significant difference was observed between the current-peak of 2.00 mM glucose with 2.00 ppm $Cu(NO_3)_2$ and 4.00 ppm $Cu(NO_3)_2$ (Figure 3-5Af and 3-6Ag). The additional concentration of $Cu(NO_3)_2$ beyond 4.00 ppm leads to a reduction in current-peak of glucose as shown for the 5.00 ppm $Cu(NO_3)_2$ concentration (Figure 3-6Ah). The trend of this electro-catalytic behavior of Cu for the enhancement of glucose current-peak suggests 2.00 ppm $Cu(NO_3)_2$ as the optimal value for glucose detection.

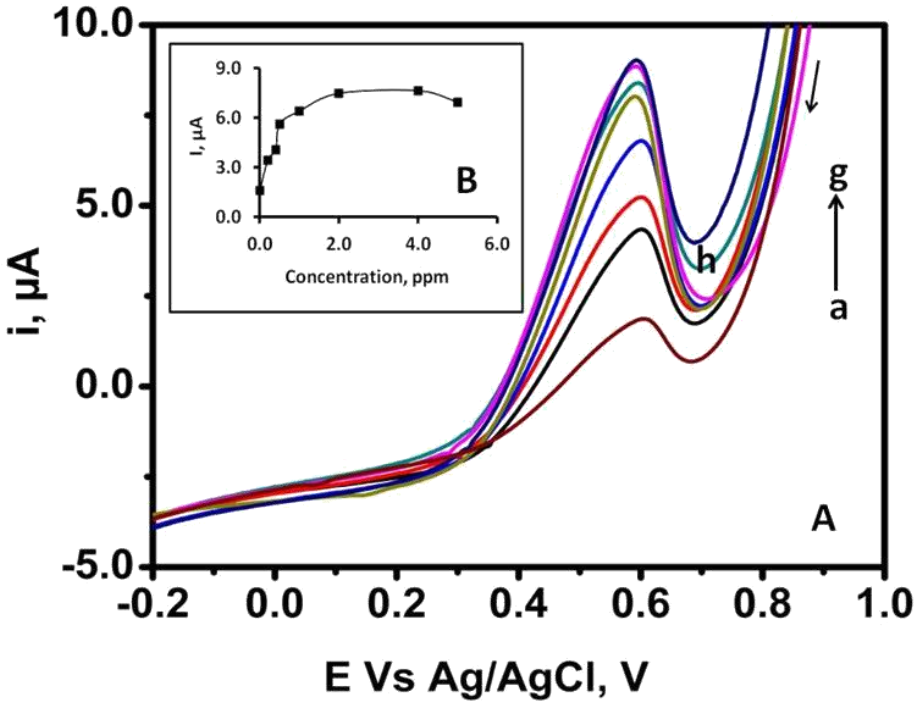

Figure 3- 6: CSLSV of 2.00 mM glucose in 0.10M NaOH at different concentration of $Cu(NO_3)_2$ (ppm) (A) and corresponding bar chart (B). (a) 0.00 (b) 0.20, (c) 0.40, (d) 0.50, (e) 1.00, (f) 2.00, (g) 4.00 and (h) 5.00.

3.3.5 Parameters Optimization

To ensure an effective performance of CSLSV, accumulation potential, accumulation time, sample interval and scan rate are very important parameters to be optimized. Effect of these parameters on the current-peak of 1.00 mM glucose was shown in the presence of 2.00 ppm Cu and represented with a bar chart in Figure 3-7. Accumulation potential on 1.00 mM glucose current-peak in the presence of 2.00 ppm $Cu(NO_3)_2$ was represented by Figure 3-7A after continuous stirring for 30 s. Accumulations by stirring the solution in an open circuit with no potential applied (Figure 3-7Aa) for 30 s give a remarkable current-peak. Improvement of the peak was noticed when -0.20 V potential was applied, but a decrease in peak intensity was observed as the potential value increased towards more positive (-0.10, 0.00 and 0.10 V). -0.20 V accumulations potential gives the best current-peak for 1.00 mM glucose and accumulation time (Figure 3-7B) was investigated at the optimum accumulation potential. Scan rate (Figure 3-7C) and sample interval (Figure 3-7D) were studies consecutively at the optimum value of other parameters.

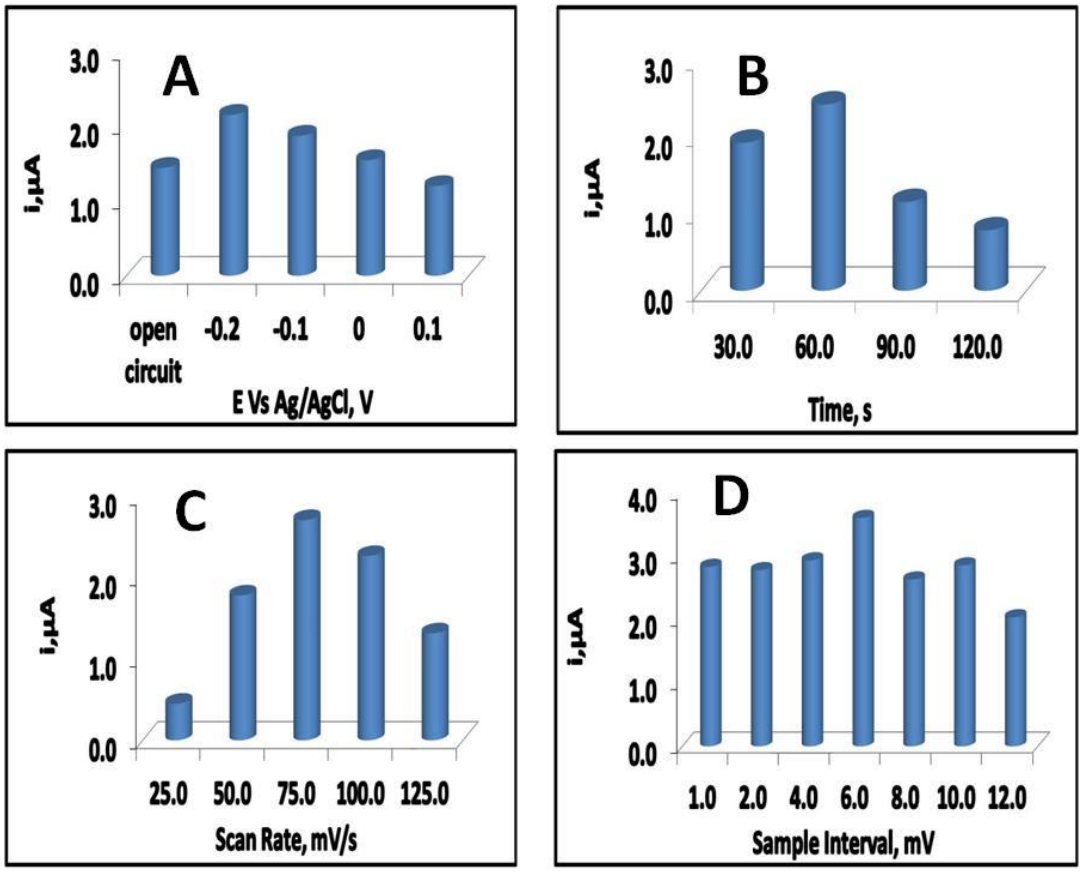

Figure 3-7: Bar Charts showing the corresponding peak heights for the optimized electrochemical parameters of Cathodic LSV for glucose detection; (A) accumulation potential, (B) accumulation time, (C) scan rate, and (D) Sample interval.

3.3.6 Electro-catalytic activity of Copper in Glucose Oxidation

Effects of Copper (Cu) as an effective electrocatalyst of glucose on the surface of GPE at optimized parameters (-0.20 V accumulation potential, 60 s accumulation time, 6.00 mV sample interval and 75.00 mV scan rate) for 1.00 mM glucose in the presence of 2.00 ppm $Cu(NO_3)_2$ were adequately demonstrated in Figure 3-8. A well-defined current peak of glucose without interferences from Cu redox species was obtained. Figure 3- 8a represents the voltammogram of a 0.10 M NaOH (blank glucose concentration) in the absence of 2.00 ppm $Cu(NO_3)_2$ while Figure 3- 8b is the corresponding voltammogram in the presence of 1.00 mM glucose without Cu. Figure 3- 8c represents the voltammogram of a 0.10 M NaOH (blank glucose concentration) in the presence of 2.00 ppm $Cu(NO_3)_2$. A huge enhancement greater than 10 multiples folds (> 1,000 %) of current-peak of Figure 3- 10b was observed in Figure 3-8d as a result of the addition or spiking of 2.00 ppm $Cu(NO_3)_2$. This result shows an amazing electro-catalysis activity of Cu in 0.10 M NaOH for glucose oxidation as a potential cost-saving approach for glucose sensor fabrication.

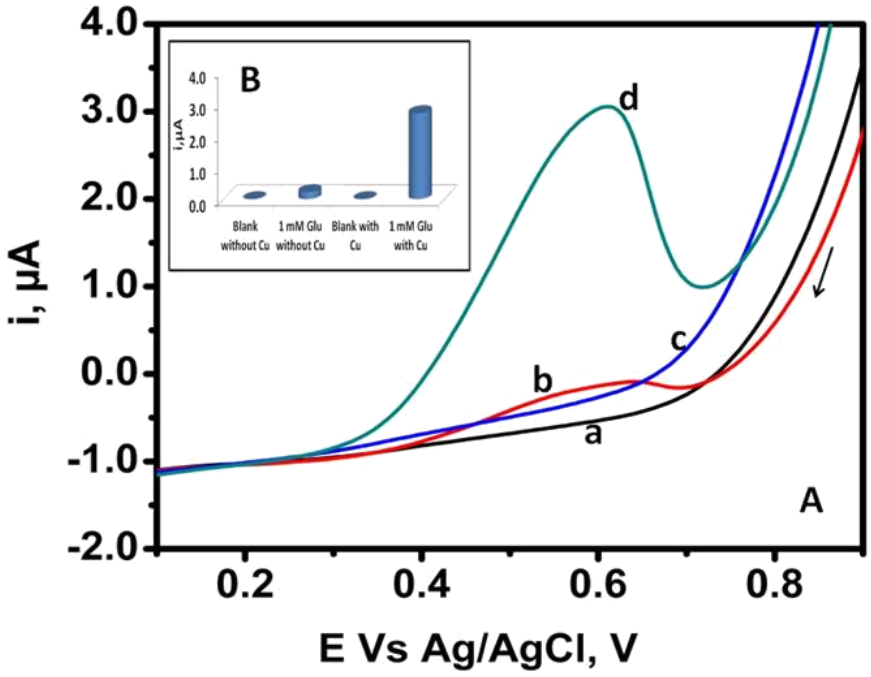

Figure 3-8: CSLSVs at optimized conditions in 0.10M NaOH for effect of $Cu(NO_3)_2$ on 1.00 mM glucose. (A) and corresponding bar chart (B).(a) blank in the absence of 2.00 ppm $Cu(NO_3)_2$, (b) 1.00 mM glucose in the absence of 2.00 ppm $Cu(NO_3)_2$, and (c) blank in the presence of 2.00 ppm $Cu(NO_3)_2$ and (d) 1.00 mM glucose in the presence of 2.00 ppm $Cu(NO_3)_2$.

3.3.7 Electroanalytical Performance

CSLSVs of oxidation of glucose on GPE in a medium comprises of 0.10 M NaOH and 2.00 ppm $Cu(NO_3)_2$ at optimized conditions are presented in Figure 3-9. By comparing the average values of 3 replicate successive additions of different concentrations (mM) of glucose. The response of the bared GPE to different concentrations of glucose can be observed from the voltammograms where an increase in the current-peak corresponding to the oxidation of glucose as the concentration of glucose increases from 0.20 – 4.00 mM as can be seen from Figure 3-9A. This is a very rare observation attribute to a solid electrode response to glucose oxidation without any surface modification which will obviously reduce the cost of sensor fabrication for real-life glucose sensing technology.

Corresponding calibration curve for the GPE response to glucose is shown in Figure 3-9B. Glucose concentration linear dependent between the linearity of 0.06 mM and 4.00 mM exhibited by the electrode is given as $i(\mu A) = 3.5985C_{glu} + 0.0143$ with a correlation coefficient (R^2) of 0.9927 and sensitivity of 315 $\mu AmM^{-1}cm^{-2}$. Estimated limit of detection by signal to noise ratio equals 3 (S/N = 3) is 1.36 µM. Performance of the sensor was found to compete favorably as enumerated in Table 3-2 with previous published articles on the use of copper as an electro-catalyst for non enzymatic glucose detection. This performance can be attributed to simultaneous adsorption of glucose on the surface containing Cu^+ due to the similarity in the reduction potential of Cu^{2+} to Cu^+ and oxidation potential of glucose. This coincidence will lead to the removal of catalytic hydrogen atom by Cu^+ which is the rate determining step of the electro-oxidation of glucose as predicted by Pletcher on 1984 [40].

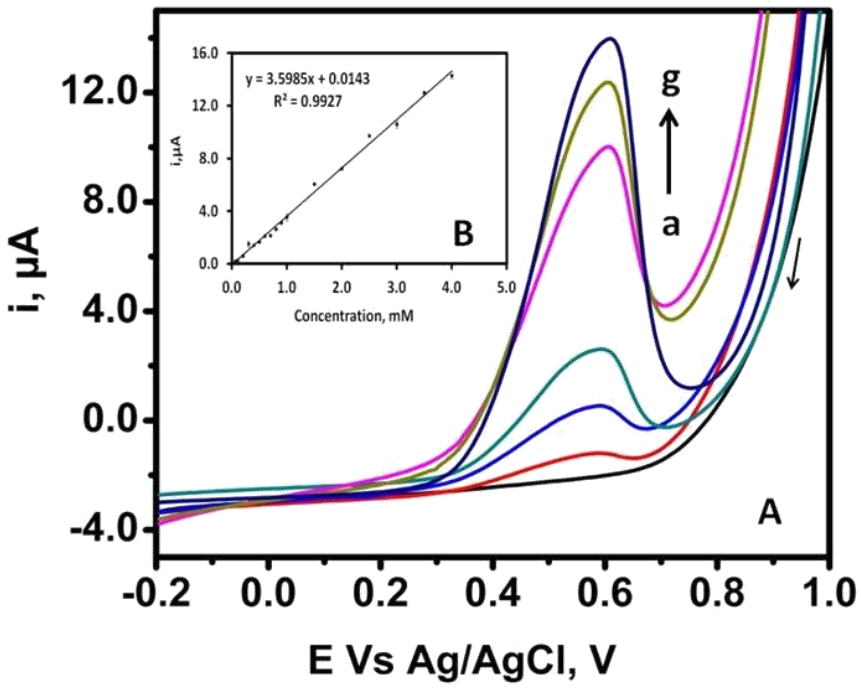

Figure 3-9: CSLSVs of different concentrations (mM) of glucose in 0.10M NaOH plus 2.00 ppm $Cu(NO_3)_2$ (A); (a) 0.00 (b) 0.20, (c) 0.40, (d) 1.00, (e) 2.00, (f) 3.00 and (g) 4.00. (B) Corresponding calibration curve showing from 0.06 – 4.00 mM concentration.

Table 3-2: Electroanalytical performance of different forms of copper modified electrodes for glucose detection

Electrode Materials	**Techniques**	**LOD (µM)**	**Linear range (mM)**	**Sensitivity ($\mu AmM^{-1}cm^{-2}$)**	**Medium**	**Ref.**
Bared GP	CSLSV	1.36	0.06 - 4	315	0.10 M NaOH with Cu std solution	Present work
CuNcs-MWCNTs\GC	Amperometry	1	Up to 7.5	1096	0.1 M NaOH	[191]
CuO-Np-CC		1	Up to 1.22	1245.9		
CuO-Nw-CC	Amperometry	1	Up to 1.12	2973.2	0.1 M	[177]
CuO-Ns-CC		1	Up to 1	4901.9	NaOH	
CuNps-MWCNTs\GC	Amperometry	0.5	0.01 – 0.3	714	0.02 M NaOH	[192]
CuNps-RGO\GC	Amperometry	0.2	0.005 – 1.4	604	0.1 M NaOH	[193]
CuNps-GS\GC	Amperometry	0.5	Up to 4.5		0.1 M NaOH	[65]
CuNws\GC	Amperometry	1	Up to 3	420	0.05 M NaOH	[194]
Cu-Psi\CP	Amperometry	0.2	0.001-0.19 ,0.19 – 2.3	-	0.1 M NaOH	[66]
CuO polyhedron-Nafion\GC	Amperometry	0.33	Up to 4	1112	0.1 M NaOH	[67]
CuNps\GP	DPV	0.44	1 - 6	1467	0.1 M NaOH	[175]
Cu-PMo_{12}-GR\GC	Amperometry	0.03	0.001 - 1	-	0.1 M NaOH	[69]
Cu-RGO\FP	Amperometry		0.002 – 2 2 - 13	50.4[a]	0.1 M NaOH	[70]

CSLSV: cathodic sweep linear scan voltammetry; **DPV:** differential pulse voltammetry; **GP:** graphite pencil; **CC:** carbon clothes; **GC:** glassy carbon; **FP:** flexible paper; **GS**: graphene sheet; **RGO:** reduced graphene oxide; **Psi;** Porous silicon; **PMo_{12} :** Phosphomolybdic acid; **Ns:** nano sheet; **Nw:** nanowire; **Np:** nano particle; **a:** $mAmM^{-1}cm^{-2}$

3.3.8 Effect of Potentials Interference Compounds on Glucose Detection

Co-existence of some saccharides (such as fructose), amino acid (alanine) and ascorbic acid (AA) along with glucose in real life samples necessitate the investigation to prove the potency of the sensor in the presence of potential interferences. Concentrations of AA and some other interferences are always below 0.10 mM compared to the physiological level of glucose which has been estimated to be between 3.00 to 8.00 mM [195]. Based on the physiological level ratio of glucose concentration to its potential interferences, 0.10 mM of AA (Figure 3-10A), fructose (Figure 3-10B) and alanine (Figure 3-10C) respectively were used as an interference concentration against 1.00 mM glucose. CSLSVs of 0.10 mM of AA, fructose, and alanine in the absence of 1.00 mM glucose are shown in Figure 3-10Aa, 3-10Ba, and 3-10Ca respectively. It can be observed that none of the interference current-peak signals was found around the electro-decomposition potential of glucose in the absence of any interference presented by Figure 3-10Ab, 3-10Bb and 3-10Cb. Addition of 1.00 mM glucose into the solution containing 0.10 mM AA, fructose and alanine respectively (Figure 3-10Ac, 3-10Bc and 3-10Cc) show no significant change in the current peak when compared with the current peak of glucose in the absence of interferences. Apart from the slight change in the background noise of the current-peak which does not significantly affect the current- peak of 1.00 mM glucose, the percentage increase in 1.00 mM glucose current peaks as a result of all the study interference are not more than 5 %. The interference study confirms the capability of GPE as a potential transducer for a glucose sensor in the presence of potential interferences.

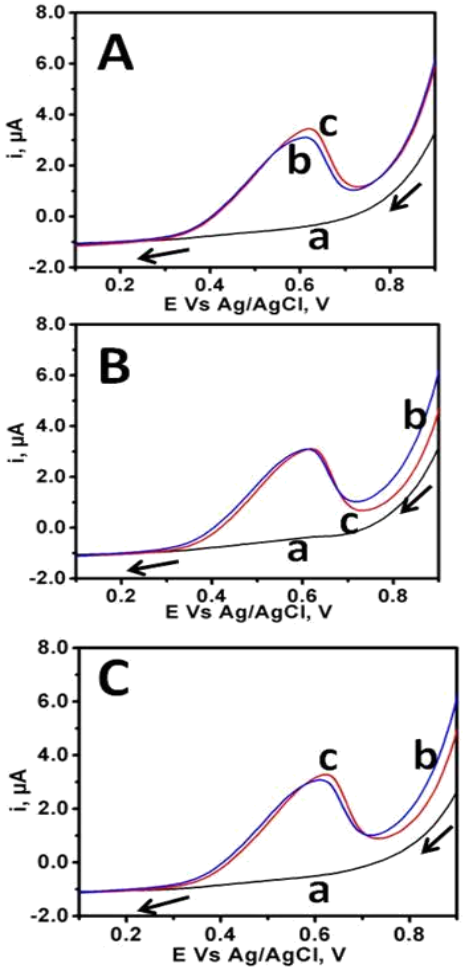

Figure 3-10: CSLSVs of various potential interferences of glucose in 0.10 M NaOH plus 2.00 ppm $Cu(NO_3)_2$ (A) AA, (B) Fructose and (C) alanine. (a) 0.10 mM interference in the absence of glucose, (b) 1.00 mM glucose in the presence of interferences, and (c) 1.00 mM glucose in the absence of 0.10 mM interferences.

3.3.9 Voltammetric Determination of Glucose in Serum Sample

The developed technique was tested using a serum sample obtained from a healthy patient in King Fahd University Teaching Hospital. Protein-free serum sample of 200 dilution times in 0.10 M NaOH was used for analysis of glucose by spiking of a series of standard glucose solutions. Results of the serum sample analysis were enumerated in Table 3-3. About 0.04 mM glucose concentration equivalent to about 8.00 mM glucose concentration was found in the serum sample with a good recovery range between 97 – 110 %. This performance is an indication of the capability of the developed technique with a bared GPE in the presence of $Cu(NO_3)_2$ for a real-life application.

Table 3-3: Glucose detection in healthy human serum sample

#	Spiked Amount (mM)	Amount Found (mM)	Amount Recovered (mM)	% Recovery
1	0.50	0.04	0.49	97.00
2	1.00	0.04	1.01	101.30
3	1.50	0.04	1.52	101.56
4	2.00	0.04	1.98	98.98

CHAPTER 4

In-situ Single-step Electrochemical Silver (II) Oxide modification and Electroanalytical Determination of DL-methionine on a Bare Disposable Graphite Lead Pencil Electrode

4.1 Introduction

Based on availability, ease of use and cost-effectiveness, graphite pencil has been reported to be an efficient electrode for various electroanalytical sensor applications and possible future sustainable transducers for numerous environmental related laboratory and industrial studies [17, 178-182]. To maximize the potential of disposable graphite lead pencil electrode (DGLPE) for sensing targets compounds or element in trace level, there is a need for enhancement of its electro-catalytical activities. However, various forms of silver compounds (AgCs) as an alloy, oxide film and nanoparticle have been reported as an essential constituent in the fabrication of advanced electrode materials for enhanced electron transferability as a supercapacitor [196-198], transistor for amplifying electrical systems [199], semiconductor diode for emitting light [200, 201], solar cell [202] and conversion of greenhouse gas to a useful product through hydrogen evolution inhibition [203]. Application of Ag electrode in voltammetric sensor application is limited based on its characteristic redox peaks but is found to improve electrocatalytic properties of other electrodes [204], thereby used as a modifier in many sensor applications. Few of these Ag modified electrodes include a screen printed electrodes for nitrite detection by flow injection amperometric technique [205], voltammetric investigation and detections of some essential antibiotics by a film made of Ag- amalgam [206], Zinc-AgNps framework electrode for peroxide detection [207] and an immunosensor film made of AgNps and graphene oxide [208].

Methionine is not naturally produced in the body but abundant in almost all human consumptions (nuts, meat, chicken, cheese, fish, egg, dairy, beans, vegetables, etc.). Being a precursor to many essential amino acids (homocysteine, cysteine, taurine,

glutathione, glycine, threonine) [120], it has been credited to be involved in many detoxifying processes, protects cells from pollutants, slows cell aging, absorption and bioavailability of some macronutrients, aiding excretion, and prevents excess fat build-up. The presence of sulfur in its side chain has made redox reaction easy and found to help in improving the growth of cell which necessitates its use as an additive in pharmaceutical products [121]. High level of plasma methionine have found not to possess any adverse effect on human, but its role in elevating homocysteine level is a significant concern as a result of metabolic disorder reactions [122] especially for noninsulin dependent diabetes (non-cardiovascular disease) [124, 125]. Folic acid, vitamins C, B-6 and B-12 supplements have been recommended for the moderation of an integral part of the methionine cycle [127] but still not effective. The emergence of neurological disorder diseases such as Alzheimer [137-139], long-term central nervous disorder disease (Parkinson) [140] and many other reduced oxygen species-related diseases associated with residual methionine. Methionine restriction diet (MRD) is the recent potent diagnosis to treat or prevent some chronic health conditions including cancer, depression, insulin sensitivity, and resistance. MRD has been reported to improve renal insulin in aged kidney, improve glucose tolerance and decrease fasting glucose[9], remodeling of white adipose tissue and reverse of malfunction liver in mice [10]. MRD is not limited to mitigation of diabetes mellitus but has been attributed to prevention of cancer cell growth and lifespan extension hypothesis strategy in animals and human [145, 146]. All these consequences of methionine are concerns for effective detection of methionine in body plasma.

Due to the complex nature of methionine, there is a need for its separation from other sulfur-containing compounds before detection. Low sensitivity, longer analysis time and cost-effectiveness have been a challenge for the sustainability of rugged chromatographic, [147-149], flow analysis [151] and colorimetric [150] techniques developed for its routine analysis. However, expensive, delicate and tedious modified electrodes such as electropolymerized film of non peripheral copper–amine complex [156], composite nanotube comprises of Pt and TiO_2 on glassy carbon electrode (TiO_2-Pt/CNT/GCE) [155] and nanofilm electrochemically synthesized by molecular imprint on graphite pencil electrode (MWCNT-NFMIP/GPE) [154] have been reported. Other complicated electrode systems reported for methionine detections includes aminic nicotine gold nanoparticle [209], oxygen electrochemically controlled graphene oxide [153], acrylic acid complex ZnO modified carbon paste [210], carbon ceramics electrode (CCE) modified with nickel powder prepared by sol-gel methods [211] and a bimetallic nanoparticle comprises of silver and gold on GCE (Au-Ag/GCE) [152]. There is a need for the development of a simple, cost-effective, proficient and efficient electroanalytical method for electroanalytical determination of methionine.

The present work is aimed at developing a facile single step electroanalytical technique by in-situ DGLPE modification with $AgNO_3$ solution and determination of DLM for the fabrication of a cost-effective, prompt and ease-to-use electrochemical sensor.

4.2 Experimental

4.2.1 Chemicals

1000 mg/L ± 4.00 Ag standard prepared in nitric HNO_3 standard solution AAS specification by Fluka were used as obtained. H_2SO_4, HCl, NaOH pellet, a 3M acetate buffer solution pH 5.00, DL-methionine, L-ascorbic acid, L-alanine, and L-cysteine were supplied by Sigma-Aldrich. 0.10 M Phosphate buffer solutions (PBS) of pH 4.5, 7.00 and 9.00 were prepared by mixing appropriate volumes of 0.10 M monosodium phosphate and disodium phosphate prepared with double distilled water from their anhydrous salts. All solutions were prepared with double distilled water obtained from Aquatron water still A4000D water purification system.

4.2.2 Electrochemical Cell and Procedure

A system comprises of 3electrodes system were utilized with 0.10 M NaOH and phosphate buffer solution (PBS) as supporting electrolyte. PBS was prepared with an appropriate mixture of sodium phosphate mono and di-basic anhydrous salts. A working electrode made of graphite pencil whose fabrications, descriptions along with its working principle have been widely reported [183]. A platinum wire and Ag\AgCl saturated KCl were connected with CHI potentiostat workstation (CHI1232A, CH Instruments Inc, Austin, TX, USA) as a counter and reference electrodes respectively for all electroanalytical measurements. Approximately 10 mm length of 0.50 mm diameter

graphite lead corresponding to about 16.10 mm^2 surface area propelled out of the vertically positioned pencil through a Teflon hole to make contact with the supporting electrolyte. The electrical contact of the graphite lead was achieved by soldering copper wire with the metallic part of the pencil.

Electroanalytical techniques adapted for the electrochemical studies are cyclic voltammetry and linear scan voltammetry for the analytical performance of the developed technique at room temperature and cathodic sweeping at the quiescent condition.

4.2.3 Surface Characterization of Disposable Graphite Lead Pencil Electrode

Image of DGLPE was recorded with FE-SEM instrument by TESCAN LYRA 3 from the Center of Research Excellence in Nanotechnology (CENT), King Fahd University of Petroleum and Minerals (KFUPM), Kingdom of Saudi Arabia (KSA). X-ray photon Spectroscopy (XPS) investigation was performed with a Thermos-Scientific ESCALAB-250Xi instrument with monochromatic Al Kα radiation (hv = 1486.6 eV) installed in the Physics Department, KFUPM, KSA. Data obtained from XPS was processed with Thermo Avantage 5.51 version, Surface Chemical Analysis software.

4.2.4 Real Sample Collection and Preparation

Collection of the serum sample was achieved with the assistant of Imam Abdulrahman Teaching Hospital (King Fahd University, Hospital) blood bank section from a healthy patient. Serum sample stored in the refrigeration was defrosted, and 450 µL aliquot was taken and treated with methanol (900 µL) in ratio 1:2 to separate protein from the serum sample. Separation of the precipitated protein was achieved with a clear supernatant of the serum sample after centrifugation of mixture for 20 minutes at 2000 rpm and subsequently filtered with a Millipore filter of 0.45 µm.

4.3 Results and Discussion

4.3.1 Influence of pH and Different Electrolytes on DL-methionine Redox Reactions on Graphite Pencil Electrode

Electrochemical activity of GPE towards oxidation of 0.50 mM DL-methionine (DLM) in the presence of 29.43 µM $AgNO_3$ solution were investigated in different electrolytes (H_2SO_4, HCl, acetate buffer (pH 5.00), PBS (pH 4.50, 7.00 and 9.00) and NaOH solutions) by cyclic voltammogram (CV) and presented as Figure 4-1A. It can be observed that NaOH solution (pH 13.70 ± 0.20) was the only electrolyte that shows electrochemical activity towards oxidation of DLM on GPE with secondary oxidation in the cathodic region of the CV at about 0.63 V along with an oxidation peak present between 0.15 V and 0.45V in all the screened electrolytes. For clarity purposes, 0.10 M

PBS pH 7.00 ± 0.20 will be used as a representative of other electrolytes that could not be oxidized DLM and compared with 0.10 M NaOH pH 13.70 ± 0.20 to investigate details of DLM redox reaction. Cyclic voltammograms (CVs) of showing various redox reactions of DLM in 0.10 M PBS pH 7.00 ± 0.20 and 0.10 M NaOH pH 13.70 ± 0.20 were shown in Figure 4-1B and 4-1C respectively. It can be observed that the presence of 0.50 mM DLM in both PBS pH 7.00 ± 0.20 and 0.10 M NaOH pH 13.70 ± 0.2 as shown in Figure 4-1B and 4-1C (red) respectively could not generate any redox peaks when compared with their corresponding voltammograms (black) which represent the CV of 0.10 M PBS pH 7.00 ± 0.20 and 0.10 M NaOH pH 13.70 ± 0.2 respectively without 0.50 mM DLM. A peak attributed to oxidation of Ag^0 to Ag^+ between 0.20 and 0.40 V as reported by Wan et al. 2013 [212] can also be observed in Figure 4-1B and 4-1C (blue) as present in other electrolytes in Figure 4- 1A due to the presence of 29.43 µM $AgNO_3$ solution in the electrolyte. Addition of 0.50 mM DLM into PBS containing 29.43 µM $AgNO_3$ solutions could not generate additional peak for DLM as shown in Figure 4-1B (cyan). Surprisingly, a very sharp secondary oxidation peak can be observed in Figure 4-1C (cyan) as a result of the addition of 0.50 mM DLM to NaOH electrolyte containing 29.43 µM $AgNO_3$ solutions. So, oxidation of DLM on the surface of GPE can only be initiated by the presence of $AgNO_3$ in NaOH electrolyte. The presence of a characteristic peak of the oxidation of Ag^+ to Ag^{2+} at about 0.80 V shown in Figure 4-1C (blue) can be responsible for the oxidation of DLM. A pulse radiolysis investigation can support this observation reported for Ag^{2+} in the metal-induced oxidation of methionine by hydroxyl radical ($OH^{\bullet}$) readily available mechanism which generates a sulphonium center

(Zwitterionic methionine) as an intermediate in both cyclic of aliphatic depending on pH and can latter oxidized to methionine sulphoxide [213, 214].

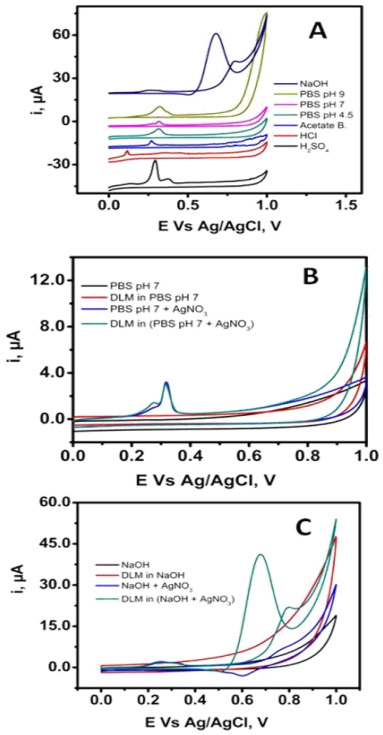

Figure 4-1: Cyclic voltammograms of 0.50 mM DL-methionine (**A**) in the presence of 29.43 µM $AgNO_3$ solution in different electrolytes; 0.10 M H_2SO_4 (black), 0.10 M HCl (red), 0.10 M acetate buffer (blue), 0.10 M Phosphate buffer solution (PBS) pH 4.50 ± 0.20 (cyan), 0.10 M PBS pH 7.00 ± 0.20 (magenta), 0.10 M PBS pH 9.00 ± 0.20 (lime-green) and 0.10M NaOH pH 13.70 ± 0.20 (navy blue). **(B)** 0.10 M Phosphate buffer solution (PBS) pH 7.00 ± 0.20 and **(C)** 0.10M NaOH pH 13.70 ± 0.20 of DL-Methionine in presence and absence of 29.43 µM $AgNO_3$; blank [PBS pH 7.00 and NaOH] (black), 0.50 mM DL-methionine (red), 29.43 µM $AgNO_3$ in blank (blue) and 0.50 mM DL-methionine in 29.43 µM $AgNO_3$ (cyan).

Electrochemical redox reaction of $AgNO_3$ on the surface of GPE was further studied in PBS and NaOH electrolyte by multiple cycles CV. Figure 4-2A and 4-2B represent 25 cycles of 29.43 µM $AgNO_3$ solution in PBS and NaOH respectively. The current attributed to oxidation of Ag^+ to Ag^{2+} was only observed in Figure 4-2A with a reduced currents peak after the first cycle of CV. However, apart from the Ag^+ to Ag^{2+} oxidation peak observed in Fig 4-2A, additional oxidation peak, and about 3 reduction peaks were observed in Figure 4-2B with an increase in peak current of each peak as the CV cycles increases. This redox behavior suggested that the property of a pure silver sample has been successfully induced on the surface of GPE based on the report of the formation and reduction of different silver oxides (AgOs) in NaOH electrolyte when 99.99 % silver sample was used as a working electrode [212] a and that there is propagation in the formations of oxides layers of Ag as the number of cycle increases by $OH^{\cdot}$ from NaOH of the supporting electrolyte.

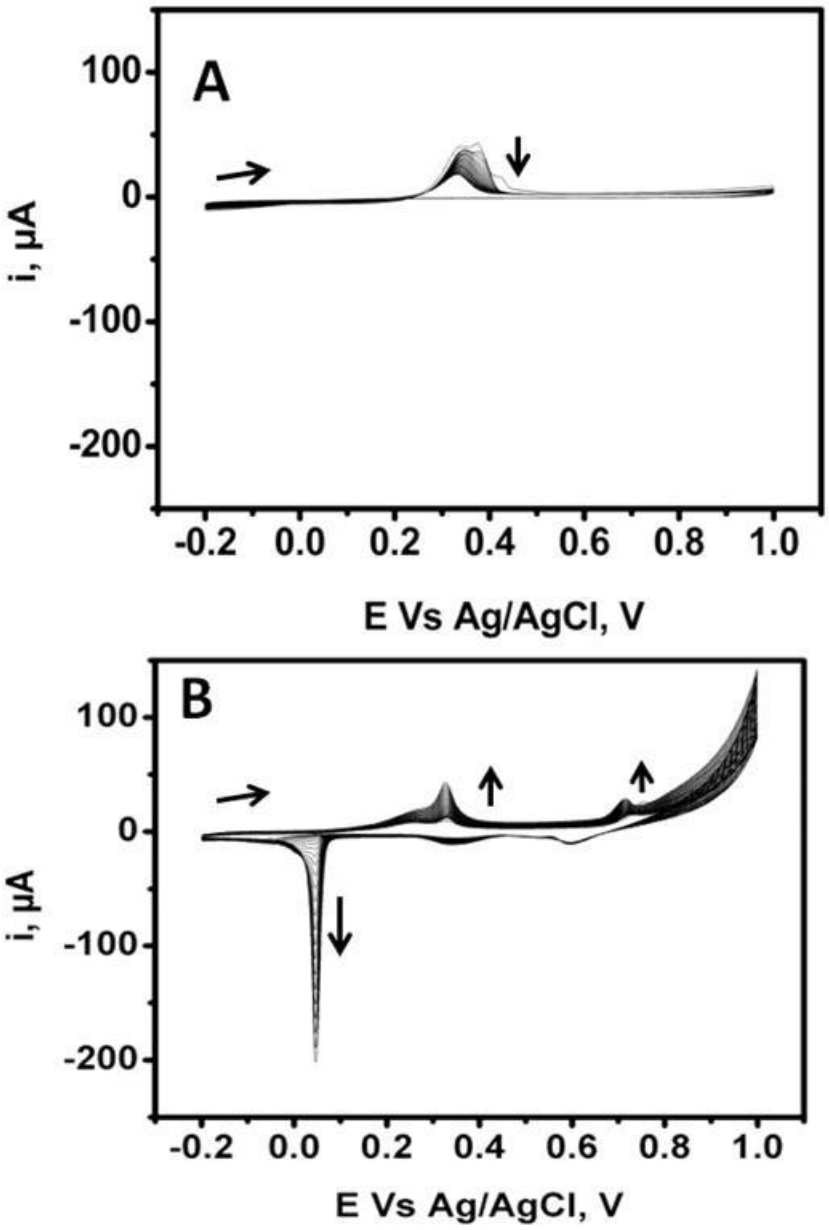

Figure 4-2: 25 cycles of CVs of 29.43 µM $AgNO_3$ solution on DGLPE in (A) 0.10 M PBS pH 7.00 ± 0.20 and (B) 0.1M NaOH pH 13.70 ± 0.20.

4.3.2 Characterization of Disposable Graphite Lead Pencil Electrode Surface

Effects of the oxides layers on the surface of DGLPE (Figure 4-3) were further investigated by FE-SEM / EDX analysis after 25 cycles CV. Figures 4- 3A and 4- 3B show the image of DGLPE in the presence and absence of 29.43 µM $AgNO_3$ solution respectively while their corresponding EDX spectrum is presented in Figure 4-3C. Formation of spherical shape Ag oxides can be observed in both Figure 4-3Ba and 4- 3Bb on DGLPE surface containing 29.43 µM $AgNO_3$ solution in PBS and NaOH respectively. By comparison, the formation of elemental silver (Ag) is more evident in NaOH (Figure 4-3Bb) than PBS (Figure 4-3Ba) medium. EDX spectrum analysis (Figure 4-3C) of the images further confirmed the presence of Ag on the DGLPE in both medium with a higher weight % in NaOH as enumerated in Table 4-1

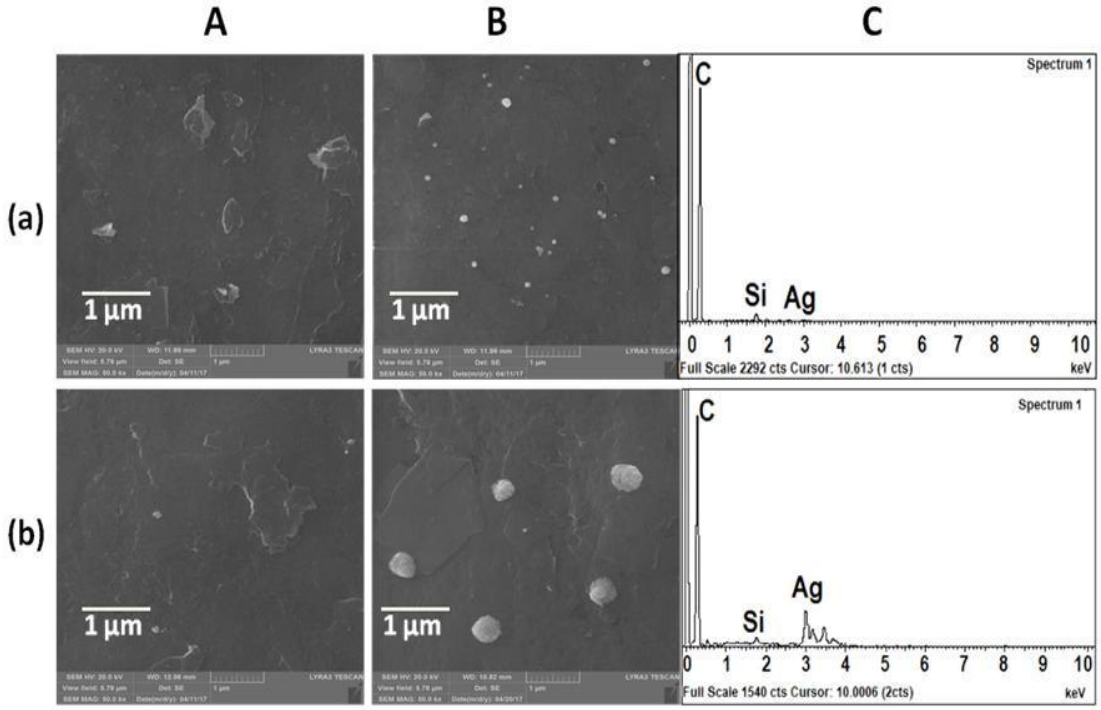

Figure 4-3: FE-SEM images of GPE surface after 25 cycles of cyclic Voltammograms in different medium **(A)** GPE in Absence of 29.43 µM $AgNO_3$ solution **(B)** GPE in presence of 29.43 µM $AgNO_3$ solution, **(C)** Corresponding EDX Analysis. (a) 0.10 M Phosphate buffer solution (PBS) pH 7.00 ± 0.20 and (b) 0.10M NaOH pH 13.70 ± 0.20.

Table 4-1: EDX elemental weight % composition of DGLPE treated with Different Concentration of $AgNO_3$ Solution in 0.10 M PBS pH 7.00 and 0.10 M NaOH.

$AgNO_3$ (µM)	**0.10 M PBS pH 7.00**			**0.10 M NaOH**		
	C	**Si**	**Ag**	**C**	**Si**	**Ag**
29.43	99.11	0.66	0.22	89.55	0.83	9.62
58.86	98.46	0.85	0.70	83.40	0.64	15.97

Investigation of the oxidation states of Ag presence on DGLPE surface 29.43 µM $AgNO_3$ in 0.10 M PBS and NaOH by XPS Ag3d and O1s spectra were presented in Figure 4-4. Two characteristic peaks Ag indicated as $3d_{3/2}$ and $3d_{5/2}$ can be observed at about 374 eV and 368 eV binding energy (BE) respectively in both media with higher intensity in NaOH medium (Figure 4-4Ab) than PBS (Figure 4-4Aa) confirming the presence of Ag on DGLPE surface with different oxidation state induced intensity. Further analysis of Figure 4-4A as shown in Figure 4-4A^{I} and Figure 4-4A^{II} for PBS and NaOH medium respectively reveal the presence of an additional peak of lower intensity in $3d_{5/2}$ with BE of 367.56 eV while there are no additional peaks observed in the analysis of Figure 4-4Ab. This observation is an indication of the presence of Ag in Ag_2O along with Ag in AgO in Figure 4-4a confirming the dominance of Ag_2O on the surface of DGLPE in PBS medium and AgO on the surface DGLPE in NaOH medium [215, 216]. This behavior was further observed in O1s spectra (Figure 4-4B) with the appearance of a hump on the O1s spectrum (Figure 4-4Ba) of the PBS medium compared with the O1s spectrum of the NaOH spectrum (Figure 4-4Bb). Analysis of Figure 4-4B presented as Figure 4-4B^{I} for the PBS medium reveal an additional peak with 530.22 eV BE showing the presence of O of Ag_2O in the PBS medium and O of AgO in NaOH medium (Figure 4-4B^{II}). Both Ag3d and the O1s spectra complement each other as a prove for the deposition of AgO on DGLPE in NaOH and Ag_2O on DGLPE in PBS medium with a characteristic O=C peak at about 532 eV for graphite attachment with the O of the oxides in both spectra [188]. Details information on XPS of Ag3d and O1s spectra peaks analysis on DGLPE surface for 29.43 µM $AgNO_3$ in PBS and NaOH are tabulated in Table 4-2 and 4-3 respectively.

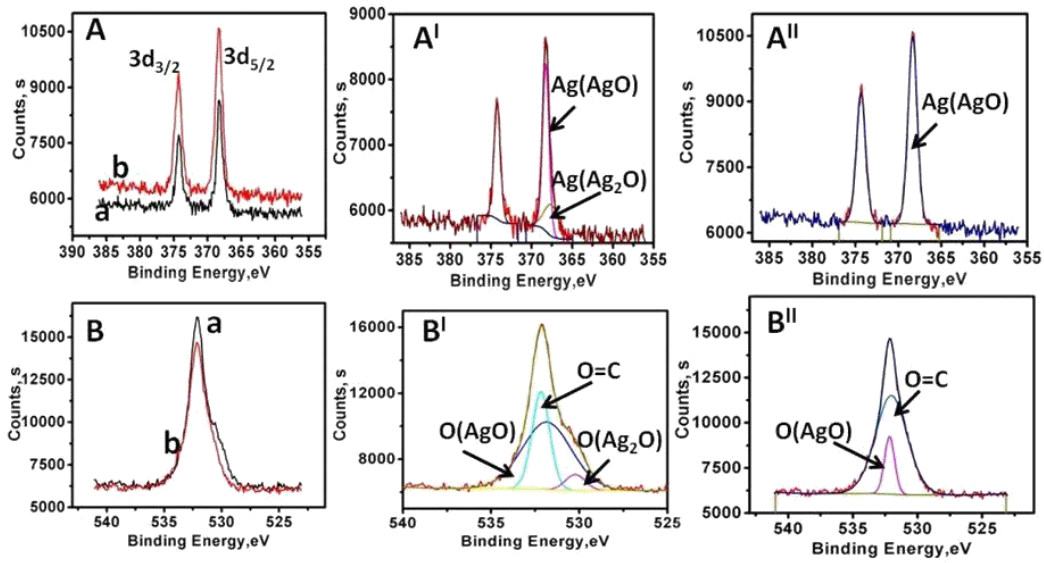

Figure 4-4: XPS analysis of (A) Ag3d and (B) O 1s on DGLPE surface after 25 cycles of CVs in a different medium. (Aa & Ba) 29.43 µM $AgNO_3$ in 0.10 M PBS pH 7.00 ± 0.20, (Ab & Bb) 29.43 µM $AgNO_3$ in 0.10 M NaOH pH 13.70 ± 0.20. (A^I) Deconvolution peaks of Aa, (A^{II}) Deconvolution peaks of Ab, (B^I) Deconvolution peaks of Ba and (B^{II}) Deconvolution peaks of Bb.

Table 4-2: XPS of Ag3d and O1s Spectra Peak Analysis on DGLPE Surface for 29.43 μM $AgNO_3$ in PBS.

Spectra	Peak's Name	BE(eV)	FWHM (eV)	Peak Area (CPS.eV)	Atomic %
Ag3d	$3d_{3/2}$ A	374.22	0.93	1783.18	44.63
	$3d_{5/2}$ B	368.26	0.93	2575.71	44.58
	3d C	367.56	2.04	1060.69	10.79
O1s	O1s A	531.84	3.28	14572.74	61.78
	O1s B	532.18	1.18	7614.79	32.29
	O1s C	530.22	1.32	1400.88	5.94

Table 4-3: XPS of Ag3d and O1s Spectra Peak Analysis on DGLPE Surface for 29.43 μM AgNO3 in NaOH.

Spectra	Peak's Name	BE(eV)	FWHM (eV)	Peak Area (CPS.eV)	Atomic %
Ag3d	$3d_{3/2}$ A	374.35	1.25	4025.98	50.03
	$3d_{5/2}$ B	368.34	1.25	5815.31	49.97
O1s	O1s A	532.03	2.87	17027.04	84.15
	O1s B	532.17	0.92	3208.20	15.85

4.3.3 Effect of $AgNO_3$ Concentration on DL-Methionine oxidation

Based on the redox peaks of Ag on the DGLPE surface and the oxidation of DLM in the cathodic region of the CV shown in Figure 4-1B, CSLSV was used for the subsequent electrochemical investigations. Amount of $AgNO_3$ solution necessary for effective oxidation of DLM needs to be optimized. Effect of the $AgNO_3$ solution on the oxidation of 0.20 mM DLM was presented in Figure 4-5. Oxidation of DLM could not be noticed in Figure 4-5Aa due to the absence of an $AgNO_3$ solution. However, introduction of $AgNO_3$ solution into the medium containing 0.10 M NaOH and 0.20 mM DLM leads to emergence of oxidation peaks of DLM around 0.65 V along with 2 reduction peaks of Ag at about 0.50 V and 0.05 V. It was observed that the peak current increases as the concentration of the $AgNO_3$ solution increases from 2.94 – 17.66 µM (Figure 4-5Ab to 4-5Ag). Peak current response of DLM to subsequent addition of $AgNO_3$ solution was shown in a corresponding inserted curve of the voltammogram presented in Figure 4-5B. Concentrations of $AgNO_3$ solution above 17.66 µM does not show significantly different in peak current of 0.20 mM DLM (Figure 4-5Ah to 4-5Aj). This could be as a result of the agglomeration of the Ag particles formed on DGLPE surface which may likely reduce or slow down the oxidation process. The optimum concentration of $AgNO_3$ solution that can effectively initiate oxidation of DLM was considered to be 17.66 µM

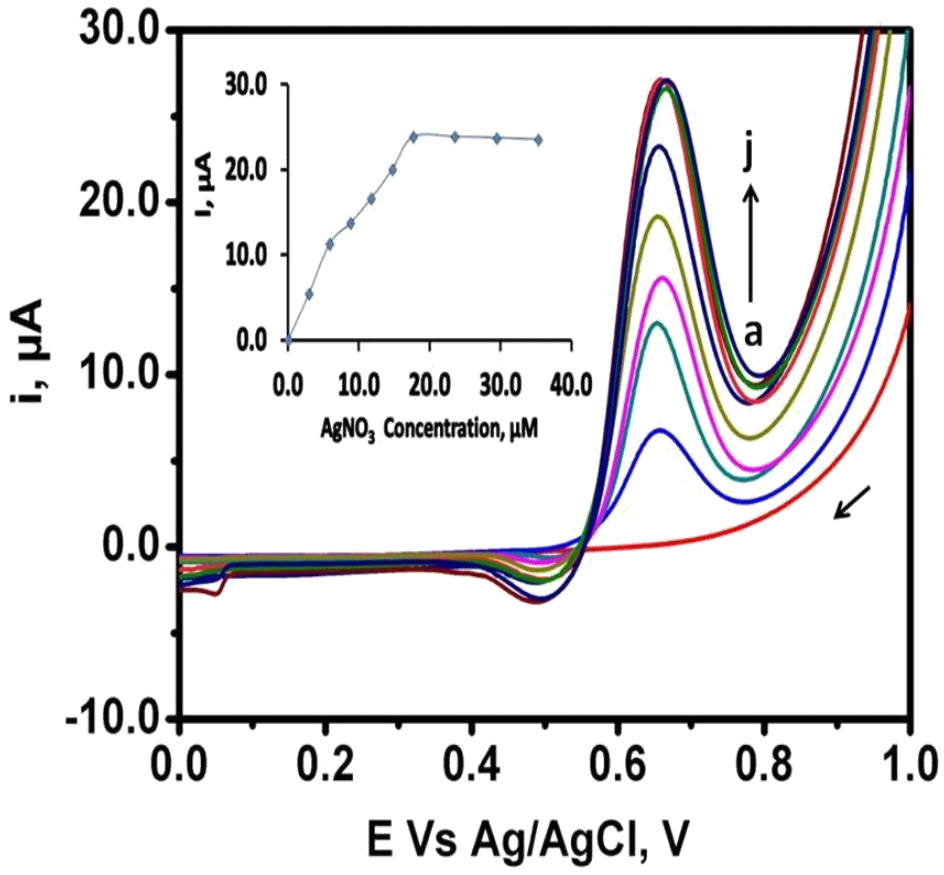

Figure 4-5: CSLSVs of 0.20 mM DL-methionine in 0.10 M NaOH pH 13.70 ± 0.20 at different concentration of $AgNO_3$ (µM) and corresponding inserted curve. (a) 0.00 (b) 2.94, (c) 5.88, (d) 8.83, (e) 11.77, (f) 14.71, (g) 17.66, (h) 23.55, (i) 29.43 and (j) 35.32.

4.3.4 Parameters Optimization

Optimization of some parameters such as accumulation potential (V), accumulation time (s), scan rate (mV/s) and sample interval (mV) are necessary for an improved voltammogram for effective DLM detection. Figure 4-6 shows the effect of accumulation potential from -0.40 V – 0.40 V on the DLM voltammogram for 30 s under stirring condition. Interestingly, the 2 reduction peaks of Ag ions observed in Figure 4-5 was found to disappear due to positive accumulation potential of 0.20 and 0.40 V (Figure 4-6d and 4-6e) compared with their corresponding -0.40 V. -0.20 V and 0.00 V (Figure 4-6a, 4-6b, and 4-6c). A positive accumulation potential might probably prevent reduction of Ag to lower oxidation states within the potential working window. Current peak of 0.20 V accumulations potential is the highest as shown in Figure 4-6B and was selected as the optimum potential. A similar investigation was carried out for accumulation time (Figure 4- 7) at 0.20 V potential from 15 s – 120 s. Corresponding bar chart of the accumulation time investigation (Figure 4- 7B) revealed 30 s accumulation time as optimum. Scan rate (Figure 4-8) and sample interval (Figure 4-9) were also studied at the optimum values of other parameters. There no significant effect of the sample interval on the oxidation current peak of DLM (Figure 4-9B) but 100 mV\s scan rate shows a better performance regarding the peak current (Figure 4-8B) among the tested scan rate.

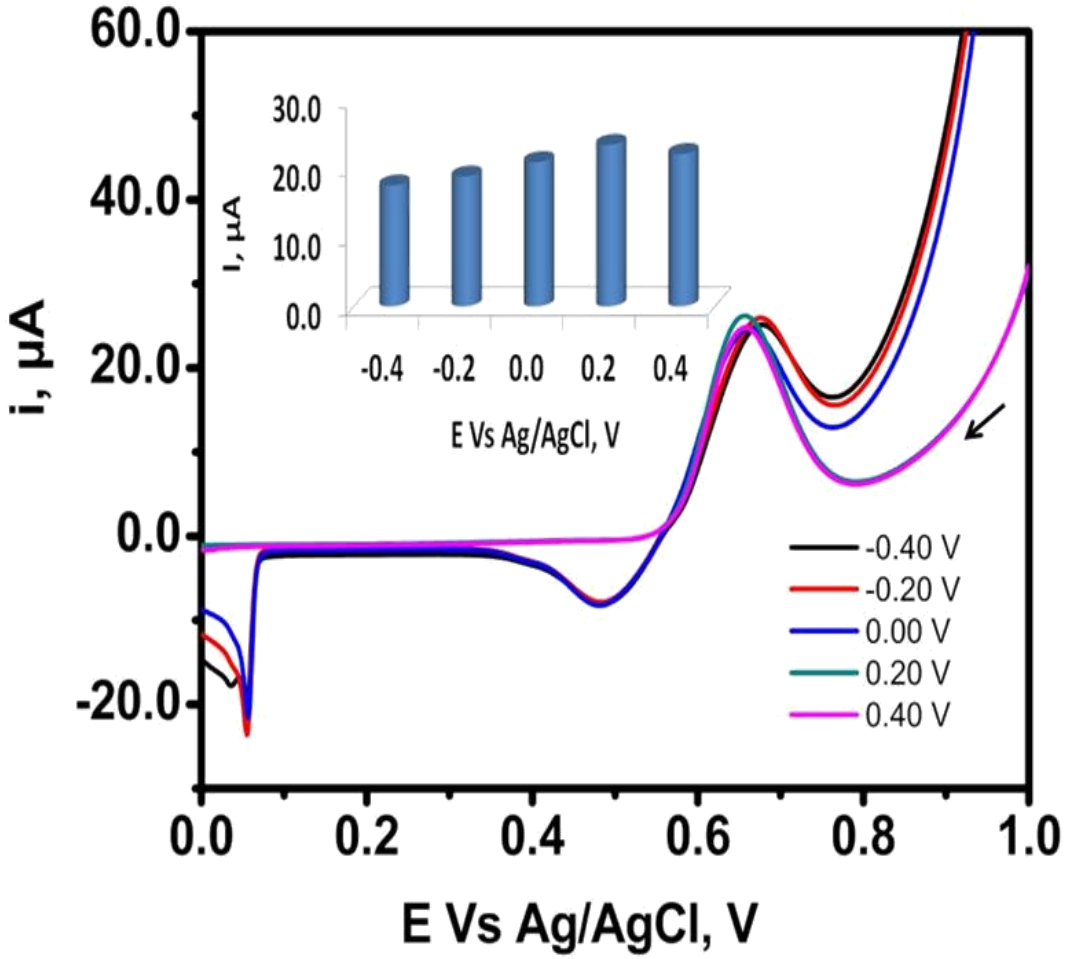

Figure 4-6: CSLSVs of 0.20 mM DL-methionine in 0.10 M NaOH pH 13.70 ± 0.20 in the presence of 17.66 µM $AgNO_3$ for different accumulation potential (mV) at 30 s accumulation time and corresponding inserted bar chart; -0.40 V (black), -0.20 V (red), 0.00 V (blue), 0.20 V (cyan) and 0.40 V (magenta).

.

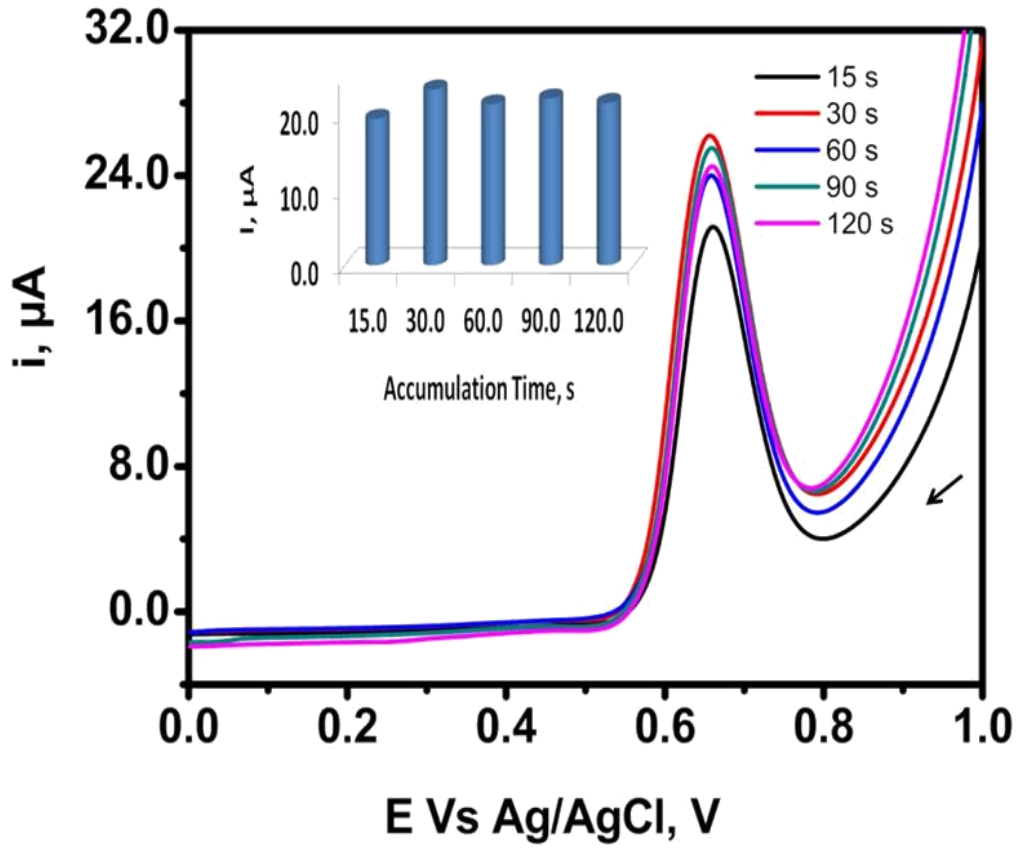

Figure 4-7: CSLSVs of 0.20 mM DL-methionine in 0.1M NaOH pH 13.70 ± 0.20 in the presence of17.66 µM $AgNO_3$ for different accumulation time (s) at optimized accumulation potential and corresponding inserted bar chart; 15 s (black), 30 s (red), 60 s (blue), 90 s (cyan) and 120 s (magenta).

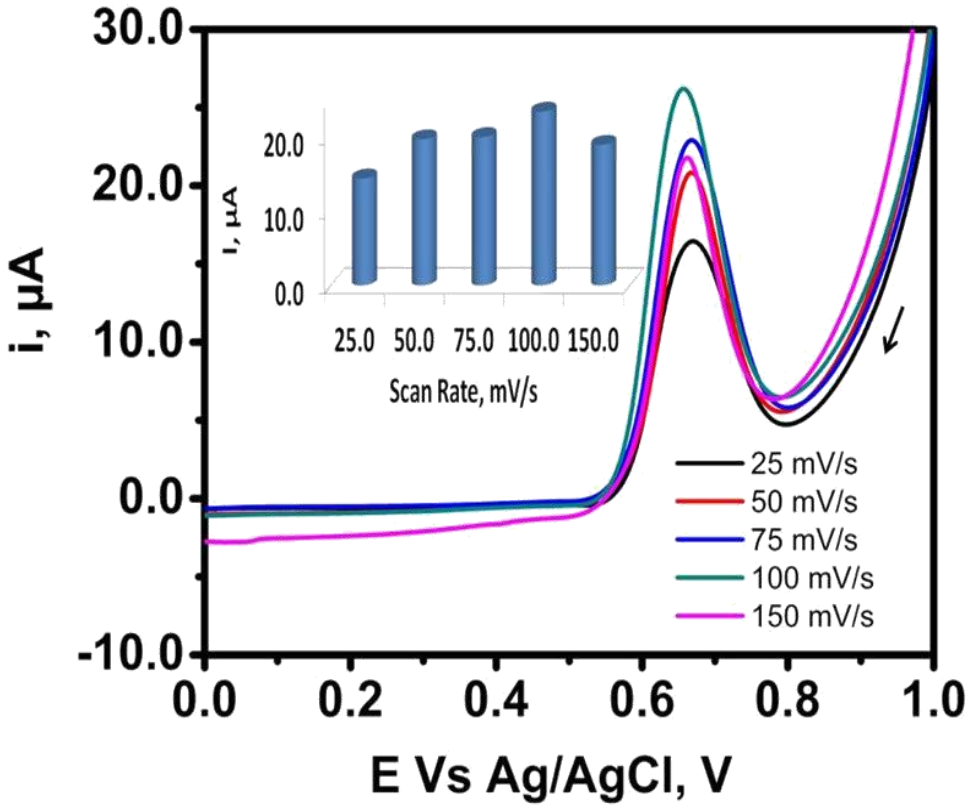

Figure 4-8: CSLSVs of 0.20 mM DL-methionine in 0.1M NaOH pH 13.70 ± 0.20 in the presence 17.66 µM $AgNO_3$ for different scan rate (mV/s) at optimized accumulation potential and time, and corresponding inserted bar chart; 25 mV/ s (black), 50 mV/s (red), 75 mV/s (blue), 100 mV/s (cyan) and 150 mV/s (magenta).

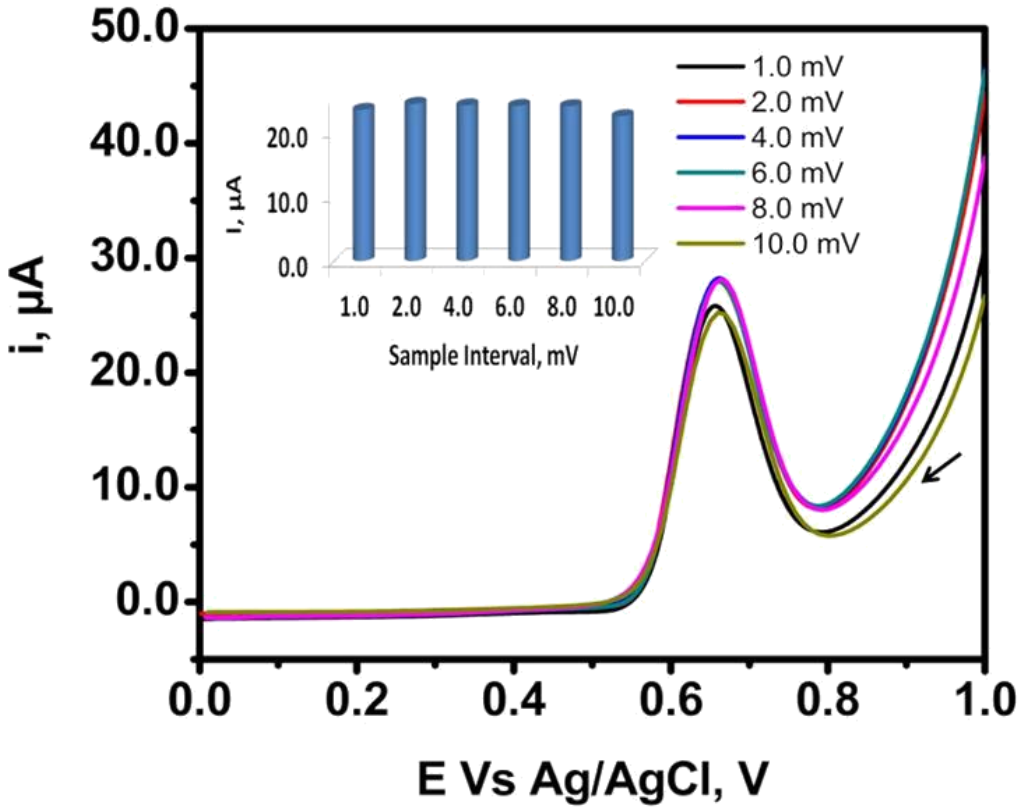

Figure 4-9: CSLSVs of 0.20 mM DL-methionine in 0.10 M NaOH pH 13.70 ± 0.20 in the presence of 17.66 µM $AgNO_3$ for different sample interval (mV) at optimized accumulation potential, accumulation time and scan rate and corresponding inserted bar chart; 1.0 mV (black), 2.0 mV (red), 4.0 mV (blue), 6.0 mV (cyan), 8.0 mV (magenta) and 10.0 mV (lime-green).

4.3.5 Electroanalytical Performance

Performance of the developed sensor presented in Figure 4-10 was ascertained by constructing a calibration curve with voltammogram of the mean value of 3 replicated successive additions of different concentrations of DLM in 0.10 M NaOH and 3 ppm $AgNO_3$ solution at the optimized conditions. A characteristic reduction peak of Ag^{2+} to Ag^{+} that is responsible for the initiation of DLM oxidation similar to what was observed in Figure 4-2B between 0.70 V and 0.60 V can be observed in Figure 4-10Aa in the absence of DLM. Possible conversion of Ag^{+} to Ag^{2+} in the supporting electrolyte by the initial applied 0.20 V accumulation potential for 30 s can be attributed to CLSV response to the reduction peak by DGLPE. This peak can still be observed despite the addition of 0.01, 0.02 and 0.04 mM of DLM that generate an oxidation peak with a deflection around 0.65 V potential in Figure 4-10Ab, 4-10Ac, and 4-10Ad respectively. Moreover, as the concentration of DLM is increased from 0.06 – 0.50 mM as shown in Figure 4-10Ae to 4-10Ak, Ag reduction peak can no longer be observed due to the relatively higher current generated by oxidation of DLM on DGLPE surface.

Calibration curve for the corresponding voltammogram of DLM is shown in Figure 4-10B. DLM concentration linear dependent between the linearity of 0.01 mM and 0.50 mM exhibited by the electrode is given as $i(\mu A) = 73.314C_{DLM} + 1.1459$ with a correlation coefficient (R^2) of 0.9847 and sensitivity of 4553.66 $\mu AmM^{-1}cm^{-2}$. Limit of quantification (LOQ) is 10 µM with an estimated limit of detection (LOD) by signal to noise ratio equals 3 (S/N = 3) of 0.04 µM. Performance of the sensor was found to compete favorably and supersede some previous published articles that involve tedious

immobilization techniques and very expensive materials for synthesis of different chemically modified electrode such as bimetallic nanoparticles, metallic doped ceramics electrode, multiple wall nanoparticles, reduced graphene, polymeric-metallic composites and different complicated electrode system for methionine detection in terms as LOD as enumerated in Table 4-4.

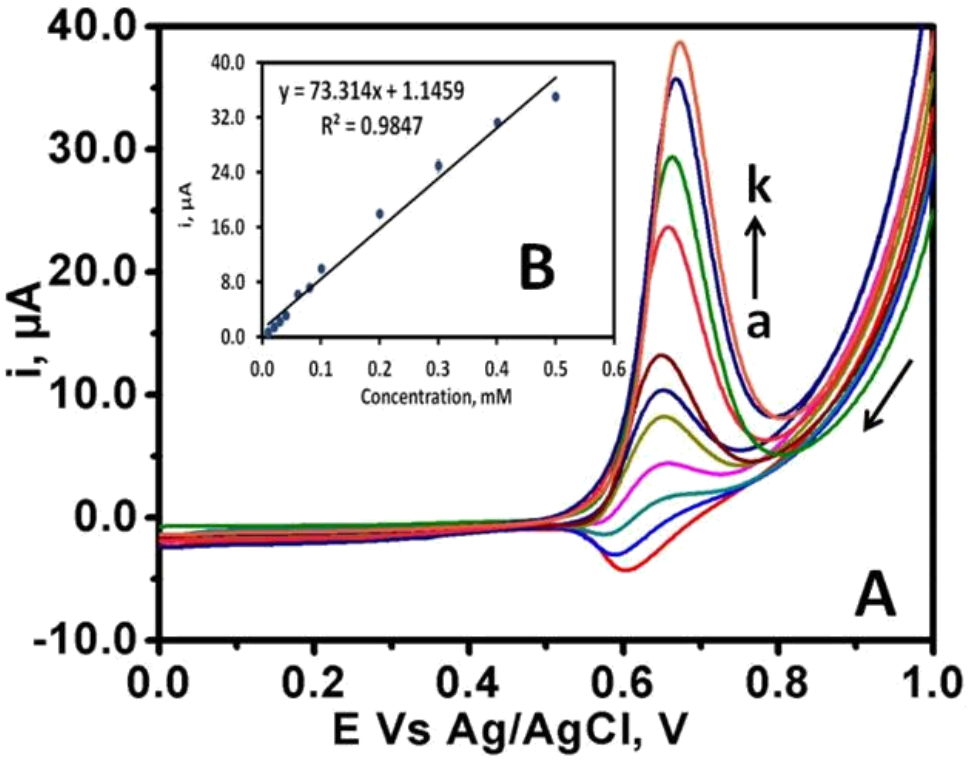

Figure 4-10: CSLSVs of different concentrations (mM) of DL-methionine in 0.10 M NaOH pH 13.70 ± 0.20 plus 3.00 ppm $AgNO_3$ (A) and corresponding calibration curve (B). (a) 0.00 (b) 0.01, (c) 0.02, (d) 0.04, (e) 0.06, (f) 0.08, (g) 0.10, (h) 0.20, (i) 0.30, (j) 0.40 and (k) 0.50.

Table 4-4: Performance Comparison of Different Modified Electrode with Bared Disposable Graphite Lead Pencil Electrode in the Presence of $AgNO_3$ for Methionine Determination.

Transducer	Medium	Technique	LOD (µM)	Linear Range (µM)	Ref.
Ru-Metden/CtCE	0.1 M PBS pH 7.0	Amperometry	0.60	1 - 10	[217]
CAu-Cystm/CPE	0.1 M PBS pH 7.0	DPV	0.56	1 - 100	[218]
Ni-P/CCE	0.1 M NaOH	Ch-Amp	2	2 - 90	[211]
Fullerene-C_{60}/AuE	0.1 M KNO_3	HDV	8.2	Up to 100	[219]
SPGME	0.1 M PBS pH 7.0	DPV	95	50 -5000	[220]
p-4α-Cu^{II}TAPc/GCE	0.2 M PBS pH 4.0	DPV	0.027	50 - 500	[156]
TiO_2-Pt/CNT/GCE	0.1 M PBS pH 7.0	Amperometry	0.1	0.5 - 100	[155]
MWCNT-NFMIP/DGLPE	0.1 M PBS pH 2.0	DPCSV	0.02	0.08 – 10	[154]
RGO-GCE	0.1 M PBS pH 5.5	DPV	100	450 - 4950	[153]
Ag-Au (BMNp)/GCE	0.1 M PBS pH 7.0	LSV & ch-Amp	30	50 - 500	[152]
Bare DGLPE	0.1 M $NaOH/AgNO_3$	CLSV& Amp	0.42	10 - 500	This work

Ru: Ruthenium (II); Metden: Metallodendrimer; CAu: Colloidal Gold; Cystm: Cysteamine; Ni-P/CCE: Nickel Powder Doped Carbon Ceramic Electrode; SPGME: Screen Printed Graphite Macroelectrode; p-4α-Cu^{II}TAPc: 1,8,15,22-tetraaminophthalocyanato-copper(II); NFMIP: Nano film molecular Imprinted; BMNp: Bimetallic Nanoparticle; CNT: Carbon Nanotube; MWCNT: Multiple wall Carbon Nanotube; RGO: reduced graphene CtCE: Conducting Composite Electrode; DGLPE: Renewable Graphite Lead Pencil Electrode; GCE: glassy Carbon Electrode; CLSV: Cathodic Linear Scan Voltammetry; DPV: Differential Pulse voltammetry; Ch-Amp: Chronoamperometry

4.3.6 Amperometric Response, Interference, Reproducibility and Stability Studies

Amperometric response of the developed sensor to successive addition of 20 µM DLM at 0.65 V for the different time interval is shown in Figure 4-11A. The sensitivity of the sensor to effective oxidation of DLM with very promising responses was observed for 9 consecutive addition of 20 µM for 100 s interval (Figure 4-11a). However, the ability of the transducer to respond to a higher range of concentrations was demonstrated for 19 consecutive addition of 20 µM DLM for 50 s interval (Figure 4-11Ab). This result shows that the developed technique can be utilized for both voltammetric and amperometric technique for the determination of DLM.

Interference studies of DLM with ascorbic acids (AA), L-alanine (Aln) and cysteine (Cyt) which are representative of essential vitamins and amino acids that can co-exist with DLM in human serum sample were investigated with amperometric technique at the same 0.65 V (Figure 4-11B). Addition of 100 µM DLM shows a very sharp response in the amperomogram at about 120 s, but no response can be observed for the consecutive spiking of 20 µM AA, An and Cyt respectively. However, a very good response indicating the selectivity of DLM can also be observed when another 100 µM was added at about 380 s. Interference compounds added for the second periods between 400s and 700 s show no amperometric response of the interference and further confirm the selectivity of the sensor to DLM detection. The magnitude of current in the amperomogram to demonstrate the selectivity of GPE to DLM as a result of series addition of DLM and interferences (AA, Aln and Cyt) were enumerated in Table 4-5. It can be observed between 30 s and 100s that the current is stable at about 1.13 µA in the

blank solution. However, a significant increase in the current value to about 4.30 µA was noticed when 100 µM was added at about 120 s. Consecutive additions of AA, Aln and Cyt at about 170 s, 220 s, and 320 s respectively to the mixture yield slight different in current value showing non selectivity to GPE. Similar trends were noticed as another series of DLM and interferences were added to confirm the selectivity of GPE to DLM. The ability of the sensor to be sensitive to DLM by its third response at about 700 s after additions of 2 series of interference compounds is proof of its stability in the presence of interferences.

Reproducibility of GPE for DLM oxidations in NaOH in the presence of $AgNO_3$ solution was demonstrated as shown in Figure 4- 12. The standard deviation of 1.42 and a relative standard deviation of 4.32% was obtained for seven consecutive measurements of the same concentration of DLM. Besides, long-term stability study of the sensor recorded continuously for 1800 s (30 minutes) for the response of 0.50 mM after a well established stable current of 0.10 M NaOH plus 17.66 µM $AgNO_3$ on GPE is presented as Figure 4-13. A stable current of the amperomogram can be observed for the 30 minutes of the study with less than 5 % reduction in peak current of 0.50 mM DLM.

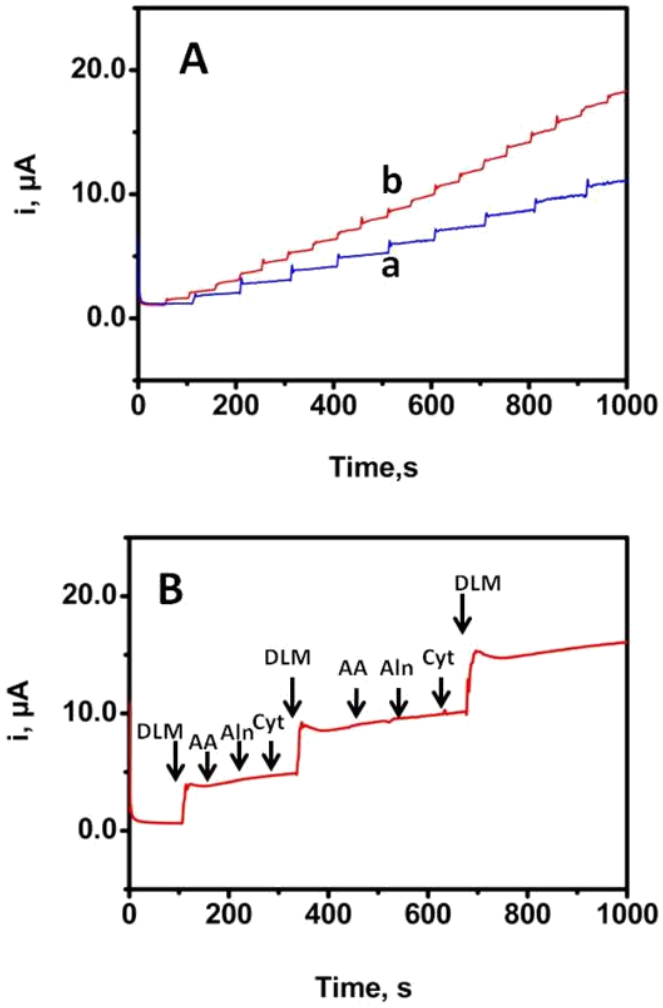

Figure 4-11: Amperometry studies at 0.65 V of DL-methionine in 0.10 M NaOH pH 13.70 ± 0.20 on DGLPE in the presence of 3.00 ppm $AgNO_3$ solution. (A) The response of subsequent additions of 20 µM DL-methionine for (a) 9 times addition for 100 s interval and (b) 19 times addition for 50 s interval. (B) Interferences studies of 20 µM AA, Alanine and Cysteine with 0.1 mM DL-methionine (1:5 molar concentrations).

Table 4-5: Selective Response of DL-methionine in the Presence of Series Concentration of Ascorbic acids (AA), L-alanine (Aln) and L-cysteine (Cyt)

Time (s)	Serial Addition of DLM and Interferences (µM)	Approximate Current (µA)	Remarks
30 - 100	Blank solution	1.13	Stable background
120	100 µM DLM	4.31	Significant response
170	20 µM AA	4.33	
220	20 µM Aln	4.70	
320	20 µM Cyt	4.90	
340	100 µM DLM	9.62	Significant response
460	20 µM AA	9.50	
520	20 µM Aln	9.77	
650	20 µM Cyt	10.30	
690	100 µM DLM	15.70	Significant response

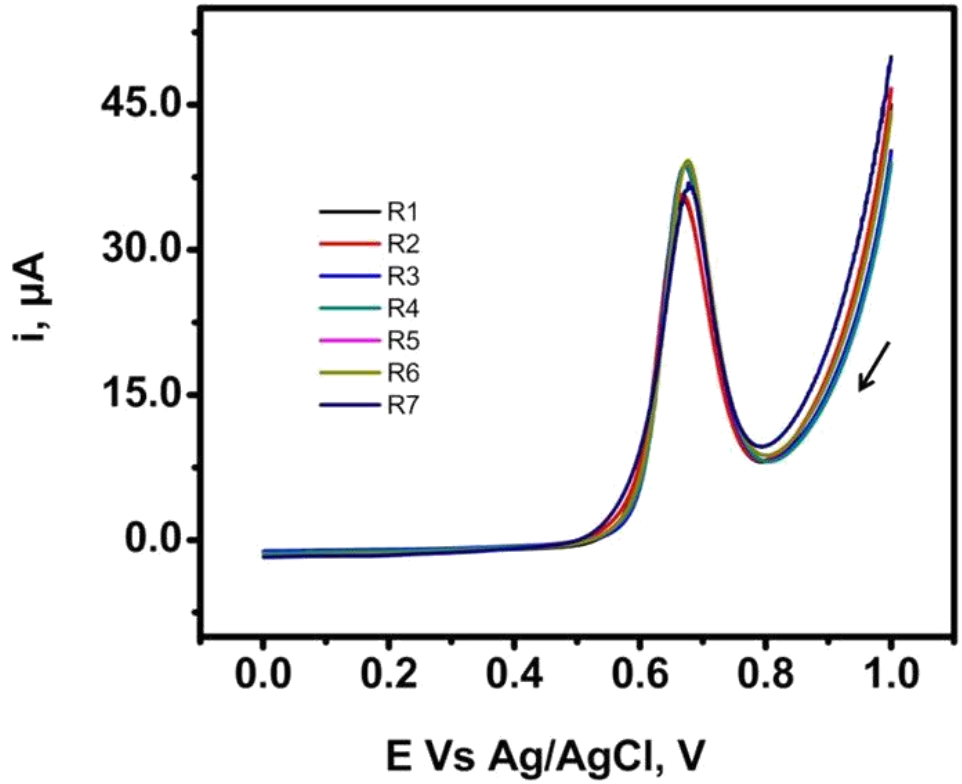

Figure 4-12: CSLSVs showing 7 repeated measurements of 0.04 mM DL-methionine in 0.10 M NaOH pH 13.70 ± 0.20 plus 17.66 µM $AgNO_3$.

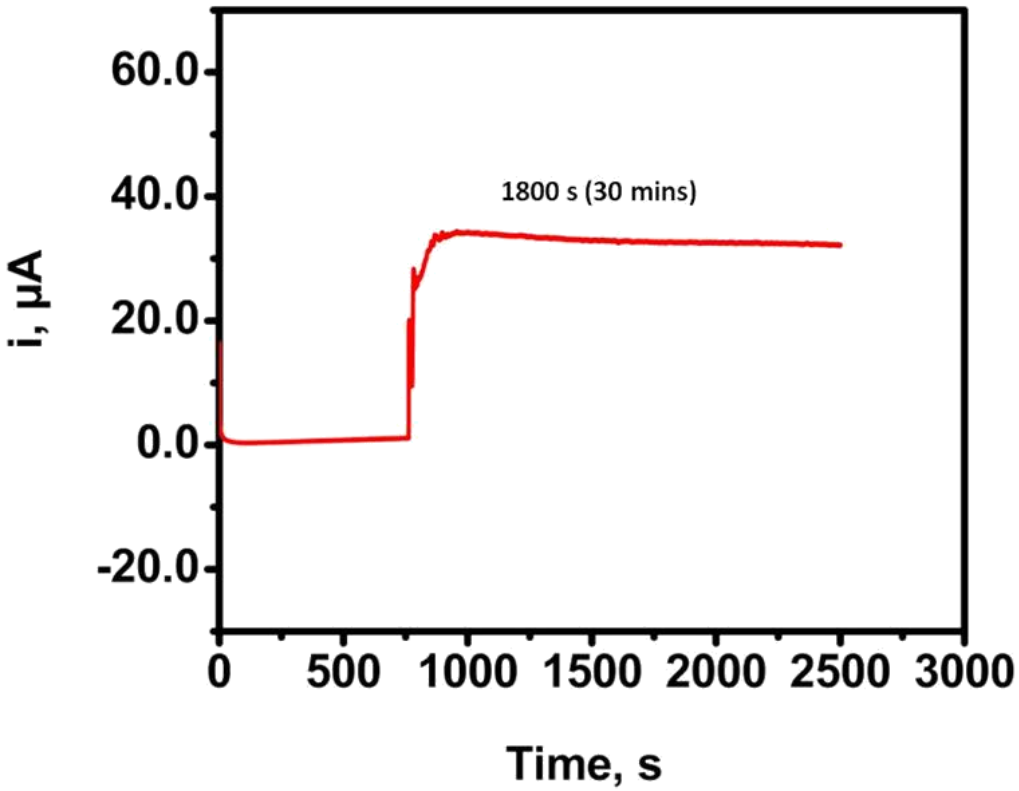

Figure 4-13: Amperogram recorded for 0.50 mM DL-methionine in 0.10 M NaOH pH 13.70 ± 0.20 plus 17.66 µM $AgNO_3$.

4.3.7 Application of the Developed Technique on Serum Sample

DLM was analyzed by standard addition method from a serum sample obtained from a healthy patient in King Fahd University Teaching Hospital. The sample was treated to make it a protein free, and 50 µL was a spike in the 0.1 M NaOH to make 100 times dilution of the serum. A good response of the serum on DGLPE can be observed in Figure 4-14Ab at about 0.65 V corresponding to the DLM signal in the serum sample when carefully compared with Figure 4- 14Aa representing the blank voltammogram. Successive addition of 0.05 mM DLM standard solution gives a remarkable response observed in Figure 4-14Ac to 4-14Ag for 0.05 – 0.25 mM of DLM whose analysis was enumerated in Table 4- 6. About 9.69 µM concentration of DLM was detected in the serum sample with a good recovery range between 98 – 109 %. This result indicates a high concentration of DLM in the serum sample of the patient and recommendation of MRD along with regular DLM evaluation to prevent the consequence of residue, and excess metabolism of DLM should be considered by the patient. Performance of the developed technique on the serum sample is an indication of its capability for real-life application.

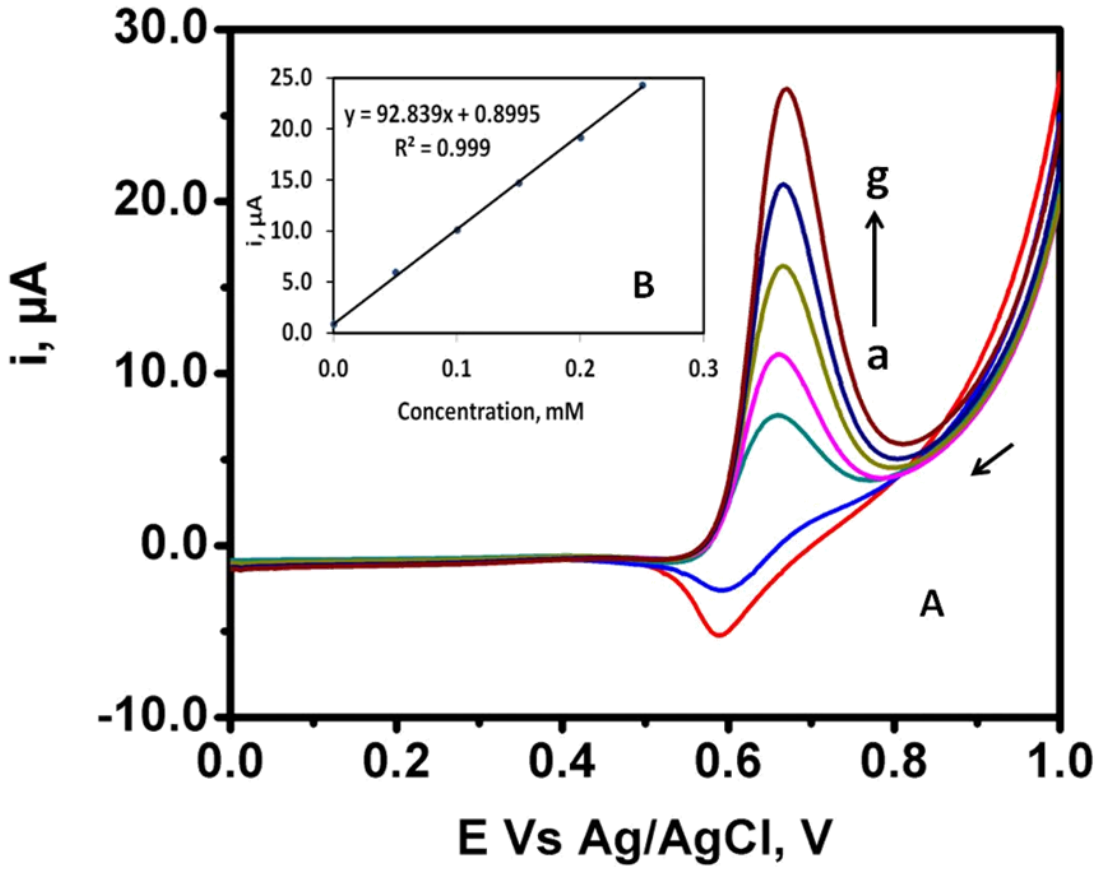

Figure 4-14: CSLSVs of standard addition of different concentrations (mM) of DL-methionine in 0.1 M NaOH pH 13.70 ± 0.20 plus 3 ppm $AgNO_3$ to serum sample (A) and corresponding calibration curve (B). (a) blank (b) 50 µL serum , (c) 0.05, (d) 0.10, (e) 0.15, (f) 0.20 and (g) 0.25.

Table 4-6: DL-Methionine Detection in Healthy Human Serum Sample

#	Spiked Amount (mM)	Amount Recovered (mM)	Amount Found (µM)	% Recovery
1	0.05	0.055	9.69	109.88
2	0.10	0.099	9.69	99.32
3	0.15	0.149	9.69	99.38
4	0.20	0.197	9.69	98.34
5	0.25	0.252	9.69	100.99

CHAPTER 5

Electrochemical Inspired Copper (II) Complex on Disposable Graphite Pencil Electrode for Effective Simultaneous Detections of Hypoxanthine, Xanthine, and Uric acid

5.1 Introduction

Efficiency of different forms of copper ions nanoparticle, composites, and complexes have been demonstrated for numerous industrial applications involving electrochemical reduction of CO_2 in fuels [221], methanol and ethanol oxidations [222-226], reductions of some important environmental pollutants [227, 228], oxygen [229, 230], hydrogen evolution reactions [231] and electrochemical sensing of peroxides [232-237]. However, practical applications of copper compounds are limited and unattractive due to non selectivity as a result of interferences of some redox peaks of copper ($Cu^{3+/2+}$, $Cu^{2+/1}$ and $Cu^{1+/0}$) with targeted compounds and or atoms [238-240] and challenges of immobilization of a stable copper complexes on solid electrode without electrochemical fouling on immobilized solid electrodes [241, 242]. Appreciable redox activity and stability of copper complex on the solid electrode can be achieved in basic medium, but the neutral medium is characterized prominently with fouling of solid electrode [243-246].

Many clinical disorders such as diabetes, high cholesterol, obesity, gout, kidney diseases, hypertension and heart disease have been attributed to the ratio of hypoxanthine (HXA) and Xanthine (XA) and abnormal level of Uric acid (UA) in the body as a result of altered purine metabolic reactions [129-132] which affect the normal physiological range of these purines degradation products. Development of an electroanalytical technique that can efficiently detect UA, XA, and HXA simultaneously in biological samples is a very important factor to be considered for proper monitoring of the human metabolic process. Several robust analytical methods have been reported for the simultaneous detections of

UA, XA, and HXA including electrophoresis [247], liquid chromatographic separation techniques regarded as high-performance chromatography [248] and several electrochemical techniques. In an attempt to overcome some challenges such as proximity of the oxidation potentials of HXA and XA on bare solid electrodes, lack of selectivity and sensitivity along with time consumption of some enzymes free electrochemical methods have been developed [249, 250]. Numerous organic and inorganic composite materials have been immobilized on bared electrodes. Mesoporous graphitized carbon on glassy carbon electrode (GCE) [251], poly-(bromo cresol blue) and poly-(L-methionine) on GCE [250, 252], Ultrathin in-laying carbon paste electrode (CPE) composite containing single-wall carbon nanotube (SWCNT) [249], pre-anodized screen print electrodes (SPE) of nontronite [253], film comprises of graphene and poly-(L-arginine), poly-pyro catechol violet and multiple wall carbon nanotube (MWCNT) composites [254, 255], tetracarboxylic acid and dopamine polymers [256], polymer based on purines [257], sulfonic acid functionalized nitrogen-doped graphene [258], cobalt doped cerium oxide (Co-CeO_2) on GCE [259] and electrochemically reduced graphene oxides (ERGO) [260] electrode for simultaneous determinations of UA, XA and HXA have been reported.

We are utilizing the efficacy of DGPE in electrochemical sensors applications [17, 182] to develop a simple, easy-to-use, cost-effective and sensitive electrochemical methods based on the electrochemical inspired copper complex on DGPE for simultaneous detections of UA, XA, and HXA.

5.2 Experimental

5.2.1 Chemicals

1000 ppm ± 4.0 Cu standard prepared in nitric HNO_3 standard solution AAS specification by Fluka were used as obtained. NaOH pellet, Uric acid, Xanthine, and Hypoxanthine were supplied by Sigma-Aldrich. 0.1 M phosphate buffer solution (PBS) pH 7.0 ± 0.2 as supporting electrolyte was prepared by mixing appropriate volumes of monosodium phosphate and disodium phosphate standard solutions prepared with double distilled water. All solutions were prepared with double distilled water obtained from Aquatron water still A4000D water purification system. Stock solutions of uric acid, Xanthine and Hypoxanthine were prepared by dissolving with 0.1 M NaOH solution before make up to with double distilled water in ratio 1: 4.

5.2.2 Electrochemical Cell and Procedure

A working electrode made of graphite pencil whose fabrications, descriptions along with its working principle have been widely reported [183]. A platinum wire and Ag\Agcl saturated KCl were connected with CHI potentiostat workstation (CHI1232A, CH Instruments Inc, Austin, TX, USA) as a counter and reference electrodes respectively for all electroanalytical measurements. Approximately 10 mm length of 0.5 mm diameter graphite lead corresponding to about 16.10 mm^2 surface area propelled out of the vertically positioned pencil through a Teflon hole to make a contact with the supporting

electrolyte. The electrical contact of the graphite lead was achieved by soldering copper wire with the metallic part of the pencil.

5.2.3 Surface Characterization of Disposable Graphite Pencil Electrode By Raman Spectroscopy

The surface of the DGPE that was electrochemically prepared by the accumulation of UA, XA, HXA and Cu in PBS pH 7.0 ± 0.2 without scanning were investigated with iHR320, HORIRA Raman spectrometer integrated with 300 mW green laser 532 nm laser wavelengths and CCD detector.

5.2.4 Computational Studies

Calculations were performed in the gaseous phase with the aid of GAUSSIAN 09 software package [261]. Density Function Theory (DFT) with hybrid function of 3 dimensional parameters of Lee, Yang and Parr (DFT-B_3LYP) with flexible triple-zeta valence polarized (TZVP) basic set was used to perform the calculation with the support High-performance Computing (HPC) facility in the Information Technology Centre (ITC), King Fahd University of Petroleum and Minerals (KFUPM), Saudi Arabia.

5.2.5 Real Samples Collections and Preparation

A urine sample was taken from a healthy person and filtered with a Millipore filter of 0.45 µm before use for analysis. However, serum sample collection was achieved with the assistant of Dammam University Teaching Hospital (King Fahd University, Hospital) blood bank section from a healthy patient. Serum sample stored in the refrigeration was defrosted, and 450 µL aliquot was taken and treated with methanol (900 µL) in ratio 1:2 to separate protein from the serum sample. Separation of the precipitated protein was achieved with a clear supernatant of the serum sample after centrifugation of mixture for 20 minutes at 2000 rpm and subsequently filtered with a Millipore filter of 0.45 µm.

5.3 Results and Discussion

5.3.1 Effect of $Cu(NO_3)_2$ on Uric Acid, Xanthine and Hypoxanthine Redox Reactions

In order to study the effect of Cu^{2+} (introduced as $Cu(NO_3)_2$) on 100 µM UA, 50 µM XA and 50 µM HXA, CV experiment were conducted in a potential window between 0.00 V and 1.50 V with 0.10 mV/s scan rate in the presence and absence of the 3 analytes (UA, XA and HXA) and $Cu(NO_3)_2$ as shown in Figure 5- 1 in 0.10 M PBS pH 7.00 ± 0.20. Figure 5- 1a represents CVs in the absence of both analytes and $Cu(NO_3)_2$ while Figure 5-1c represent in the presence of 2 mg/L $Cu(NO_3)_2$ without analytes. It is obvious that no oxidation peaks of any forms of Cu can be observed in Figure 5-1c. This observed

behavior may be as a result of either no redox reactions of Cu in the tested medium or the Cu present is below the detection limit of the transducer. Oxidation peaks of 100 µM UA, 50 µM XA and 50 µM HXA can be observed around 0.40 V, 0.80 V, and 1.10 V respectively on the anodic segment of the CV in Figure 5-1b with their corresponding low-intensity reversible peaks with potential slightly lower than their oxidized peaks in the cathodic segment of the CV showing reversible nature reaction nature of UA, XA and HXA. Enhance peaks of the same concentrations of UA, XA and HXA in Figure 5-1b were observed in Figure 5-1d due to the addition of 2 mg/L $Cu(NO_3)_2$ along with a slight shift toward positive potentials when compared with the corresponding oxidation potentials of UA, XA and HXA observed in Figure 5-1b. Interaction of $Cu(NO_3)_2$ with UA, XA and HXA might be responsible for the enhancement of peaks observed in Figure 5-1d.

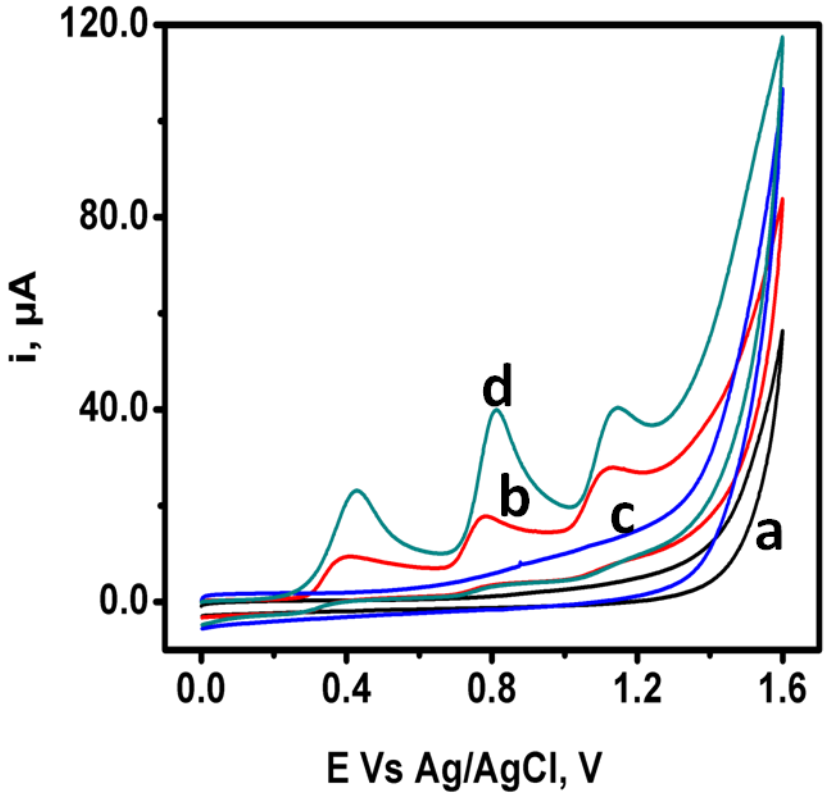

Figure 5-1: CVs of 100 µM UA, 50 µM XA and 50 µM HXA in 0.1 M Phosphate buffer solution (PBS) pH 7.00 ± 0.20. (a) Blank without $Cu(NO_3)_2$, (b) analytes without 2 mg/L $Cu(NO_3)_2$, (c) Blank with 2 mg/L $Cu(NO_3)_2$ and (d) analytes with 2 mg/L $Cu(NO_3)_2$.

5.3.2 Electrochemical Parameters and $Cu(NO_3)_2$ Concentration Optimization

Effect of concentration of $Cu(NO_3)_2$ (mg/L), accumulation potential (V) and accumulation time (s) were investigated with square wave voltammetry (SWV) techniques to utilized the reversed peaks observed in Figure 5-1 to generate a well defined peak differential oxidation peaks for UA, XA, and HXA. Square wave voltammograms (SWVs) showing oxidation peaks behaviors of 50 µM UA, 25 µM XA and 25 µM HXA to the addition of different concentration of $Cu(NO_3)_2$ is shown in Figure 5- 2A with 0.10 V accumulation potential for 30 s. Figure 5-2Aa show the SWVs in the absence of $Cu(NO_3)_2$ with about 0.35 V, 0.75 V and 1.15 V oxidation potentials for UA, XA, and HXA respectively. Enhanced peak currents were observed by addition of 0.50 mg/L (Figure 5- 2Ab) and 1.00 mg/L (Figure 5-2Ac) of $Cu(NO_3)_2$ in almost the same peak potentials observed in Figure 5-2Aa possibly due to the limited amount of $Cu(NO_3)_2$ in the medium. However, continuous slight positive shift in potentials due to the presence of an appreciable amount of $Cu(NO_3)_2$ concentration was observed in Figure 5-2Ad, 5-2Ae and 5-2Af for 3.00 mg/L, 4.00 mg/L and 5.00 mg/L concentration of $Cu(NO_3)_2$. Addition of 4.00 mg/L concentration $Cu(NO_3)_2$ to 50 µM UA, 25 µM XA and 25 µM HXA shows the maximum current peaks as illustrated in the inserted calibration curve in Figure 5-2A.

Accumulation potentials were studied with 4.00 mg/L of $Cu(NO_3)_2$ at the different potential for 30 s and presented as Figure 5-2B. Peak current was observed to be relatively low at 0.20 V (Figure 5-2Ba) but improved with lower potential of 0.10 V

(Figure 5-2Bb) suggesting a favorable condition for copper complex formation on GPE for better current peak enhancement. Further enhancements with a positive shift in potential were observed with negative potentials -0.10 V, -0.30V and -0.50 V presented as Figure 5-2Bc, 5-2Bd and 5-2Be respectively. The shift in peak towards a positive potential can be attributed to possible coordination of $Cu(NO_3)_2$ with phosphate ions of the PBS before diffusion to the electrode surface. Current peaks obtained for the 3 analytes at with -0.30 V potential was found to be superior to the current peaks obtained for -0.50 V and thereby assumed to be the best accumulation potential for the enhancement of the UA, XA and HXA peaks with $Cu(NO_3)_2$.

Moreover, contact time of the electrode with 4.00 mg/L $Cu(NO_3)_2$ at -0.30 V potential before electro-oxidation is a very important electrochemical parameter that needs to be explored for proper utilization of $Cu(NO_3)_2$ complex enhancement capability. Results obtained for the accumulation time investigation is presented as Figure 5-2C. Lower current peak is obvious as shown in Figure 5-2Ca for 15 s accumulation time before oxidation of the 3 analytes and relatively slightly low potentials than other longer accumulation time's investigation. This behavior might be suggesting a time-dependent property of the electrode for complexation of $Cu(NO_3)_2$ with the analyte for current peak enhancement. Increase in peak current of the 3 analytes was observed to increase as the accumulation time increases from 30 s – 120 s as shown in Figure 5-2Cb to 5-2Ce. A drastic reduction of current peaks of all the analyte was observed at 150 s accumulation presented as Figure 5-2Cf possibly due to saturation of the electrode surface with $Cu(NO_3)_2$ complexation.

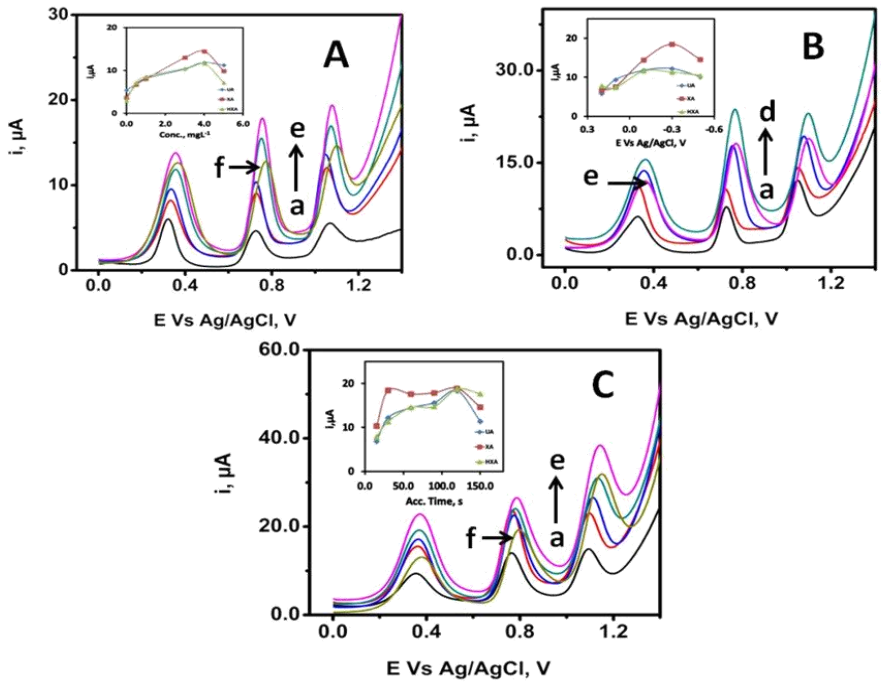

Figure 5-2: SWVs of 50 µM UA, 25 µM XA & 25 µM HXA in 0.1 M PBS pH 7.00 ± 0.2 (A) Effect of Concentration (mg/L) of $Cu(NO_3)_2$ with accumulation potential of -0.10 V for 30 s and its corresponding bar chart of the current peak. (a) 0.00, (b) 0.50, (c) 1.00, (d) 3.00, (e) 4.00 and (f) 5.00. (B) Effect of accumulation potential (V) for 30 s in the present 4 mg/L $Cu(NO_3)_2$ and its corresponding bar chart of the current peaks. (a) 0.20, (b) 0.10, (c) -0.10, (d) -0.30 and (e) -0.50 (C) Effect of accumulation time (s) at -0.30 V accumulation potential in the present 4 ppm $Cu(NO_3)_2$ and its corresponding bar chart of the current peak. (a) 15 (b) 30 (c) 60 (d) 90 (e) 120 and (f) 150.

5.3.3 Disposable Graphite Pencil Electrode Electrochemical Redox process

Electrochemical activities involved in the redox process of the electrode were studied with CV at different scan rate (V/s) as shown in Figure 5-3. Successive increase in the current peaks of the 3 analytes was observed in Figure 5-3A for 0.025 – 0.150 V/s scan rates. Voltammograms pattern presented by CV experiments in Figure 5-3A has been reported as the behavior of an electrode process that predominantly undergoes adsorption process rather than diffusion process whose adsorption phenomenon expression is express in equation 5.1 below and can be used to estimate the average surface coverage (Γ) of the electrode [262-264].

$$\boldsymbol{i_p = \frac{n^2 F^2 A \Gamma \upsilon}{4RT}} \qquad (\mathbf{5.1})$$

where n is the number of electron transfer, A (cm^2) is electrode area, υ is scan rate, and Γ (mol/cm^2) is the electroactive surface coverage concentration.

Equation 5.1 was utilized to estimate the electroactive surface coverage concentrations (Γ) of the 3 analytes on GPE after plotting peak current (i_p) against scan rate (υ) with linear equation along with R^2 values of $i_p(\mu A) = 141.07C_{UA} + 3.4078$ (R^2 = 0.9969), $i_p(\mu A) = 155.15C_{XA} + 12.3520$ (R^2 = 0.9891) and $i_p(\mu A) = 357.14C_{HXA} - 0.3352$ (R^2 = 0.9821) for UA, XA and HXA respectively. Average values of Γ for the all the investigated scan rates were found to be 2.29 x 10^{-12} mol/cm^2, 2.52 x 10^{-12} mol/cm^2 and

5.79×10^{-12} mol/cm^2 respectively for UA, XA and HXA and were observed to be in order of the magnitudes of peak current presented for the scan rate experiment in Figure 5-3A.

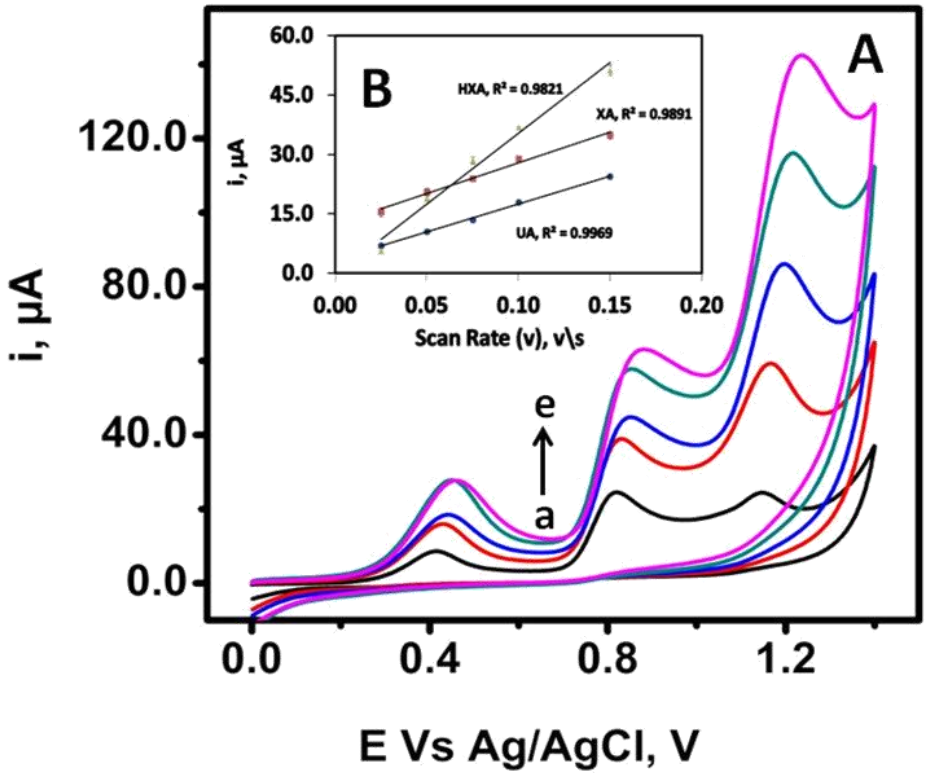

Figure 5-3: CVs (A) showing effect of scan rate (V/s) with 50 µm UA, 25 µM XA & 25µM HXA in the presence of 4 mg/L $Cu(NO_3)_2$ at -0.30 V accumulation Potential for 120s and its corresponding calibration curves (B). (a) 0.025 V/s, (b) 0.050 V/s , (c) 0.075 V/s , (d) 0.100 V/s and (e) 1.500 V/s.

5.3.4 Raman Spectroscopy Investigation

Raman spectra of DGPE after electrochemical accumulation at -0.30 V for 2 minutes without scanning in the presence and absence of $Cu(NO_3)_2$ and the 3 analytes in PBS pH 7.00 ± 0.20 were shown in Figure 5-4. Two important peaks attributed to the features of perfect stacked layered graphite which are the G-band of first order at about 1580 cm^{-1} and the 2D-band between 2600 cm^{-1} and 2700 cm^{-1} can be observed in Figure 5-4a representing a Raman spectrum of DGPE without any electrochemical reaction. A minimal disorder and defect of a graphitic layer of DGPE are consolidated with a very low intensity of the D-band peak observed at about 1350 cm^{-1}. The intensity of the D-band has been reported to be proportional to the extent of defect present in the graphite sample [265, 266]. Similar features for the G-band, 2D-band, and D-band in Figure 5-4a were observed in Figure 5-4b representing Raman spectra with the electrochemical process in PBS pH 7.00 ± 0.20 in the absence of the 3 analytes and $Cu(NO_3)_2$. This shows that electrochemical accumulation at 0.30 V for 2 minutes in PBS pH 7.00 does not affect the graphitic features of DGPE. Addition of $Cu(NO_3)_2$ to PBS shows complexation property of $Cu(NO_3)_2$ [267] with phosphate ions (PO_4^{3-}). A huge peak at about 1100 cm^{-1} was observed in Figure 5-4c corresponding that might likely be attributed to copper phosphate [$Cu_3(PO_4)_2$] complex which has been reported as a characteristic peak for different $Cu_3(PO_4)_2$ minerals [268]. A similar peak was observed in Figure 5-4d in the presence of UA, XA, and HXA without $Cu(NO_3)_2$ which can be explained as complexation of each of the analytes with PO_4^{3-} in PBS forming corresponding phosphoric compounds[269-271]. Spectra of Figure 5-4c and 5-4d are characterized by a

very high background that masked the 2D-band peaks of DGPE. This behavior indicates fluorescence property of phosphate compounds complexes formed on the surface of DGPE in the presence of $Cu(NO_3)_2$ and the 3 analytes respectively [272-276]. Although fluorescence in Raman spectroscopy is a challenge that has attracted several efforts such as the use of multiple wavelengths, statistical techniques and Surface Enhanced Raman Spectroscopy (SERS) for spectra peak enhancement [277-279] but are necessary to explain the characteristics of the electrochemical initiated complex on DGPE surface. Moreover, PO_4^{3-} peaks and the fluorescence property observed in Figure 5-4c and 5-4d are no longer present in Figure 5-4e when $Cu(NO_3)_2$, UA, XA, and HXA are all together in PBS. The disappearance of the PO_4^{3-} peak might be due to unfavorable or weaker interaction between PO_4^{3-} and $Cu(NO_3)_2$, UA, XA, and HXA than the interaction between $Cu(NO_3)_2$ and corresponding UA, XA, and HXA.

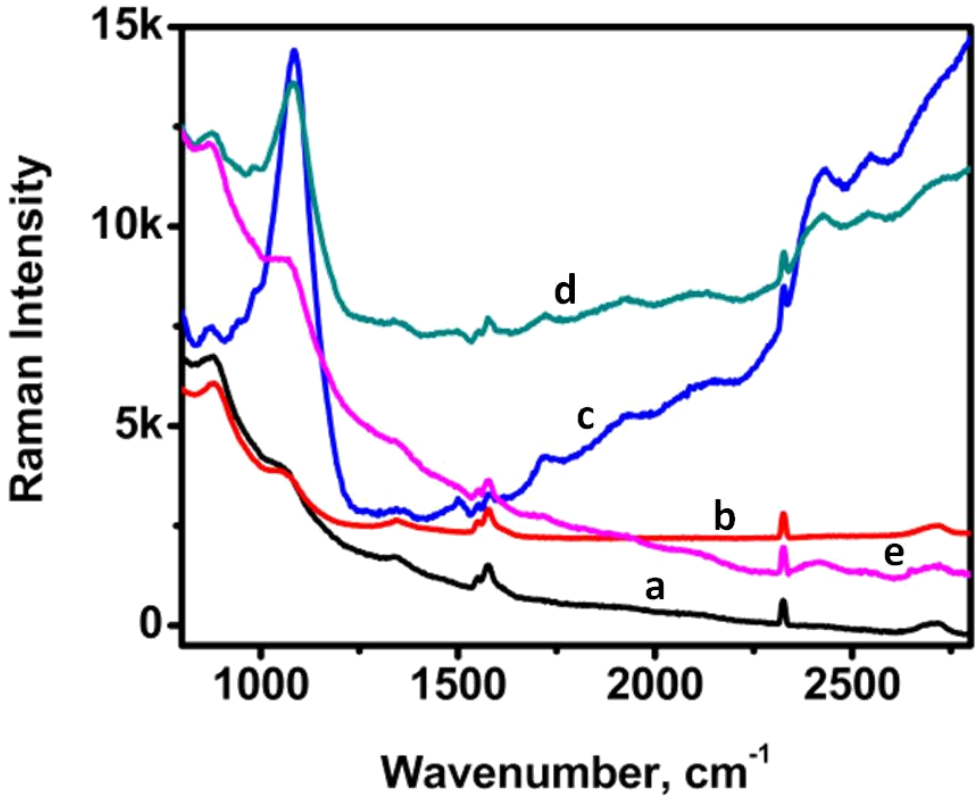

Figure 5-4: Raman Spectroscopy spectrum of Pentil graphite lead Pencil with electrochemical accumulation at -0.30V for 120 s without scanning. (a) GPE without any modification, (b) GPE in PBS pH 7.00 ± 0.20, (c) GPE with 4 mg/L $Cu(NO_3)_2$ in PBS pH 7.00 ± 0.20, (d) GPE with UA, XA & HXA (50 µM, 25 µM & 25 µM) in PBS pH 7.00 ± 0.20 and (e) GPE with 4 mg/L $Cu(NO_3)_2$ and the 3 analytes in PBS pH 7.00 ± 0.20.

5.3.5 Interaction Studies

Reasons for the disappearance of PO_4^{3-} peak need to be substantiated with interaction studies among all the concerned compounds involved in the complex formation on DGPE. Figure 5-5 shows optimized structures for the interaction of copper cluster (Cu), phosphate ion (PO_4^{3-}), UA, XA and HXA in the gaseous phase. Four copper atom cluster was utilized to investigate the interaction site of Cu by what was obtainable in experimental condition as a copper atom cannot exist alone in isolation [280]. Interaction site of PO_4^{3-} with Cu was found to be through the double bonded oxygen atom (Cu-O) with a bond length of about 2.14 Å (Figure 5-5a) and seems to be the strongest interaction of PO_4^{3-} when compared with other compounds which are simply hydrogen bonds (O-H) interactions as shown in Figure 5-5b, 5-5c and 5-5d for UA, XA and HXA respectively. The double site of O-H interaction was observed with UA with 1.96 Å and 1.67 Å bond lengths indicating a better interaction of PO_4^{3-} with UA than XA and HXA with single hydrogen bond interactions of 1.64 Å and 1.67 Å respectively. Cu was found to preferably interact with the nitrogen atom (Cu-N) as shown in Figure 5-5e, 5-5f and 5-5g for UA, XA, and HXA respectively with similar bond lengths. Additional interaction site was observed for UA involving Cu and oxygen atom (Cu-O). However, type of interactions and bond lengths are not enough to justify the disappearance of PO_4^{3-} peak in Raman in Figure 5-4e when competitions for complexation are expected among PO_4^{3-}, Cu and the 3 analytes. Binding free energy (ΔG^{θ}) of the interactions will be estimated between the free and binding ligands to determine the feasibility of their interaction as shown in equation 5.2.

Binding free energy (ΔG^{θ}) of the interaction elucidated in Table 5-1 for Cu interaction with UA, XA, HXA are -34.1241 Kcal/mol, -13.5239 Kcal/mol and -12.9943 Kcal/mol respectively. Feasibility of these complex reactions is far greater than complexation reaction of PO_4^{3-} with Cu, UA, XA and HXA which are calculated to be -0.1061 Kcal/mol, -7.2012 Kcal/mol, -8.4738 Kcal/mol and -1.9346 Kcal/mol. Summary of the interactions of $Cu(NO_3)_2$- complexes, Raman spectra and their effects on the current peaks of UA, XA and HXA is shown in Figure 5-6.

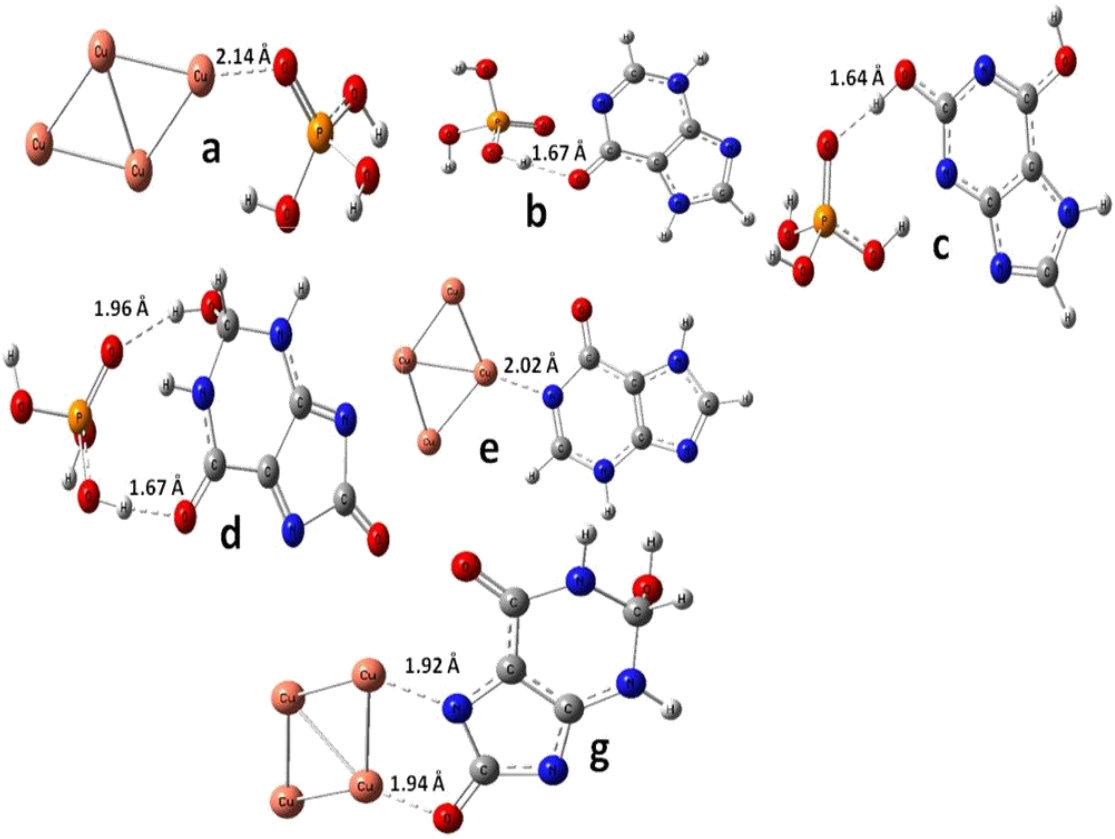

Figure 5-5: Optimized structures for the interaction studies by frequency of copper cluster (Cu), phosphate ion (PO_4^{3-}), UA, XA and HXA in gaseous phase using by DFT method for (a) Cu- PO_4^{3-}, (b) UA- PO_4^{3-}, (c) XA- PO_4^{3-}, (d) HXA- PO_4^{3-} , (e) Cu-HXA, (f) Cu-XA and (g) Cu-UA.

Table 5-1: Free Binding Energy (ΔG^{θ}) of Cu-complexes Interactions Studies Estimated from Frequency calculation By DFT Method

Complexes	**Free Binding Energy (ΔG^{θ}) (Kcal/mol)**
Copper Cluster - Phosphate ion **(Cu - PO_4^{3-})**	-0.1061
Uric acid - Phosphate ion **(UA - PO_4^{3-})**	-7.2012
Xanthine - Phosphate ion **(XA - PO_4^{3-})**	-8.4738
Hypoxanthine - Phosphate ion **(HXA - PO_4^{3-})**	-1.9346
Copper Cluster – Hypoxanthine **(Cu – HXA)**	-12.9943
Copper Cluster –Xanthine **(Cu – XA)**	-13.5239
Copper Cluster – Uric acid **(Cu – UA)**	-34.1241

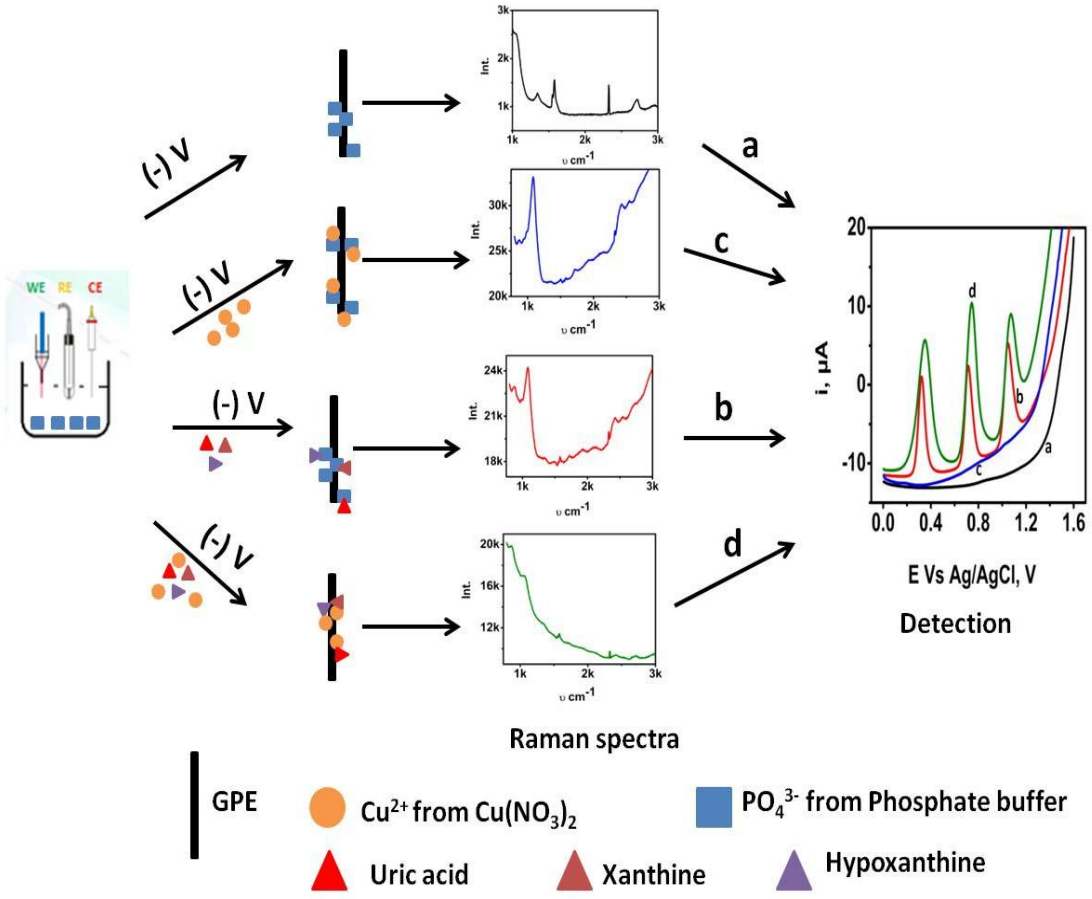

Figure 5-6: Summary of the interactions of $Cu(NO_3)_2$ - complexes, Raman spectra and their effects on the current peaks of UA, XA, and HXA.

5.3.6 Disposable Graphite Pencil Electrode Performance for Simultaneous Detection of Uric Acid, Xanthine, and Hypoxanthine

Evaluation of $Cu(NO_3)_2$ complexes of UA, XA, and HXA electrochemically prepared at applied -0.30V for 120 s with 4 mg/L $Cu(NO_3)_2$ on DGPE for simultaneous determination of UA, XA, and HXA in PBS pH 7.00 ± 0.2 is shown in Figure 5-7. Voltammograms showing linear proportionality of successive increase in the concentration of UA, XA and HXA mixtures and their corresponding current peaks are shown in Figure 5-7A. Calibration curves are shown in Figure 5-7A, 5-7B and 5-7C are representing linear correlations between current peaks and concentrations of UA, XA, and HXA respectively. Two linear range of 1 - 40 µM and 100 – 300 µM were observed for XA with correlations of $i_p(\mu A) = 0.6659C_{XA} + 2.7479$ (R^2 = 0.9907) and $i_p(\mu A) = 0.1422C_{XA} + 16.8280$ (R^2 = 0.9962) respectively while a single wide linear range of 2 - 80 µM for UA and 0.1 - 10 µM for HXA were achievable with correlations of $i_p(\mu A) = 0.168C_{UA} + 5.5472$ (R^2 = 0.9925) and $i_p(\mu A) = 1.4258C_{HXA} + 2.7451$ (R^2 = 0.9902) respectively. Limit of detection (LOD) estimated by signal to noise ratio (S/N = 3) are 0.0144, 0.0050 and 0.0049 µM for UA, XA and HXA respectively. A lot of improvement in term of performance of the developed method despite its cost effectiveness, fast, ease-to-use and in-situ simple electrochemical immobilization approach made it a suitable candidate for simultaneous detection of UA, XA and HXA when compared with other method elucidated in Table 5-2.

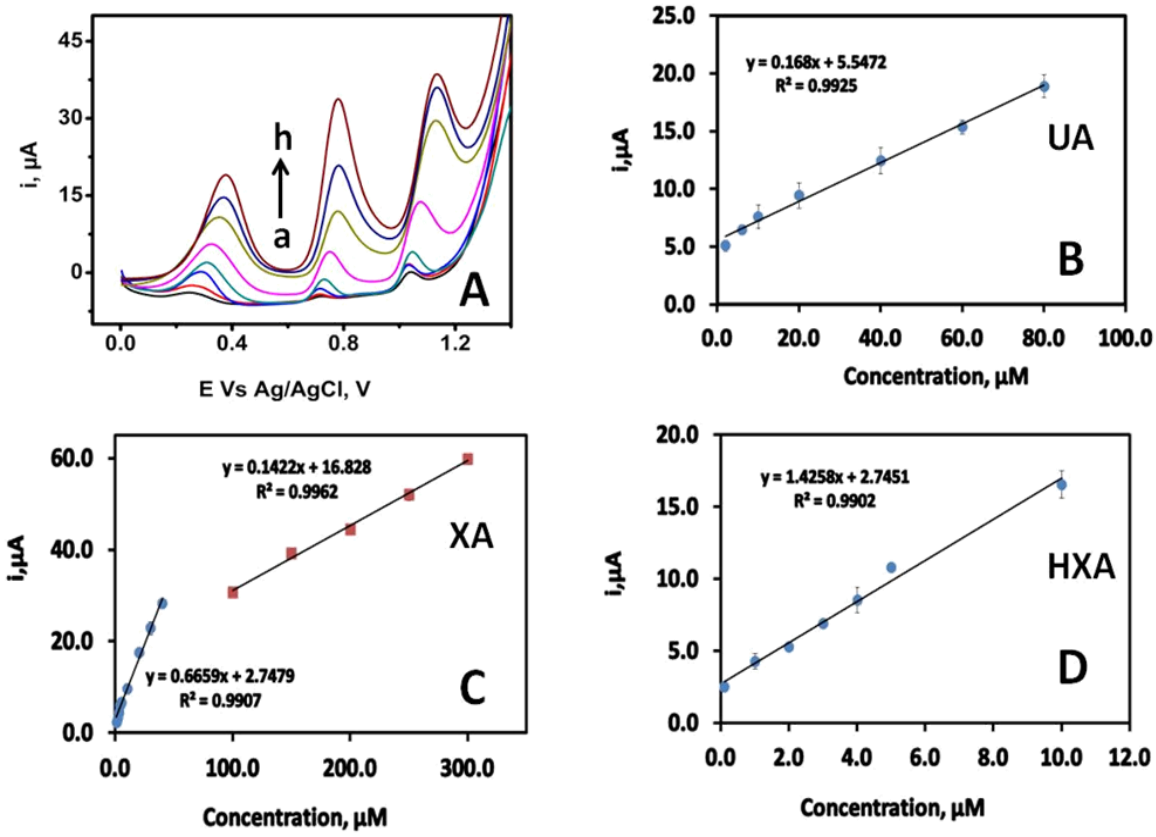

Figure 5-7: (A) SWVs are showing linear proportionality of successive increase in the concentration of UA, XA and HXA mixtures and their corresponding current peaks. a (0.2 µm UA, 0.1 µM XA & 0.1µM HXA); b (0.4 µm UA, 0.2 µM XA & 0.2µM HXA); c (2 µm UA, 1 µM XA &1µM HXA); d (6 µm UA, 3 µM XA & 3µM HXA); e (10 µm UA, 5 µM XA & 5µM HXA); f (20 µm UA, 10 µM XA & 10µM HXA); g (40 µm UA, 20 µM XA & 20µM HXA); and h (80 µm UA, 40 µM XA & 40 µM HXA). B, C, and D is linear correlations between current peaks and concentrations of UA, XA and HXA respectively.

Table 5-2: Comparison of the Developed Method with Electrochemical Methods for Simultaneous Detections of UA, XA, and HXA

Electrode	Medium	Linear range (µM)			Detection limit (µM)			Ref.
		UA	XA	HXA	UA	XA	HXA	
DGPE[1]	4 mg/L Cu in PBS pH 7.00	2 - 80	1–40, 100-300	0.1 - 10	0.014	0.005	0.005	This work
Co-CeO_2 np/GCE[2]	PBS pH 5.00	1-2200	0.1-1000	1-600	0.12	0.096	0.36	[259]
ERGO/HAD/GCE[3]	Physiological pH	5-1000	5-300	5-300	0.08	0.1	0.32	[260]
PCV/MWTs-COOH/GCE[4]	PBS pH 6.60	0.3-80	0.1-100	0.5-90	0.16	0.05	0.2	[255]
PYTS-NG/GCE[5]	PBS pH 7.90	9-1000	8-800	8-200	0.33	0.083	0.23	[258]
P6-TG/GCE[6]	PBS pH 7.00	2-1600	2-800	1-500	0.06	0.3	0.1	[257]
BCP/GCE[7]	PBS pH 6.50	0.5-120	0.1-100	0.2-80	0.2	0.06	0.12	[252]
PTCA/PDAox/GCE[8]	PBS pH 3.00	1.8-238	5.2-289	3.8-293	0.6	1.7	1.3	[256]
P-(L-arg)/ERGO/GCE[9]	PBS pH 6.50	0.1-10	0.1-10	0.2-20	0.05	0.05	0.1	[254]
NTSPE[10]	PBS pH 7.50	2-40	2-40	4-30	0.42	0.07	0.34	[253]

[1] Disposable graphite pencil electrode, **[2] Cobalt-doped cerium oxide nanoparticle**

[3] Electrochemical reduced graphene/hexadiamine **[4] Poly-(pyrocatechol violet)/functionalized multi-walled carbon nanotube**

[5] Nitrogen-doped graphene functionalized with sulfonic group **[6] Purine based polymer**

[7] Poly-(bromocresol purple) **[8] 3,4,9,10-perylene tetracarboxylic acid composite**

[9] Poly-(L-arginine)/graphene composite **[10] Nontronite coated screen-printed electrode**

GCE – Glassy carbon electrode

5.3.7 Reproducibility and Interference Studies

The response of the mixture of 100 µM of UA, 50 µM of XA and 50 µM of HXA were recorded for 6 (n = 6) consecutive measurements on fresh $Cu(NO_3)_2$ complex DGPE surface to determine the reproducibility of the developed method Figure 5-8. Standard deviations of 0.22, 0.28 and 0.47 along with relative standard deviations (RSD) of 1.50 %, 1.59 %, and 3.10 % were obtained for UA, XA and HXA respectively. Interferences studies with potential interferences were also evaluated with iron (Fe), zinc (Zn), methionine, alanine and glucose showing less than 5 % variation in the current peaks of the mixture of UA, XA, and HXA in the present and absence of the interference compounds (Figure 5-9).

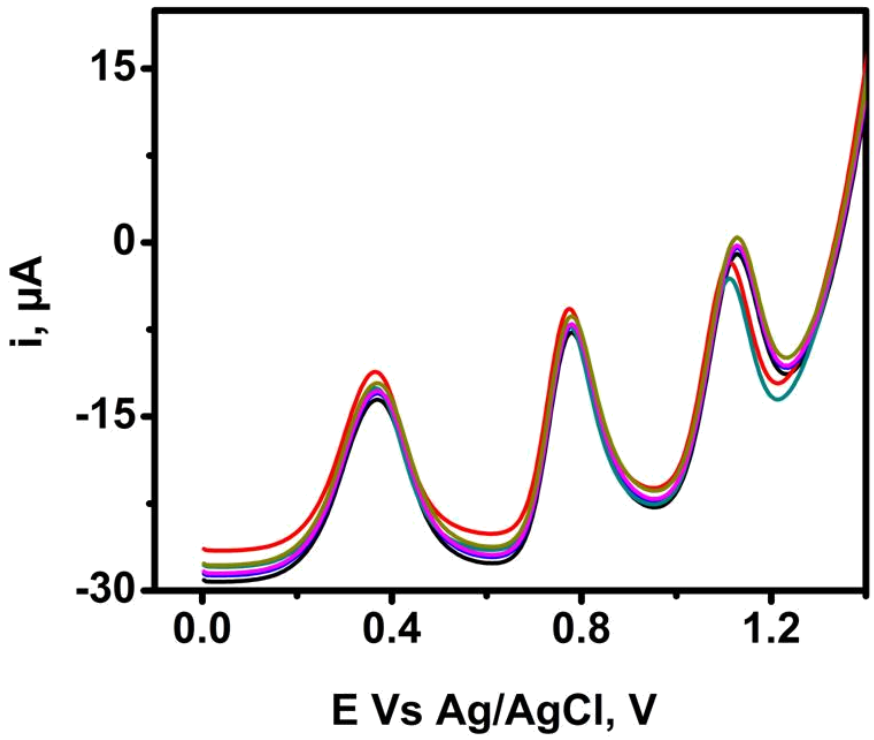

Figure 5-8: SWVs showing 6 repeated scanning in the same mixture of 100 µM UA, 50 µM XA & 50µM HXA on the $Cu(NO_3)_2$- complex DGPE surface DGPE.

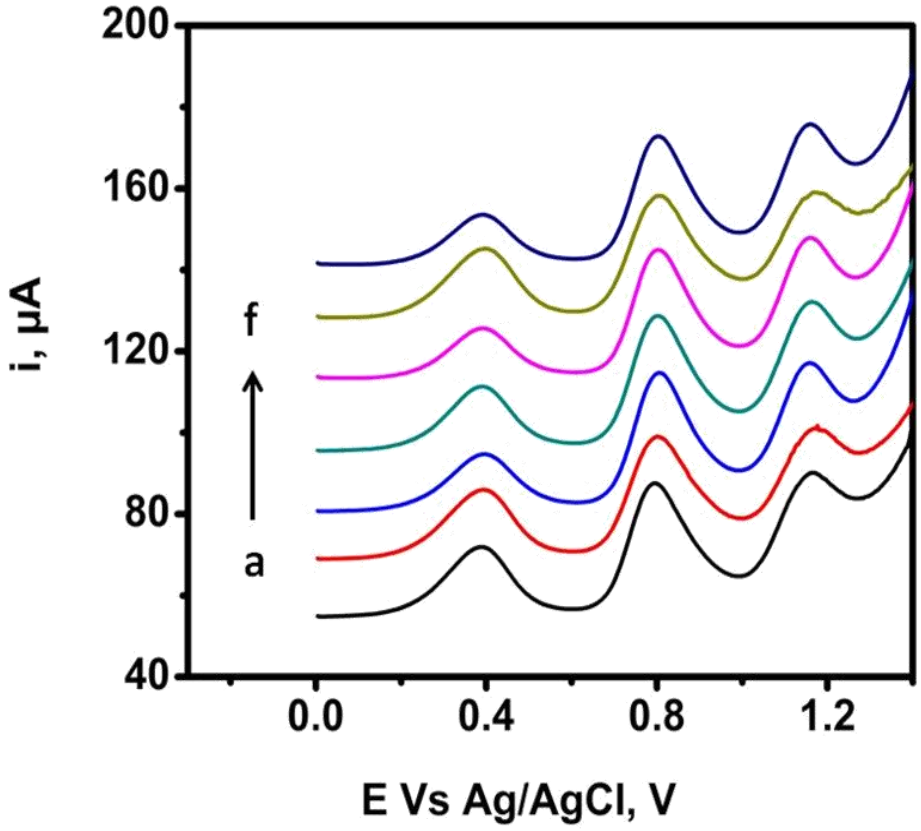

Figure 5-9: SWVs showing effect of interferences on the mixture of 100 µM UA, 50 µM XA & 50µM HXA on the Cu(NO3)2-complex DGPE surface in (a) absence of interference and in the presence of (b) 20 µM methionine, (c) 20 µM glucose, (d) 20 µM alanine, (e) 1 mg/L Fe and (f) 1 mg/L Zn.

5.3.8 Detection of Uric Acid, Xanthine, and Hypoxanthine in Serum and Urine Samples

Standard addition method was used to determine concentrations of UA, XA and HXA in human serum and urine for real sample analysis. Voltammograms showing 200 times dilution of serum sample and 400 times dilution urine sample are shown as Figure 5-10Ab and 5-10Bb respectively. Peaks corresponding to UA, XA, and HXA in both samples can be observed around 0.30 V, 0.70 V, and 1.10 V respectively. Mixtures containing a different concentration of UA, XA and HXA were spiked, and the result obtained for both samples are tabulated in Table 5-3 with an impressive percentage recoveries between 96.58 % and 108 %. So, the developed electrochemical method could be effectively used to determine UA, XA, and HXA in biological samples.

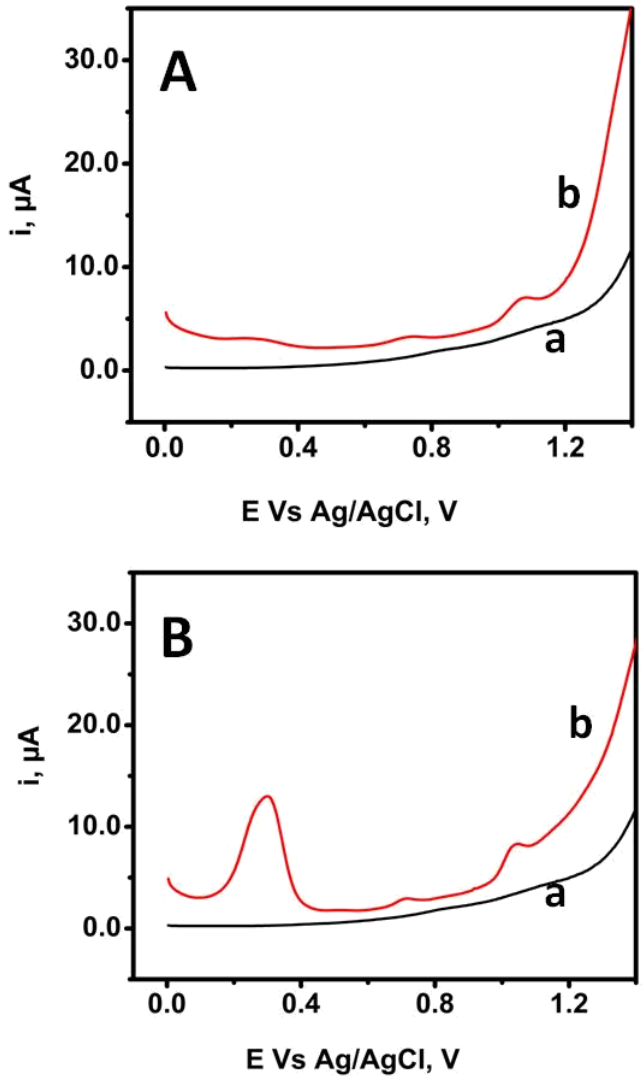

Figure 5-10: Response UA, XA and HXA in human serum (A) and urine (B) on the developed electrochemical method. (a) PBS pH 7.00 ± 0.20 and (b) 20 µL serum and 10 µL urine in 5.00 mL solution for A and B respectively.

Table 5-3: Application of the Developed Method on Human serum and urine sample

Sample	UA added (µM)	UA Found (µM)	% UA Rec.	XA added (µM)	XA Found (µM)	% XA Rec.	HXA added (µM)	HXA Found (µM)	% HXA Rec.
	1.00	1.08	108.00	3.00	3.15	105.11	1.00	1.03	103.08
Serum	2.00	2.19	109.99	10.00	9.84	98.35	3.00	3.17	105.99
	3.00	9.95	99.52	20.00	20.00	100.00	10.00	9.94	99.43
	1.00	1.09	108.81	2.00	1.97	98.84	1.00	1.05	104.58
Urine	2.00	2.11	105.49	10.00	10.83	108.30	2.00	1.99	99.92
	3.00	2.89	96.58	20.00	19.54	97.64	3.00	2.99	99.53

***Rec. - Recovery**

CHAPTER 6

Effect of Supporting Electrolyte on Simultaneous Determinations of Ascorbic acid, Uric acid, Xanthine and Hypoxanthine on Bare Graphite Pencil Electrode

6.1 Introduction

Ascorbic acid (AA) is an essential food additive that provides much-needed micronutrient in diets [281]. It is commonly prescribed as a drug or in its natural form (Vitamin C) for the prevention and treatment of many common illness such as catarrh, infertility, scurvy (swollen gum, shortness of breath, joint pain), liverwort, cancer, AIDS and so on due to its tremendous and important characteristic of being a water-soluble antioxidant, strong electron donating molecule [282]. AA is an activator of defense mechanism in many biological processes involving gene expression, cell division, physiological functions like scavenger for neuron protections and many metabolic processes [283, 284]. Importance of AA as a possible marker for oxidative stress in human has been emphasized through a study pointing out that oxidative stress is as result of an imbalance between reactive oxygen species involving AA, UA and other co-existing molecules [11, 285]. Determination of AA along with other molecules such as UA, XA and HXA is very important for the proper diagnosis of gout, kidney, heart and many other clinical ailments.

The possibility of the overlapping signal of UA and AA on carbon and metallic solid based electrodes due to the proximity of electro-oxidation potentials, low sensitivity and foul up effect in voltammetry techniques is a major challenge for simultaneous detections of both compounds in biological samples [286]. Numerous complicated electrode systems have been designed to overcome these challenges. A sensor made from titanium nitride compound on GCE (CL-TiN-GCE) [287], inter-digital gold microelectrode composite of graphene, nucleotide and platinum (Pt) nanoparticle (PtNP-Gr-FMN) [288]

and poly (glyoxal hydroxyanil) on GCE [289] for simultaneous determination of AA and UA. Many complicated electrode systems of Au, Zn, Pt, Pd, Rh. Ir, Ni NPs, polymers, and graphene oxides have been reported for simultaneous determination of UA, AA and dopamine (DA) [290-296], a nanocomposite of tin oxides electrodes for simultaneous detection of UA and AA along with folic acid and epinephrine injection [297, 298].

However, mesoporous graphitized carbon on glassy carbon electrode (GCE) [251], poly-(bromo cresol blue) and poly-(L-methionine) on GCE [250, 252], Ultrathin in-laying carbon paste electrode (CPE) composite containing single-wall carbon nanotube (SWCNT) [249], pre-anodized screen print electrodes (SPE) of nontronite [253], film comprises of graphene and poly-(L-arginine), poly-pyro catechol violet and multiple wall carbon nanotube (MWCNT) composites [254, 255], tetra carboxylic acid and dopamine polymers [256], polymer based on purines [257], sulfonic acid functionalized nitrogen-doped graphene [258] and electrochemically reduced graphene oxides (ERGO) [260] have also been reported for simultaneous determinations of UA, XA and HXA and AA, DA, UA, XA, HXA in urine and serum samples[299].

Slight variation in the composition of graphite pencils leads (HB, 2B, 4B, 2H, and 4H) as revealed by the silica-alumina ratio (Si/Al) from X-ray photoelectron spectroscopy (XPS) analysis and Raman spectroscopy [300] have been reported. BGPE is a material that combines both non-metallic and metallic properties, comprise approximately 30 % clay and 65 % wax balanced with polymeric wax [301, 302]. Despite the challenges of bared solid electrode for electrochemical method determinations of AA, UA, XA and HXA, we are utilizing the efficacy of disposable BGPE in electrochemical sensors

applications [17, 182] to develop a simple, cost-effective, facile and efficient electrochemical method for simultaneous determination of AA, UA, XA and HXA.

6.2 Experimental

6.2.1 Chemicals

NaOH pellet, Xanthine, Uric acid, Ascorbic acid, and Hypoxanthine were used as supplied by Sigma-Aldrich. Different pH of 0.10 M phosphate buffer solutions was prepared by mixing the required proportions of mono and di sodium phosphate standard solutions. All stock solutions were prepared with double distilled water obtained from Aquatron water still A4000D water purification system except Xanthine, Uric acid, and Hypoxanthine that were initially dissolved with 0.10 M NaOH and later makeup to a standard solution with double distilled water.

6.2.2 Electrochemical cell and Procedure

A working electrode made of graphite pencil whose fabrications, descriptions along with its working principle have been widely reported [183]. A platinum wire and Ag\Agcl saturated KCl were connected with CHI potentiostat workstation (CHI1232A, CH Instruments Inc, Austin, TX, USA) as a counter and reference electrodes respectively for all electroanalytical measurements. Approximately 10 mm length of 0.5 mm diameter

graphite lead corresponding to about 16.10 mm^2 surface area propelled out of the vertically positioned pencil through a Teflon hole to make contact with the supporting electrolyte. The electrical contact of the graphite lead was achieved by soldering copper wire with the metallic part of the pencil.

6.2.3 Bulk Graphite Pencil Sample Characterization

A bulk sample of BGPE was prepared by grinding about 8 pieces of graphite HB pencil lead with pestle and mortal and used directly without any modification. Raman spectrum was obtained with iHR320, HORIRA Raman spectrometer CCD detector integrated with 300 mW green laser 532 nm laser wavelengths. Crystalline and graphitic phases in its XRD pattern were identified with XRD Miniflex, CuKα radiation (λ = 1.5406 Å), equipped with Rigaku PDXL software in the 2θ range of 5° to 60°. Textural properties were investigated with N_2 adsorption-desorption instrument at −196 °C by micromeritics ASAP 2020. Adsorption part was utilized to calculate the surface area by Brunauer, Emmet, and Teller (BET) method, and the pore size distribution and pore volume by Barret, Joyner and Halenda (BJH) method.

6.2.4 Real Sample Collection and Preparation

A urine sample was taken from a healthy person and filtered with a Millipore filter of 0.45 µm before use for analysis. However, serum sample collection was achieved with the assistant of Dammam University Teaching Hospital (King Fahd University, Hospital)

blood bank section from a healthy patient. Serum sample stored in the refrigeration was defrosted, and 450 µL aliquot was taken and treated with methanol (900 µL) in ratio 1:2 to separate protein from the serum sample. Separation of the precipitated protein was achieved with a clear supernatant of the serum sample after centrifugation of mixture for 20 minutes at 2000 rpm and subsequently filtered with a Millipore filter of 0.45 µm.

6.3 Results and Discussion

6.3.1 Redox Process Ascorbic Acid and Uric Acid on Glassy Carbon Electrode and Graphite Pencil Electrode

CVs showing comparison redox process of Ascorbic Acid (AA) and UA on bare glassy carbon electrode (BGCE) and bare graphite pencil electrode (BGPE) are shown in Figure 6-1 PBS pH 7.00 ± 0.20. CVs of 500 µM of AA on BGCE (Figure 6-1Aa) and BGPE (Figure 6-1Ab) and CVs of 500 µM of UA on BGCE (Figure 6-1Ba) and BGPE (Figure 6-1Bb) are compared. It can be observed that BGPE is more sensitive to AA and UA as revealed in Figure 6-1A and 6-1B. There are several advantages of BGPE over BGCE that can be responsible for its superior sensitivity. Its electroactive surface area is adjustable depending on the volume of the testing solution while that of GCE is fixed no matter the volume of testing solution. Other advantages as reported include availability of lead pencil, lower cost, lower background noise, good reproducibility, time-consuming cleaning procedures between electrochemical measurements and analysis of low concentration sample without pre-concentration or deposition steps [301]. CVs of the

mixture of 500 µM AA and 500 µM UA is shown in Figure 6-1C. Resolution of oxidation peaks of AA and UA can be observed on BGCE (Figure 6-1Ca) while complete overlapping of AA and UA oxidation peaks were observed on BGPE (Figure 6-1Cb). BGCE is characterized by low sensitivity and good peak resolution while BGPE posses higher sensitivity with no peak resolution for AA and UA. A clearer picture of Figure 6-1Cb is shown in Figure 6-1D for the comparison of 500 µM AA (Figure 6-1Da), 500 µM UA (Figure 6- 1Db) and a mixture of 500 µM AA and 500 µM UA (Figure 6-1Dc) on BGPE. Proffering solution to the challenge of the complete overlapping signal observed in Figure 6-1Dc will be a good step towards achieving sensitive and selective simultaneous determination of AA and UA, XA and HXA on BGPE.

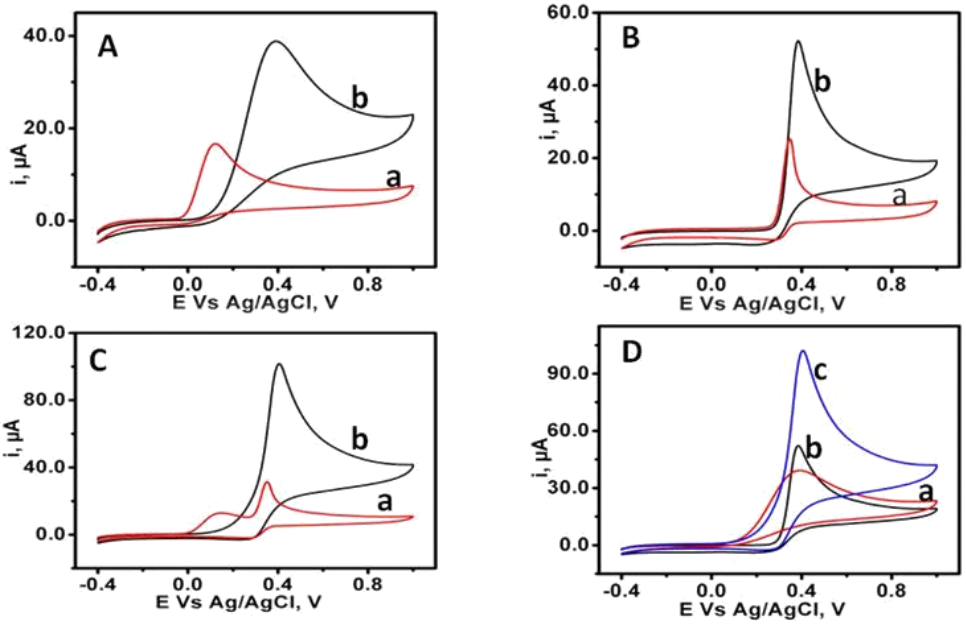

Figure 6-1: CVs showing oxidation peak behavior of AA and UA on BGCE and BGPE in 0.1 M Phosphate buffer solution (PBS) pH 7.00 ± 0.2. (A) 0.50 mM of AA (a) BGCE and (b) BGPE. (B) 0.50 mM of UA (a) BGCE and (b) BGPE. (C) 0.50 mM UA & 0.50 mM AA (a) BGCE and (b) BGPE and (D) BGPE (a) 0.50 mM AA, (b) 0.50 mM UA and (c) 0.50 mM UA & 0.50 mM AA.

6.3.2 Characterization of Bulk Graphite Pencil

X-ray diffraction (XRD) pattern for the bulk powdered sample of BGPE is presented as Figure 6-2A. Two distinct crystalline planes as a fingerprint of pristine graphite at about 27° for (002) plane strong diffraction peak and about 55° for (004) plane relatively weaker diffraction can be observed. These two diffraction peaks and some other very low peaks for (100) and (101) planes as shown in the inserted plots of Figure 6-2A conform to many reported XRD profile to categorize modified and un-modified graphite and thereby justify BGPE as a pristine graphite material [303-306].

Raman spectrum is shown in Figure 6-2B is a claim to support both metallic and non-metallic properties of graphite as indicated by the doublet peak of the G-band of graphite observed at about 1580 cm^{-1} as the main feature of identifying pristine graphite from graphene product [307]. Perfect stacked graphite layered property of BGPE is revealed by G-band and 2D- band peaks at about 1580 cm^{-1} and about 700 cm^{-1} for G-band and 2D-band respectively along with the defect characteristic peak (D-band) observed at about 1350 cm^{-1} [265, 266].

N_2 adsorption-desorption curve revealing the adsorption isotherm type of BGPE is shown in Figure 6-2C. The presence of hysteresis as a result of the desorption indicates that BGPE is a type IV adsorption isotherm material with mesoporous properties that are expected to be characterized with a pore size between 2 nm and 50 nm [308]. BGPE Pore size distribution and pore volume estimated with the adsorption part of the isotherm by BJH method were found to be 43.7 nm and 0.093 cm^3g^{-1} respectively while the BET

estimated surface area is about 8.18 m^2g^{-1} as shown in the inserted curve in Figure 6-2C for the pore size distribution.

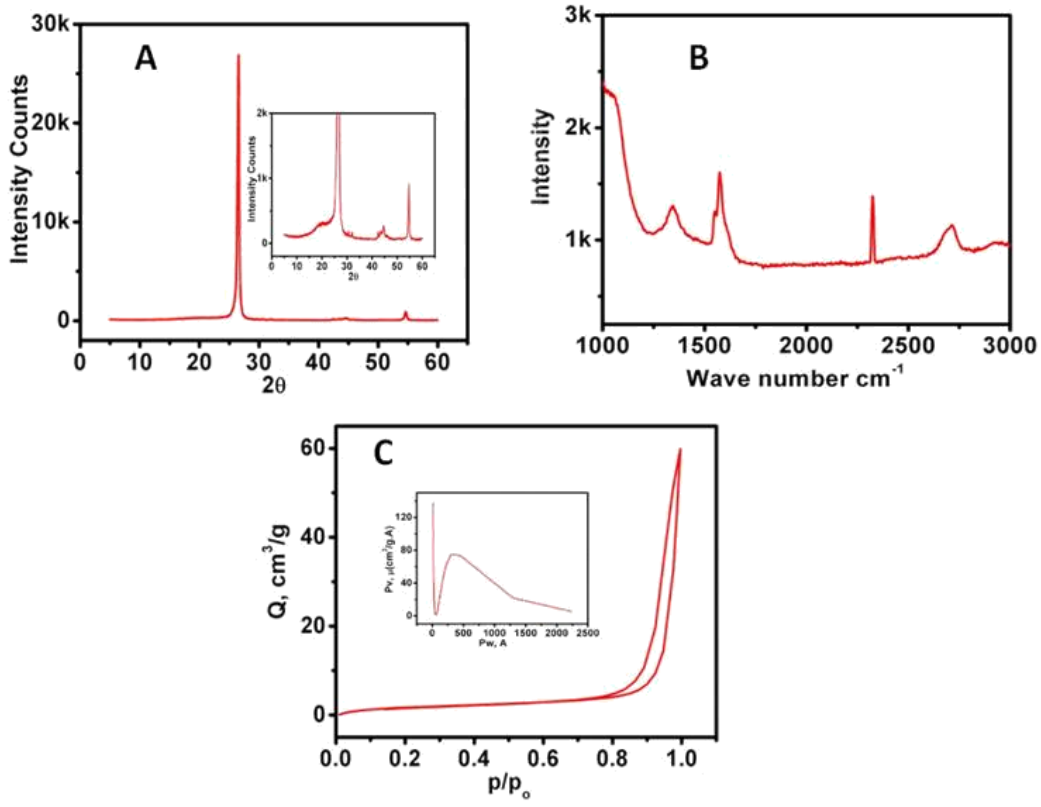

Figure 6-2: Characterization of bulk GPE (A) XRD pattern, (B) Raman spectrum and (C) N_2 adsorption-desorption curve with the pore size distribution curve.

6.3.3 Effect of pH on Oxidation Peaks of Ascorbic Acid, Uric Acid, Xanthine and Hypoxanthine

SWVs of the effect of pH on the resolution of AA and UA oxidation peaks for simultaneous detections of AA, UA, XA and HXA in PBS of pH values from 9.00 to 4.35 are shown in Figure 6-3A. Effect of pH in voltammetry technique involves shifting of oxidation potential towards higher potential as pH decreases and towards lower potential as pH increases. The relationship between pka values of analytes and pH of the medium can be utilized to effect the separation of compounds with different pKa values. Value of pKa for UA, XA and HXA have been reported as 5.50, 7.70 and 8.80 respectively [247] and AA with pKa values of 4.10. These pKa values are a good indication of the possible resolution of AA and UA which will be proportional to their oxidation peak potentials. As shown in Figure 6-3Aa, Figure 6-3Ab and Figure 6-3Ac for PBS pH 9.00, 8.00 and 7.00 respectively, only 3 peaks can be observed from about 0.25 V, 0.45 V and 0.90 V slightly shifting towards positive potential as pH of the medium decreases from 9.00 – 7.00 despite the presence of 500 µM AA, 50 µM UA, 50 µM XA and 100 µM HXA. This shows that there is no resolution of the oxidation peaks of AA and UA as earlier observed in Figure 6-1Cb. However, the appearance of the forth peak can be observed at about 0.40 V in PBS pH 6.00 (Figure 6-3Ad). As the pH of the medium decreases further, shifting of the appeared peak and other 2 at higher potential continue while the peak with the lowest potential (AA) remains partially constant. Complete separation of the overlapped peak can be observed in Figure 6-3Ae and 6-3Af with a slightly different resolution between the two peaks for PBS pH 5.00 and 4.35 respectively.

SWVs showing oxidation peaks of 500 µM AA, 50 µM UA, 50 µM XA and 100 µM HXA in 0.10 M PBS 4.35 for both BGCE and BGPE are shown in Figure 6-3B. Obvious separations of the 4 analytes can be observed in both BGCE (Figure 6-3Ba) and BGPE (Figure 6-3Bb). However, the resolution between AA and UA were observed to be very wide (about 0.20 V) on BGCE, but less than 0.10 V is observed with BGPE but can still be utilized to simultaneously determine AA, UA, XA, and HXA simultaneously.

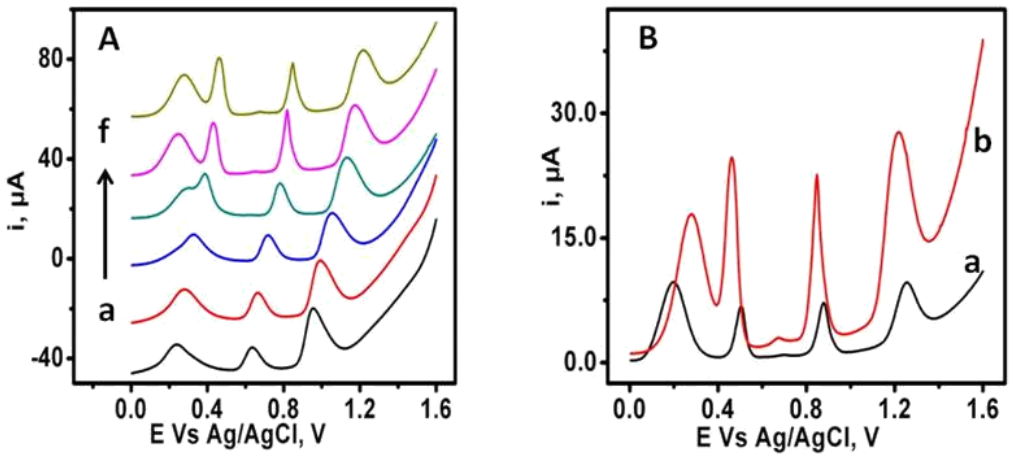

Figure 6-3: SWVs (A) of 0.50 mM AA, 0.05 µM UA, 0.05 mM XA and 0.10 mM HXA in different pH of 0.1 M PBS. (a) pH 9.00, (b) pH 8.00, (c) pH 7.00, (d) pH 6.00, (e) pH 5.00 and (f) pH 4.35 and (B) comparison of same concentrations of analytes on (a) BGCE and (b) BGPE.

6.3.4 Scan Rate Effect

Effect of scan rate to investigate redox process of the electrode was studied with CV at different scan rate from 0.025 – 0.150 V/s for 500 µM AA, 50 µM UA, 50 µM XA and 100 µM HXA in 0.10 M PBS 4.35 are shown in Figure 6-4. It can be observed from Figure 6-4A that the oxidation current peaks of the 4 analytes were proportionally increase as the scan rate increases with a noticeable minimal reverse peaks showing the reversible nature of all the investigating analytes. This behavior exhibited by CVs experiments in Figure 6-4A can be further investigated to validate adsorption process of the BGPE by estimating the average surface coverage (Γ) of the electrode with the generally acceptable equation for adsorption process of a reversible reaction[262-264] shown in equation 6.1.

$$\boldsymbol{i_p = \frac{n^2 F^2 A \Gamma \upsilon}{4RT}} \qquad (\mathbf{6.1})$$

where n is the number of electron transfer, A (cm^2) is electrode area, υ is scan rate, and Γ (mol/cm^2) is the electroactive surface coverage concentration.

Slopes obtained from the plots of current peaks (i_p) Vs scan rate (υ) (Figure 6-4B) were used to estimate average electroactive surface coverage concentrations (Γ) of the 4 analytes as 0.85 x 10^{-12} mol/cm^2, 0.93 x 10^{-12} mol/cm^2, 1.91 x 10^{-12} mol/cm^2 and 1.21 x 10^{-12} mol/cm^2 respectively for AA, UA, XA and HXA respectively on BGPE.

A good straight line with impressive correlations of $i_p(\mu A) = 52.611C_{AA} + 6.9989$ (R^2 = 0.9892), $i_p(\mu A) = 57.141C_{UA} + 2.5188$ (R^2 = 0.9800), $i_p(\mu A) = 117.61C_{XA} + 4.8199$ (R^2 = 0.9876) and $i_p(\mu A) = 74.788C_{HXA} + 4.5664$ (R^2 = 0.9965) are obtainable for AA, UA, XA and HXA respectively.

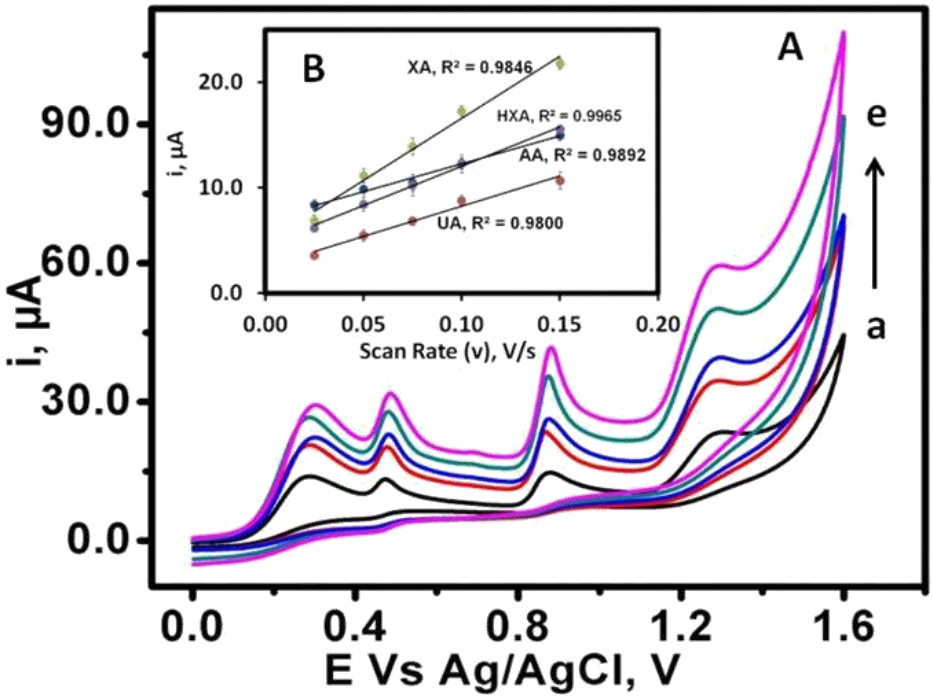

Figure 6-4: CVs (A) showing effect of scan rate (V/s) with 500 µM AA, 50 µM UA, 50 µM XA & 100 µM HXA and its corresponding calibration curves (B). (a) 0.025 V/s, (b) 0.050 V/s , (c) 0.075 V/s , (d) 0.100 V/s and (e) 1.500 V/s.

6.3.5 Parameters Optimization

SWV parameters including frequency, amplitude and sample increment were optimized and shown as Figure 6- 5. It can be observed from frequency optimization (Figure 6-5A) that current peaks of all the analytes increase from 15 Hz – 50 Hz (Figure 6-5Aa to Figure 6-5Ac). However, current peaks were observed to slightly reduce at 75 Hz (Figure 6-5Ad), and undesirable peak emerges after HXA peak. Considerations of the peak current, background current and good resolution of peaks were used as guidance for selecting the frequency of 50 Hz as the optimized parameter. Amplitude (Figure 6-5B) and sample increment (Figure 6-5C) were also investigated with the conclusion of selecting 25 mV and 4 mV as an optimized condition for amplitude and sample increment respectively based on the earlier mentioned criteria for the frequency optimization.

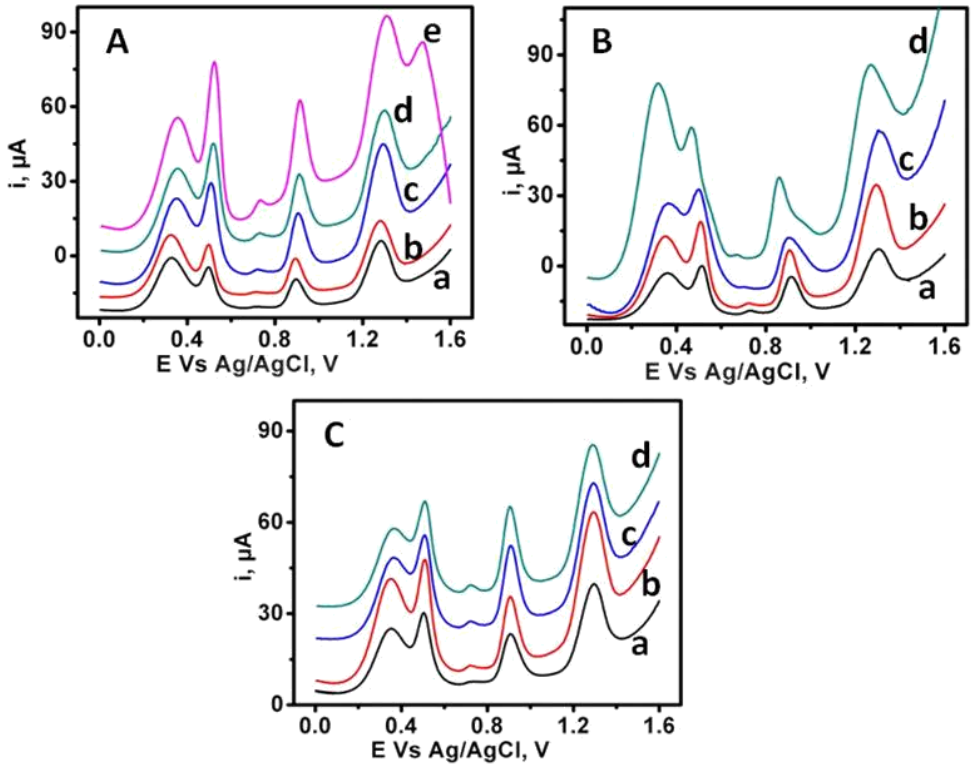

Figure 6-5: SWVs for the electrochemical parameters of 0.50 mM AA, 0.05 µM UA, 0.05 mM XA and 0.10 mM HXA in 0.10 M PBS pH 4.35. (A) Frequency (a) 15 Hz, (b) 25 Hz, (c) 50 Hz, (d) 75 Hz and (e) 100 Hz. (B) Amplitude (a) 15 mV, (b) 25 mV, (c) 50 mV and (d) 75 mV . (C) Increment (a)2 mV, (b) 4 mV, (c) 6 mV and (d) 8 mV.

6.3.6 Simultaneous and Selective Determination of Ascorbic Acid, Uric Acid, Xanthine and Hypoxanthine

Evaluation of BGPE for simultaneous determination of AA, UA, XA, and HXA were carried as shown in Figure 6-6. Figure 6-6A is SWVs containing mixtures of different compositions of AA, UA, XA and HXA from low to high concentrations (µM) (Figure 6-6Aa to Figure 6-6Aj). SWVs were found to show proportional current peaks corresponding to the concentration of AA, UA, XA and HXA in the mixture. Corresponding calibration curves for AA, UA, XA and HXA are presented in Figure 6-6B, Figure 6-6C, Figure 6-6D and Figure 6-6E respectively. Linear range of 100 µM – 1500 µM (R^2 = 0.9851), 1 µM – 100 µM (R^2 = 0.9915), 1 µM – 1500 µM (R^2 = 0.9864) and 20 µM – 300 µM (R^2 = 0.9825) and limit of detection (LOD) estimated by signal to noise ratio (S/N = 3) of 2.99 µM, 0.25 µM, 0.084 µM and 0.26 µM were obtained for AA, UA, XA and HXA respectively. Performance of BGPE was found to compete favorably when compared with other methods compose of composites, nanoparticle, polymers and several complex electrode modifications for simultaneous determinations of AA, UA, XA and HXA as shown in Table 6-1.

Selective determinations of each of the four analytes in the presence of relatively higher concentrations of other were also investigated and presented as Figure 6-7. Figure 6-7A shows SWVs of different concentrations of AA in the presence of 50 µM UA, 50 µM XA and 100 µM HXA, Figure 6-7B shows SWVs of different concentrations of UA in the presence of 500 µM AA, 50 µM XA and 100 µM HXA, Figure 6-7C shows SWVs of different concentrations of XA in the presence of 500 µM AA, 50 µM UA and 100 µM

HXA and Figure 6-7D shows SWVs of different concentrations of HXA in the presence of 500 µM AA, 50 µM XA and 50 µM UA. It can be observed in the calibrations curves inserted into Figure 6-7A, Figure 6-7B, Figure 6-7C and Figure 6-7D that linear range of 100 µM – 1500 µM (R^2 = 0.9851), 10 µM – 700 µM (R^2 = 0.9880), 10 µM – 600 µM (R^2 = 0.9778) and 20 µM – 600 µM (R^2 = 0.9804) were obtained for AA, UA, XA and HXA respectively.

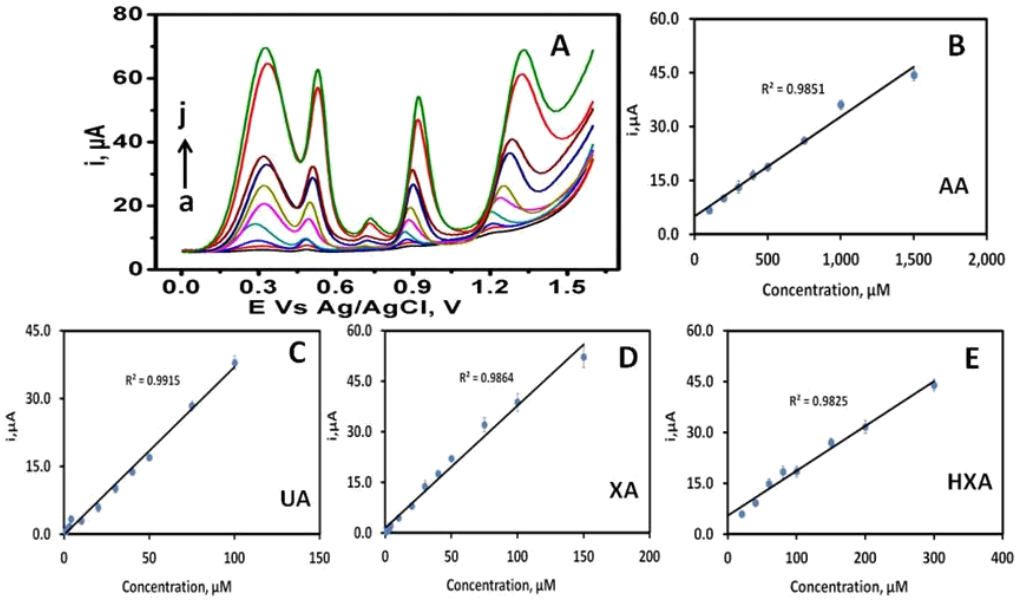

Figure 6-6: (A) SWVs showing different concentration of AA, UA, XA & HXA and the corresponding calibration curves (B), (C) , (D) and (E) for AA, UA, XA and HXA respectively. a (10 µM AA, 1 µM UA, 1 µM XA & 1 µM HXA); b (20 µM AA, 2 µM UA, 2 µM XA & 2 µM HXA); c (40 µM AA, 4 µM UA, 4 µM XA & 4 µM HXA); d (100 µM AA, 10 µM UA, 10 µM XA & 20 µM HXA); e (200 µM AA, 20 µM UA, 20 µM XA & 40 µM HXA); f (300 µM AA 30 µM UA 30 µM XA & 60 µM HXA); g (400 µM AA, 40 µM UA, 40 µM XA & 80 µM HXA); h (500 µM AA, 50 µM UA 50 µM XA & 100 µM HXA); i (750 µM AA, 75 µM UA, 75 µM XA & 150 µM HXA); and j (1000 µM AA, 100 µM UA, 100 µM XA & 200 µM HXA).

T**able 6-1:** Comparison of the Developed Method with Electrochemical Methods for Simultaneous Detections of Ascorbic Acid, Uric Acid, Xanthine and Hypoxanthine

Electrode	Medium	**Linear range (µM)**				**Detection limit (µM)**				Ref.
		AA	**UA**	**XA**	**HXA**	**AA**	**UA**	**XA**	**HXA**	
BGPE[1]	PBS pH 4.35	100-1500	1-100	1-1500	20-300	2.99	0.25	0.084	0.26	This work
PDA_{ox}-PTCA/GCE[2]	PBS pH 3.00	76-3900	1.8-238	5.1-289	3.8-293	25.3	0.60	1.70	1.30	[299]
P(GBHA)/GCE[3]	PBS pH 5.00	1–8, 10-1000	1-100	-	-	0.30	0.09	-	-	[289]
CL-TiN/GCE[4]	PBS pH 7.00	50-1500	10-300	-	-	1.52	0.28	-	-	[287]
P6-TG/GCE[5]	PBS pH 7.00	-	2-1600	2-800	1-500	-	0.06	0.3	0.1	[257]
PYTS-NG/GCE[6]	PBS pH 7.90	-	9-1000	8-800	8-200	-	0.33	0.083	0.23	[258]
Co-CeO_2 np/GCE[7]	PBS pH 5.00	-	1-2200	0.1-1000	1-600	-	0.12	0.096	0.36	[259]
ERGO-PLL/GCE[8]	PBS pH 7.40	100-1200	20-200	-	-	2.00	0.15	-	-	[290]
RGO-ZnO/GCE[9]	PBS pH 6.00	50-2350	3-330	-	-	3.71	1.08	-	-	[295]
PG/GCE[10]	PBS pH 7.00	9-2314	6-1330	-	-	0.23	0.33	-	-	[296]

[1] Bare graphite pencil electrode, **[2] Over oxidized dopamine polymer-3,4,9,10-perylenetetracarboxylic acid**

[3] Poly (glyoxal-bis(2-hydroxyanil)) **[4] Chrysanthemum-like titanium nitride**

[5] Purine based polymer **[6] Nitrogen-doped graphene functionalized with a sulfonic group**

[7] Cobalt-doped cerium oxide nanoparticle **[8] Electrodeposited reduced graphene oxide- poly L- lysine**

[9] Reduced graphene oxide zinc oxide composite **[10] Pristine graphene**

GCE – Glassy carbon electrode

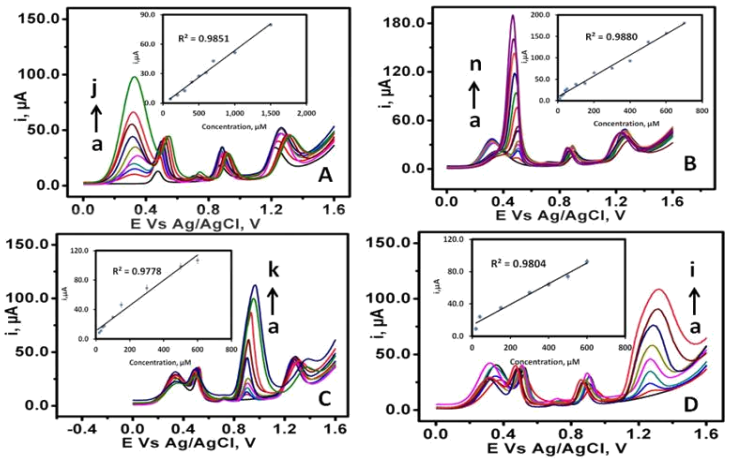

Figure 6-7: (A) SWVs showing different concentrations of AA, in the presence of 50 µM UA, 50 µM XA and 100 µM HXA (a) 0 µM , (b) 100 µM , (c) 200 µM , (d) 300 µM , (e) 400 µM , (f) 500 µM , (g) 600 µM , (h) 700 µM , (i) 1000 µM and (j) 1500 µM . (B) SWVs showing different concentrations of UA, in the presence of 500 µM AA, 50 µM XA and 100 µM HXA (a) 0 µM , (b) 10 µM , (c) 20 µM , (d) 30 µM , (e) 40 µM , (f) 50 µM , (g) 100 µM , (h 150 µM, (i) 200 µM , (j) 300 µM , (k) 400 µM , (l) 500 µM , (m) 600 µM and (n) 700 µM . (C) SWVs showing different concentrations of XA, in the presence of 500 µM AA, 50 µM UA and 100 µM HXA (a) 0 µM , (b) 10 µM , (c) 20 µM , (d) 30 µM , (e) 40 µM , (f) 50 µM , (g) 100 µM , (h) 150 µM , (i) 500 µM , (j) 500 µM and (k) 600 µM . (D) SWVs showing different concentrations of HXA, in the presence of 500 µM AA, 50 µM XA and 50 µM XA (a) 0 µM , (b) 10 µM , (c) 20 µM , (d) 40 µM , (e) 150 µM , (f) 300 µM , (g) 400 µM , (h) 500 µM and (i) 600 µM Corresponding calibration curves inserted in A, B, C and D respectively for AA, UA, XA and HXA.

6.3.7 Reproducibility and Interference Studies

Reproducibility experiments of BGPE voltammograms in 0.10 M PBS 4.35 for the mixture of 500 µM of AA, 50 µM of UA, 50 µM of XA and 50 µM of HXA were recorded for 8 (n = 8) measurements on the fresh surface of BGPE consecutively as shown in Figure 6-8. Standard deviations of the 8 measurements were calculated to be 0.74, 1.37, 1.31 and 0.53 while relative standard deviations (RSD) of 3.67 %, 3.54 %, 4.47 % and 3.88 % were estimated as AA, UA, XA and HXA respectively.

Interference studies in the presence of 2 mg/L of Co, Cu, Fe, Ni, Zn and 50 µM glucose and methionine Zn in the mixture of 500 µM AA, 50 µM UA, 50 µM XA and 100 µM HXA were shown in Figure 6-9. These potential interferences almost do not influence the shape of the 4 analytes signal and have minimal effect on the variation (± 5 %) on the current peak of the mixtures of the analytes without the interference compounds and metals.

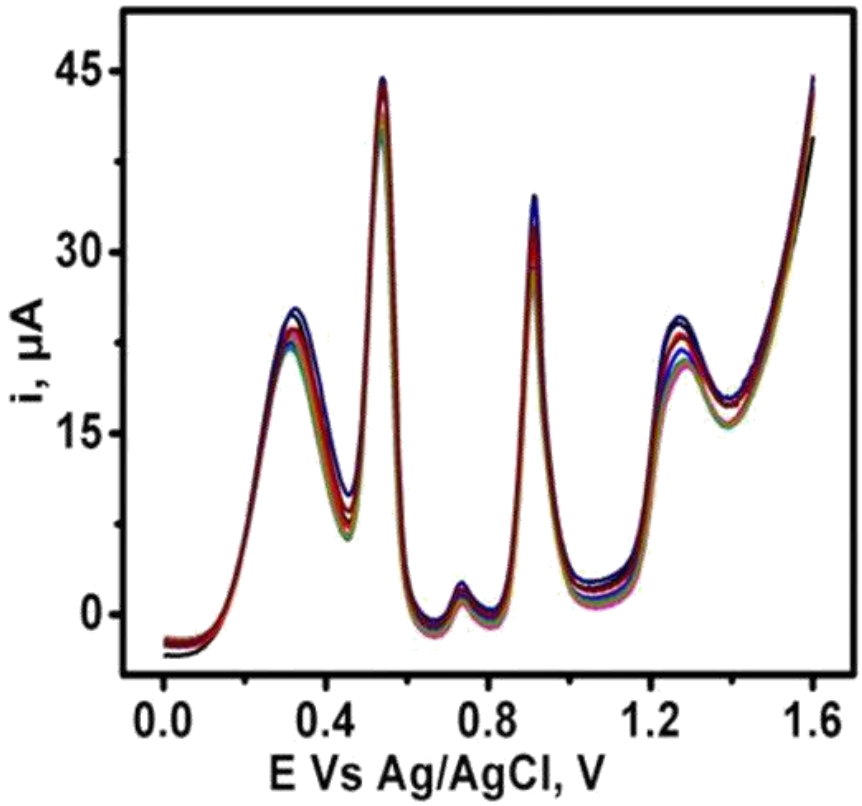

Figure 6-8: SWVs showing 8 repeated scanning on the BGPE for 500 µM AA, 50 µM UA, 50 µM XA and 50 µM HXA.

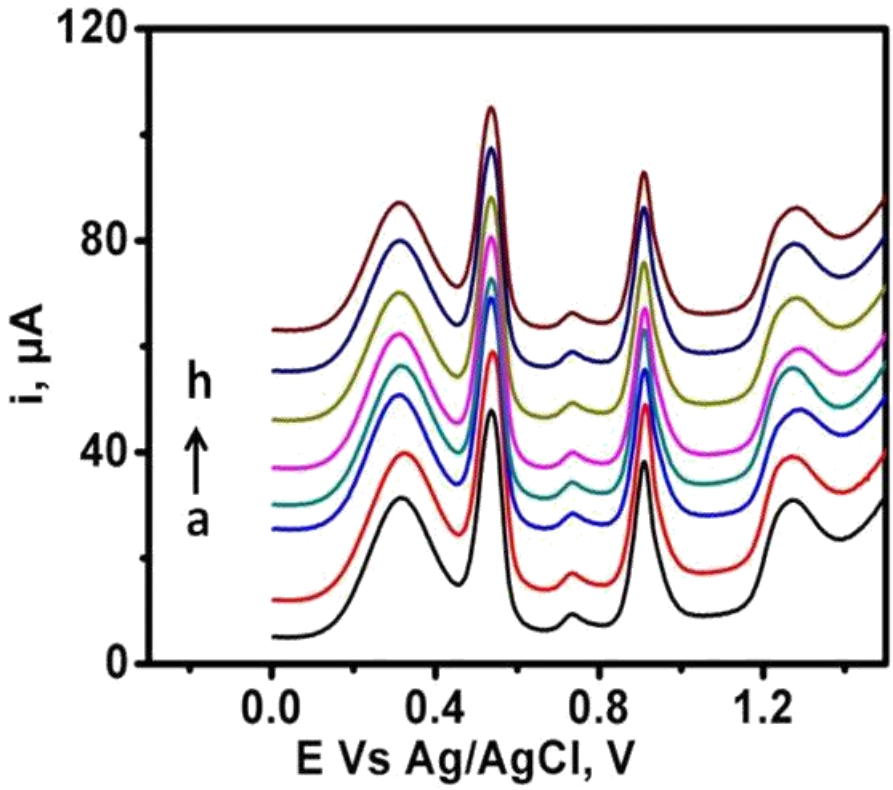

Figure 6-9: SWVs showing effect of interferences on the mixture of 500 µM AA, 50 µM UA, 50 µM XA & 100µM HXA on BGPE in the presence and absence of interference compounds. (a) absence of interference and presence of (b) 2 mg/L Co (c) 2 mg/L Cu, (d) 2 mg/L Fe, (e) 2 mg/L Ni, (f) 2 mg/L Zn, (g) 50 µM glucose and (h) 50 µM methionine.

6.3.8 Detection of Ascorbic Acid, Uric Acid, Xanthine and Hypoxanthine in Biological Samples

The presence of AA, UA, XA and HXA in human serum sample and urine sample were confirmed with the developed method as shown in the voltammograms presented in Figure 6-10A for 50 µL serum (diluted 80 times) and Figure 6-10B for 50 µL urine (diluted 200 times) with peaks corresponding to the potential of each analytes. To determine the concentration of AA, UA, XA, and HXA in the biological samples, mixtures containing a different concentration of AA, UA, XA and HXA were spiked and results were analyzed by standard addition methods and tabulated as shown in Table 6-2. Impressive % recovery between 93.95 % and 108.98 % for urine sample while 91.68% and 102.70 % for serum sample were obtained. BGPE is characterized by an excellent performance of a good transducer to be considered as a candidate for effective determinations of UA, XA, and HXA in the presence of AA.

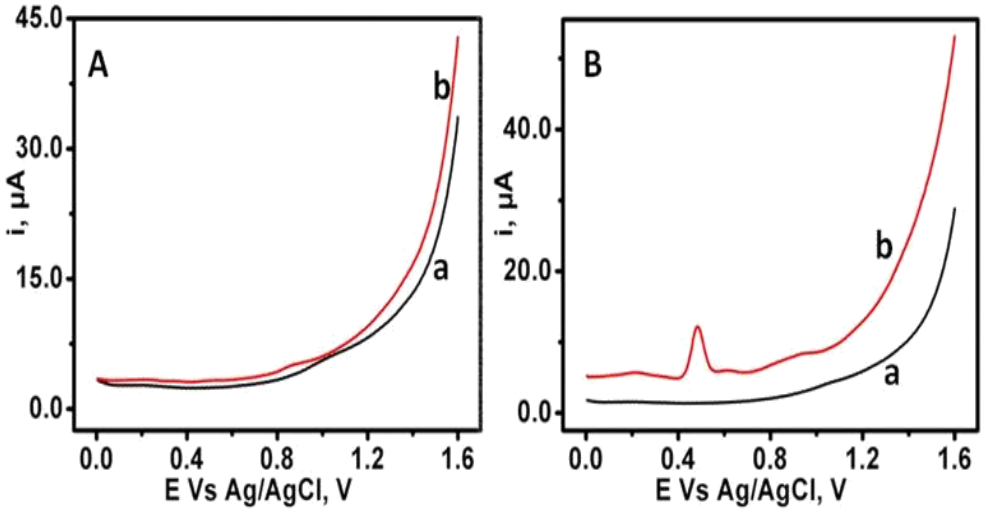

Figure 6-10: Response of Serum (A) and Urine (B) on the developed electrochemical method. (a) Blank and (b) are 50 µL serum and 20 µL urine in 5ml solution for A and B respectively.

Table 6-2: Application of the Developed Method on Human serum and urine sample

Sample	AA *A (µM)	AA*F (µM)	% AA Rec.	UA *A(µM)	UA*F (µM)	% UA Rec.	XA *A (µM)	XA*F (µM)	% XA Rec.	HXA *A(µM)	HXA *A (µM)	% HXA Rec.
	50.00	54.49	108.98	5.00	4.94	98.79	5.00	4.76	95.24	10.00	9.40	93.95
Urine	100.00	106.59	106.59	10.00	10.08	100.08	10.00	10.67	106.71	20.00	20.95	104.77
	150.00	144.25	96.17	15.00	15.01	100.09	15.00	14.64	97.57	30.00	29.57	98.58
	100.00	96.69	96.69	10.00	10.27	102.70	10.00	9.80	98.02	10.00	9.17	91.68
Serum	200.00	196.50	98.25	20.00	20.07	100.37	20.00	20.63	100.37	20.00	19.53	97.65
	250.00	255.76	102.30	25.00	24.82	99.29	25.00	24.57	98.26	30.00	30.58	101.92

***F - Found, *A –Added and Rec. - Recovery**

CHAPTER 7

CONCLUSION

Non-enzymatic electroanalytical methods based on GPE were successfully developed for all identified analytes (methionine, ascorbic acid, uric acid, xanthine, and hypoxanthine) along with glucose for mitigation of DB-M. Developed methods are comparably cost effective based on the approached that involved mostly in-situ electrochemical modifications and detections of analytes on GPE surface. Despite by-passing challenges of external chemical modifications and immobilizations of electro-catalyst on the working electrode, the performance of the GPE developed methods competes favorably with all complex and expensive electrode systems reported for each of the identified analytes.

A disposable GPE was successfully utilized to develop a voltammetric technique suitable for non-enzymatic glucose sensor fabrication. In-situ electrochemical reduction of Cu^{2+} to Cu^{+} and oxidation of an adsorbed glucose on the surface of bare GPE was found to be responsible for the enhancement of secondary oxidation peak of glucose on GPE. An impressive performance of response up to 4.00 mM linear range of glucose with a limit of detection of 1.36 µM and R^2 of 0.9927 was achieved. Redox potentials of L-ascorbic acid (AA), alanine, fructose and uric acid (UA) as potential interference compounds co-

existing with glucose could not be noticed around the current-peak of glucose which makes the sensor a candidate to be considered as a transducer for the fabrication of an effective, disposable, cost-effective and facile non-enzymatic glucose sensor.

A simple in-situ single-step AgO modification and electroanalytical determination of DLM on a bared DGLPE was also successfully developed and characterized with FE-SEM, EDX and XPS instruments. Electrochemical and electrocatalytic activity of Ag in 0..01 M NaOH pH 13.70 ± 0.20 was successfully used to initiate oxidation reaction of DLM on bare DGLPE surface with Ag^{2+} metal-induced reaction by hydroxyl radical ($OH^{\cdot}$) readily available mechanism due to the presence of AgO while other supporting electrolytes explored (H_2SO_4, HCl, Acetate buffer, PBS pH 4.50, PBS pH 7.00 and PBS pH 9.00) could not initiate oxidation of DLM. Electrode linearity dependence obtained is given as $i(\mu A) = 73.314C_{DLM} + 1.1459$ for a linear range concentration of 10 µM - 500 µM with correla ation coefficient (R^2) of 0.9847 and limit of detection of 0.42 µM. Developed method was found to be suitable for both voltammetric and amperometric techniques for the development of non enzymatic sensor of DLM in human serum in the presence of potential interferences such as ascorbic acid, L-alanine and cysteine.

Development of a novel, easy-to-use and cost-effective method for simultaneous determinations of UA, XA and HXA in human serum and urine samples on DGPE in the presence of $Cu(NO_3)_2$ solution without external electrode modification was reported for the first time. Cu(II) - complexes of UA, XA, and HXA were found to be successfully immobilized in-situ electrochemically on the surface of DGPE and utilized to generated enhanced oxidation peaks of UA, XA, and HXA in PBS pH 7.00 ± 0.20. DGPE was found to predominantly undergoes adsorption process as suggested by the effect of scan

rate of CV studies. Nature of Cu(II) - complexes of UA, XA, and HXA with phosphate ions on DGPE were found to be fluorescence according to the characterization by Raman spectroscopy. Enhancement of peaks (UA, XA, and HXA) on DGPE was as a result of stronger interaction between copper atoms and corresponding UA, XA and HXA for complex formation as revealed by DFT calculation when comparing their binding energy for complexation with phosphate ions which is predominantly a weaker hydrogen bonding interaction. Two linear range of 1 - 40 µM (R^2 = 0.9907) and 100 – 300 µM (R^2 = 0.9962) was observed for XA while 2 - 80 µM (R^2 = 0.9925) and 0.1 - 10 µM (R^2 = 0.9902) for UA and HXA respectively. The developed method was successfully utilized for simultaneous determination of the three analytes on human serum and urine with impressive recovery and was found to be efficient in the presence of glucose, methionine, alanine, iron, and zinc as potential interferences.

Lastly, development of an electroanalytical method that successfully resolved AA and UA oxidation peaks on BGPE in PBS pH 4.35 without any electrode surface modification was achieved and utilized for simultaneous and selective detection of AA, UA, XA and HXA with RSD of 3.67 %, 3.54 %, 4.47 % and 3.88 % respectively for 8 repeated measurement (n = 8). Semiconductor property, mesoporous nature and a good ordered stacked graphite layer of BGPE were revealed by XRD, N_2 adsorption-desorption and Raman spectroscopy characterization of the bulk BGPE sample. Effect of scan rate by CV techniques reveals predominant involvement of the adsorption process in its redox reaction. Capabilities of BGPE for simultaneous of detections of AA, UA, XA and HXA in the presence of potential interferences was demonstrated with less than 5 % variation in current peaks of respective analytes. The developed method was utilized to determine

AA, UA, XA and HXA in urine and serum sample with a good percentage recovery between 91.68 % and 108.98 % for urine and serum samples.

Reference

[1] S. Selim, Frequency and pattern of chronic complications of diabetes and their association with glycemic control, Diabetes & Metabolic Syndrome: Clinical Research & Reviews, 11 (2017) S311-S314.

[2] N. Nanayakkara, S. Ranasinha, A. Gadowski, S. Heritier, J. Flack, N. Wischer, J. Wong, S. Zoungas, Age, age at diagnosis and diabetes duration are all associated with vascular complications in type 2 diabetes, Journal of Diabetes and its Complications, 32 (2018) 279-290.

[3] D. Nathan, Long-term complications of diabetes mellitus, New England Journal of Medicine, 328 (1993) 1676-1685.

[4] L. Guariguata, D. Whiting, I. Hambleton, J. Beagley, U. Linnenkamp, J. Shaw, Global estimates of diabetes prevalence for 2013 and projections for 2035, Diabetes Research and Clinical Practice, 103 (2014) 137-149.

[5] S. Wild, G. Roglic, A. Green, R. Sicree, H. King, Global prevalence of diabetes, estimates for the year 2000 and projections for 2030, Diabetes Care 27 (2004) 1047-1053.

[6] International Diabetes Federation (IDF) Diabetes Atlas 7th edition, 2015.

[7] International Diabetes Federation (IDF) Diabetes Atlas 8th edition, 2017.

[8] J. Zimmerman, V. Malloy, R. Krajcik, N. Orentreich, Nutritional control of aging, Experimental Gerontology, 38 (2003) 47-52.

[9] L. Grant, E. Lees, L. Forney, N. Mody, T. Gettys, P. Brown, H. Wilson, M. Delibegovic, Methionine restriction improves renal insulin signaling in aged kidneys, Mechanisms of Ageing and Development, 157 (2016) 35-43.

[10] E. Lees, E. Król, L. Grant, K. Shearer, C. Wyse, E. Moncur, A. Bykowska, N. Mody, T. Gettys, M. Delibegovic, Methionine restriction restores a younger metabolic phenotype in adult mice with alterations in fibroblast growth factor 21, Aging Cell, 13 (2014) 817-827.

[11] R. Kanďár, The ratio of oxidized and reduced forms of selected antioxidants as a possible marker of oxidative stress in humans, Biomedical Chromatography, 30 (2016) 13-28.

[12] G. Ndrepepa, Uric acid, and cardiovascular disease, Clinica Chimica Acta, 484 (2018) 150-163.

[13] B. Uslu, S. Ozkan, Electroanalytical application of carbon-based electrodes to the pharmaceuticals, Analytical Letters, 40 (2007) 817-853.

[14] T. Huong Le, M. Bechelany, M. Cretin, Carbon felt based-electrodes for energy and environmental applications: A review, Carbon, 122 (2017) 564-591.

[15] J. Xu, X. Zhou, M. Chen, S. Shi, Y. Cao, Preparing hierarchical porous carbon aerogels based on enzymatic hydrolysis lignin through ambient drying for supercapacitor electrodes, Microporous and Mesoporous Materials, 265 (2018) 258-265.

[16] M. Carneiro, F. Moreira, R. Dutra, R. Fernandes, M. Sales, Homemade 3-carbon electrode system for electrochemical sensing: Application to microRNA detection, Microchemical Journal, 138 (2018) 35-44.

[17] A. Kawde, N. Baig, M. Sajid, Graphite pencil electrodes as electrochemical sensors for environmental analysis: a review of features, developments, and applications, RSC Advances, 6 (2016) 91325-91340.

[18] R. Wilson, A. Turner, Glucose oxidase: an ideal enzyme, Biosensors, and Bioelectronics, 7 (1992) 165-185.

[19] S. Updike, G. Hicks, The enzyme electrode, Nature, 214 (1967) 986-988.

[20] L. Clark Jr, C. Lyons, Annals of the New York Academy of Sciences, 102 (1962) 29-45.

[21] G. Guilbault, G. Lubrano, An enzyme electrode for the amperometric determination of glucose, Analytica Chimica Acta, 64 (1973) 439-455.

[22] D. Gough, J. Lucisano, P. Tse, Two-dimensional enzyme electrode sensor for glucose, Analytical Chemistry, 57 (1985) 2351-2357.

[23] J. Armour, J. Lucisano, B. McKean, D. Gough, Application of chronic intravascular blood glucose sensor in dogs, Diabetes, 39 (1990) 1519-1526.

[24] J. Wang, J. Mo, S. Li, J. Porter, Comparison of oxygen-rich and mediator-based glucose-oxidase carbon-paste electrodes, Analytica Chimica Acta, 441 (2001) 183-189.

[25] J. Wang, F. Lu, Oxygen-rich oxidase enzymes electrodes for operation in oxygen-free solutions, Journal of the American Chemical Society, 120 (1998) 1048-1050.

[26] M. Loughran, J. Hall, A. Turner, Development of a pyrroloquinoline quinone (PQQ) mediated glucose oxidase enzyme electrode for detection of glucose in fruit juice, Electroanalysis, 8 (1996) 870-875.

[27] K. Lau, S. De Fortescu, L. Murphy, J. Slater, Disposable glucose sensors for flow injection analysis using substituted 1,4-benzoquinone mediators, Electroanalysis, 15 (2003) 975-981.

[28] C. Taylor, G. Kenausis, I. Katakis, A. Heller, "Wiring" of glucose oxidase within a hydrogel made with polyvinyl imidazole complexed with [(Os-4,4′-dimethoxy-2,2′-bipyridine)Cl] + 2+1, Journal of Electroanalytical Chemistry, 396 (1995) 511-515.

[29] A. Cass, G. Davis, G. Francis, H. Allen, O. Hill, W. Aston, I. Higgins, E. Plotkin, L. Scott, A.Turner, Ferrocene-mediated enzyme electrode for amperometric determination of glucose, Analytical Chemistry, 56 (1984) 667-671.

[30] A. Mulchandani, S. Pan, Ferrocene-conjugated m-phenylenediamine conducting polymer-incorporated peroxidase biosensors, Analytical Biochemistry, 267 (1999) 141-147.

[31] S. Tsujimura, S. Kojima, K. Kano, T. Ikeda, M. Sato, H. Sanada, H. Omura, Novel FAD-dependent glucose dehydrogenase for a dioxygen-insensitive glucose biosensor, Bioscience, Biotechnology and Biochemistry, 70 (2006) 654-659.

[32] P. Hale, T. Inagaki, H. Karan, Y. Okamoto, T. Skotheim, A new class of amperometric biosensor incorporating a polymeric electron-transfer mediator, Journal of the American Chemical Society, 111 (1989) 3482-3484.

[33] S. Bao, C. Li, J. Zang, X. Cui, Y. Qiao, J. Guo, New nanostructured TiO_2 for direct electrochemistry and glucose sensor applications, Advanced Functional Materials, 18 (2008) 591-599.

[34] S. Wu, H. Ju, Y. Liu, Conductive mesocellular silica-carbon nanocomposite foams for immobilization, direct electrochemistry, and biosensing of proteins, Advanced Functional Materials, 17 (2007) 585-592.

[35] Y. Wang, F. Caruso, Enzymes encapsulation in nanoporous silica, Chemical Communications, 13, (2004) 1528-1529.

[36] J. Li, X. Lin, Glucose biosensor based on immobilization of glucose oxidase in poly(o-aminophenol) film on polypyrrole-Pt nanocomposite modified glassy carbon electrode, Biosensors and Bioelectronics, 22 (2007) 2898-2905.

[37] K. Han, Z. Wu, J. Lee, I. Ahn, J. Park, B. Min, K. Lee, Activity of glucose oxidase entrapped in mesoporous gels, Biochemical Engineering Journal, 22 (2005) 161-166.

[38] B. Wu, G. Zhang, S. Shuang, M. Choi, Biosensors for determination of glucose with glucose oxidase immobilized on an eggshell membrane, Talanta, 64 (2004) 546-553.

[39] T. Ohara, R. Rajagopalan, A. Heller, "Wired" enzyme electrodes for amperometric determination of glucose or lactate in the presence of interfering substances, Analytical Chemistry, 66 (1994) 2451-2454.

[40] D. Pletcher, Electrocatalysis: present and future, Journal of Applied Electrochemistry, 14 (1984) 403-415.

[41] L. Burke, Premonolayer oxidation and its role in electrocatalysis, Electrochimica Acta, 39 (1994) 1841-1848.

[42] Y. Huang, D. Kim, Synthesis and self-assembly of highly monodispersed quasispherical gold nanoparticles, Langmuir, 27 (2011) 13861-13867.

[43] Y. Huang, D. Kim, Dark-field microscopy studies of polarization-dependent plasmonic resonance of single gold nanorods: Rainbow nanoparticles, Nanoscale, 3 (2011) 3228-3232.

[44] Y. Huang, D. Kim, Light-controlled synthesis of gold nanoparticles using a rigid, photoresponsive surfactant, Nanoscale, 4 (2012) 6312-6317.

[45] L. Wei, Y. Fan, H. Wang, N. Tian, Z. Zhou, S. Sun, Electrochemically shape-controlled synthesis in deep eutectic solvents of Pt nanoflowers with enhanced activity for ethanol oxidation, Electrochimica Acta, 76 (2012) 468-474.

[46] L. Wei, Y. Fan, N. Tian, Z. Zhou, X. Zhao, B. Mao, S. Sun, Electrochemically shape-controlled synthesis in a deep eutectic solvents-A new route to prepare Pt nanocrystals enclosed by high-index facets with high catalytic activity, Journal of Physical Chemistry C, 116 (2012) 2040-2044.

[47] J. Zeng, A simple eco-friendly solution phase reduction method for the synthesis of polyhedra platinum nanoparticles with high catalytic activity for methanol electrooxidation, Journal of Materials Chemistry, 22 (2012) 3170-3176.

[48] Z. Xiao, C. Han, W. Kwok, H. Wang, U. Welp, J. Wang, G. Crabtree, Tuning the Architecture of mesostructures by electrodeposition, Journal of the American Chemical Society, 126 (2004) 2316-2317.

[49] P. Si, Y. Huang, T. Wang, J. Ma, Nanomaterials for electrochemical non-enzymatic glucose biosensors, RSC Advances, 3 (2013) 3487-3502.

[50] K. Toghill, R. Compton, Electrochemical non-enzymatic glucose sensors: A perspective and an evaluation, International Journal of Electrochemical Science, 5 (2010) 1246-1301.

[51] D. Feng, F. Wang, Z. Chen, Electrochemical glucose sensor based on one-step construction of gold nanoparticle-chitosan composite film, Sensors, and Actuators, B: Chemical, 138 (2009) 539-544.

[52] F. Kurniawan, V. Tsakova, V. Mirsky, Gold nanoparticles in nonenzymatic electrochemical detection of sugars, Electroanalysis, 18 (2006) 1937-1942.

[53] B. Jena, C. Raj, Enzyme-free amperometric sensing of glucose by using gold nanoparticles, Chemistry - A European Journal, 12 (2006) 2702-2708.

[54] Y. Ma, J. Di, X. Yan, M. Zhao, Z. Lu, Y. Tu, Direct electrodeposition of gold nanoparticles on indium tin oxide surface and its application, Biosensors, and Bioelectronics, 24 (2009) 1480-1483.

[55] Y. Ding, Y. Liu, L. Zhang, Y. Wang, M. Bellagamba, J. Parisi, C. Li, Y. Lei, Sensitive and selective nonenzymatic glucose detection using functional NiO-Pt hybrid nanofibers, Electrochimica Acta, 58 (2011) 209-214.

[56] Q. Shen, L. Jiang, H. Zhang, Q. Min, W. Hou, J. Zhu, Three-dimensional dendritic Pt nanostructures: Sonoelectrochemical synthesis and electrochemical applications, Journal of Physical Chemistry C, 112 (2008) 16385-16392.

[57] J. Yuan, K. Wang, X. Xia, Highly ordered platinum-nanotubule arrays for amperometric glucose sensing, Advanced Functional Materials, 15 (2005) 803-809.

[58] B. Singh, E. Dempsey, C. Dickinson, F. Laffir, Inside/outside Pt nanoparticles decoration of functionalized carbon nanofibers (Pt19.2/f-CNF80.8) for sensitive non-enzymatic electrochemical glucose detection, Analyst, 137 (2012) 1639-1648.

[59] Y. Lee, D. Park, J. Park, Fully packaged nonenzymatic glucose microsensors with nanoporous platinum electrodes for anti-fouling, Institute of Electrical and Electronics Engineers (IEEE) Sensors Journal, 8 (2008) 1922-1927.

[60] S. Joo, S. Park, T. Chung, H. Kim, Integration of a nanoporous platinum thin film into a microfluidic system for non-enzymatic electrochemical glucose sensing, Analytical Sciences, 23 (2007) 277-281.

[61] J. Wang, D. Thomas, A. Chen, Nonenzymatic electrochemical glucose sensor based on nanoporous PtPb networks, Analytical Chemistry, 80 (2008) 997-1004.

[62] J. Zhu, J. Jiang, J. Liu, R. Ding, Y. Li, H. Ding, Y. Feng, G. Wei, X. Huang, CNT-network modified Ni nanostructured arrays for high-performance non-enzymatic glucose sensors, RSC Advances, 1 (2011) 1020-1025.

[63] T. Watanabe, Y. Einaga, Design, and fabrication of nickel microdisk-arrayed diamond electrodes for a non-enzymatic glucose sensor based on control of diffusion profiles, Biosensors and Bioelectronics, 24 (2009) 2684-2689.

[64] X. Zhang, G. Wang, Y. Huang, L. Yu, B. Fang, Non-enzymatic glucose detection using Ni/multi-walled carbon nanotubes composite, Micro and Nano Letters, 7 (2012) 168-170.

[65] J. Luo, S. Jiang, H. Zhang, J. Jiang, X. Liu, A novel non-enzymatic glucose sensor based on Cu nanoparticle modified graphene sheets electrode, Analytica Chimica Acta, 709 (2012) 47-53.

[66] A. Ensafi, M. Abarghoui, B. Rezaei, A new non-enzymatic glucose sensor based on copper/porous silicon nanocomposite, Electrochimica Acta, 123 (2014) 219-226.

[67] C. Kong, L. Tang, X. Zhang, S. Sun, S. Yang, X. Song, Z. Yang, Templating synthesis of hollow CuO polyhedron and its application for nonenzymatic glucose detection, Journal of Materials Chemistry A, 2 (2014) 7306-7312.

[68] S. Pourbeyram, K. Mehdizadeh, Nonenzymatic glucose sensor based on disposable pencil graphite electrode modified by copper nanoparticles, Journal of Food and Drug Analysis, 24 (2016) 894-902.

[69] J. Xu, X. Cao, J. Xia, S. Gong, Z. Wang, L. Lu, Phosphomolybdic acid functionalized graphene loading copper nanoparticles modified electrodes for non-enzymatic electrochemical sensing of glucose, Analytica Chimica Acta, 934 (2016) 44-51.

[70] B. Wang, Y. Wu, Y. Chen, B. Weng, C. Li, Flexible paper sensor fabricated via in situ growth of Cu nanoflower on RGO sheets towards amperometrically non-enzymatic detection of glucose, Sensors and Actuators B: Chemical, 238 (2017) 802-808.

[71] Y. Xing, L. Yang, H. Kuang, X. Gao, H. Liu, Function of obestatin in the digestive system, Nutrition, 34 (2017) 21-28.

[72] D. McMillan, P. Geevarghese, Dietary Cyanide and Tropical Malnutrition Diabetes, Diabetes Care, 2 (1979) 202-208.

[73] E. Morrison, D. Ragoobirsingh, J type diabetes revisited, Journal of the National Medical Association, 84 (1992) 603-608.

[74] N. Ewald, P. Hardt, Diagnosis and treatment of diabetes mellitus in chronic pancreatitis, World Journal of Gastroenterology (WJG), 19 (2013) 7276-7281.

[75] M. Sasikala, R. Talukdar, C. Subramanyam, N. Reddy, The enigma of type 3c diabetes in chronic pancreatitis, Pancreas Open Journal, 1 (2016) 19-21.

[76] P. Hart, M. Bellin, D. Andersen, D. Bradley, Z. Cruz-Monserrate, C. Forsmark, M. Goodarzi, A. Habtezion, M. Korc, Y. Kudva, S. Pandol, D. Yadav, S. Chari, Type

3c (pancreatogenic) diabetes mellitus secondary to chronic pancreatitis and pancreatic cancer, The Lancet Gastroenterology & Hepatology, 1 (2016) 226-237.

[77] J. Zajac, A. Shrestha, P. Patel, L. Poretsky, Principles of diabetes mellitus, second edition (2010) pp 3-16.

[78] C.Bogardus, C. Weyer, D. Mott, R. Pratley, The natural history of insulin secretory dysfunction and insulin resistance in the pathogenesis of type 2 diabetes mellitus, Journal of Clinical Investment, 104 (1999) 784-794.

[79] S. Del Prato, P. Marchetti, R. Bonadonna, Phasic insulin release and metabolic regulation in Type 2 diabetes, Diabetes, 51 (2002) S109-S116.

[80] S. Del Prato, P. Marchetti, Beta- and Alpha-cell dysfunction in type 2 diabetes, Hormone and Metabolic Research, 36 (2004) 775-781.

[81] L. Piper, Z. Stewart, H. Murphy, Gestational diabetes, Obstetrics, Gynaecology & Reproductive Medicine, 27 (2017) 171-176.

[82] A. Ali, S. Shastry, R. Nithiyananthan, A. Ali, R. Ganapathy, Gestational diabetes–predictors of response to treatment and obstetric outcome, European Journal of Obstetrics & Gynecology and Reproductive Biology, 220 (2018) 57-60.

[83] A. Tiffany, M. Simas, K. Szegda, X. Liao, P. Pekow, G. Markenson, L. Chasan-Taber, Cigarette smoking and gestational diabetes mellitus in Hispanic woman, Diabetes Research and Clinical Practice, 105 (2014) 126-134.

[84] C. Kim, Maternal outcomes and follow-up after gestational diabetes mellitus, Diabetic Medicine, 31 (2014) 292-301.

[85] D. Mitanchez, Foetal and neonatal complications in gestational diabetes: perinatal mortality, congenital malformations, macrosomia, shoulder dystocia, birth injuries, neonatal complications, Diabetes & Metabolism, 36 (2010) 617-627.

[86] B. Metzger, L. Lowe, A. Dyer, E. Trimble, B. Sheridan, M. Hod, R. Chen, Y. Yogev, D. Coustan, P. Catalano, W. Giles, J. Lowe, D. Hadden, B. Persson, J. Oats, Hyperglycemia and adverse pregnancy outcome (HAPO) study associations with neonatal anthropometrics, Diabetes, 58 (2009) 453-459.

[87] T. Holder, C. Giannini, N. Santoro, B. Pierpont, M. Shaw, E. Duran, S. Caprio, R. Weiss, A low disposition index in adolescent offspring of mothers with gestational diabetes: a risk marker for the development of impaired glucose tolerance in youth, Diabetologia, 57 (2014) 2413-2420.

[88] A. Fraser, D. Lawlor, Long-term health outcomes in offspring born to women with diabetes in pregnancy, Current Diabetes Reports, 14 (2014) 489-496.

[89] A. Berry, Pancreatic enzyme replacement therapy during pancreatic insufficiency, Nutrition in Clinical Practice, 29 (2014) 312-321.

[90] J. Teichmann, J. Riemann, Prevalence of exocrine pancreatic insufficiency in women with obesity syndrome: assessment by pancreatic fecal elastase 1, International Scholarly Research Network (ISRN), Gastroenterology, 2011 (2011) 1-5.

[91] R. Kandimalla, V. Thirumala, P. Reddy, Is Alzheimer's disease a Type 3 Diabetes? A critical appraisal, Biochimica et Biophysica Acta (BBA) - Molecular Basis of Disease, 1863 (2017) 1078-1089.

[92] E. Pedditizi, R. Peters, N. Beckett, The risk of overweight/obesity in mid-life and late-life for the development of dementia: A systematic review and meta-analysis of longitudinal studies, Age and Ageing, 45 (2016) 14-21.

[93] S. Brenner, Alzheimer's disease and other neurodegenerative diseases may be due to nutritional deficiencies secondary to unrecognized exocrine pancreatic insufficiency, Medical Hypotheses, 102 (2017) 89-90.

[94] J. Ma, H. Wang, Q. Li, Y. Zhang, J. Pan, Q. Qiang, X. Xin, H. Tang, J. Ding, S. Chen, Starvation triggers Aβ42 generation from human umbilical vascular endothelial cells, Federation of Europeans Biochemical Societies (FEBS) Letters, 584 (2010) 3101-3106.

[95] K.H. Herzig, A.K. Purhonen, K.M. Räsänen, J. Idziak, P. Juvonen, R. Phillps, J. Walkowiak, Fecal pancreatic elastase-1 levels in older individuals without known gastrointestinal diseases or diabetes mellitus, BMC Geriatrics, 11 (2011).

[96] A. Dasgupta, A. Wahed, Chapter 6 - Lipid metabolism and disorders, in: Clinical Chemistry, Immunology and Laboratory Quality Control, Elsevier, San Diego (2014) 85-105.

[97] A. Dasgupta, A. Wahed, Chapter 7 - Carbohydrate metabolism, diabetes, and hypoglycemia, in: Clinical Chemistry, Immunology and Laboratory Quality Control, Elsevier, San Diego (2014) 107-126.

[98] Y. Horikawa, N. Oda, N. Cox, X. Li, M. Orho-Melander, M. Hara, Y. Hinokio, T. Lindner, H. Mashima, P. Schwarz, L. Del Bosque-Plata, Y. Oda, I. Yoshiuchi, S. Colilla, K. Polonsky, S. Wei, P. Concannon, N. Iwasaki, J. Schulze, L. Baier, C. Bogardus, L. Groop, E. Boerwinkle, C. Hanis, G. Bell, Genetic variation in the

gene encoding calpain-10 is associated with type 2 diabetes mellitus, Nature Genetics, 26 (2000) 163-175.

[99] S. O'Rahilly, I. Barroso, N. Wareham, Genetic factors in type 2 diabetes: The end of the beginning, Science, 307 (2005) 370-373.

[100] J. Florez, K. Jablonski, N. Bayley, T. Pollin, P. De Bakker, A. Shuldiner, W. Knowler, D. Nathan, D. Altshuler, TCF7L2 polymorphisms and progression to diabetes in the Diabetes Prevention Program, New England Journal of Medicine, 355 (2006) 241-250.

[101] S. Grant, G. Thorleifsson, I. Reynisdottir, R. Benediktsson, A. Manolescu, J. Sainz, A. Helgason, H. Stefansson, V. Emilsson, A. Helgadottir, U. Styrkarsdottir, K. Magnusson, G. Walters, E. Palsdottir, T. Jonsdottir, T. Gudmundsdottir, A. Gylfason, J. Saemundsdottir, R. Wilensky, M. Reilly, D. Rader, Y. Bagger, C. Christiansen, V. Gudnason, G. Sigurdsson, U. Thorsteinsdottir, J. Gulcher, A. Kong, K. Stefansson, Variant of transcription factor 7-like 2 (TCF7L2) gene confers risk of type 2 diabetes, Nature Genetics, 38 (2006) 320-323.

[102] K. Owen, M. McCarthy, Genetics of type 2 diabetes, Current Opinion in Genetics and Development, 17 (2007) 239-244.

[103] D. Dabelea, R. Hanson, R. Lindsay, D. Pettitt, G. Imperatore, M. Gabir, J. Roumain, P. Bennett, W. Knowler, Intrauterine exposure to diabetes conveys risks for type 2 diabetes and obesity: A study of discordant sibships, Diabetes, 49 (2000) 2208-2211.

[104] K. Ong, M. Ahmed, D. Dunger, P. Emmett, M. Preece, Association between postnatal catch-up growth and obesity in childhood: A prospective cohort study, British Medical Journal, 320 (2000) 967-971.

[105] J. Jimenez-Chillaron, M. Patti, To catch up or not to catch up: Is this the question? Lessons from animal models, Current Opinion in Endocrinology, Diabetes and Obesity, 14 (2007) 23-29.

[106] J. Jimenez-Chillaron, M. Hernandez-Valencia, A. Lightner, R. Faucette, C. Reamer, R. Przybyla, S. Ruest, K. Barry, J. Otis, M. Patti, Reductions in caloric intake and early postnatal growth prevent glucose intolerance and obesity associated with low birthweight, Diabetologia, 49 (2006) 1974-1984.

[107] M. Lazar, How obesity causes diabetes: Not a tall tale, Science, 307 (2005) 373-375.

[108] T. Graham, Q. Yang, M. Blüher, A. Hammarstedt, T. Ciaraldi, R. Henry, C. Wason, A. Oberbach, P. Jansson, U. Smith, B. Kahn, Retinol-binding protein 4 and insulin resistance in lean, obese, and diabetic subjects, New England Journal of Medicine, 354 (2006) 2552-2563.

[109] K. Wellen, G. Hotamisligil, Inflammation, stress, and diabetes, Journal of Clinical Investigation, 115 (2005) 1111-1119.

[110] S. Shoelson, J. Lee, A. Goldfine, Inflammation and insulin resistance, Journal of Clinical Investigation, 116 (2006) 1793-1801.

[111] S. Gesta, Y. Tseng, C. Kahn, Developmental Origin of Fat: Tracking obesity to its source, Cell, 131 (2007) 242-256.

[112] J. Manson, M. Stampfer, G. Colditz, W. Willett, B. Rosner, C. Hennekens, F. Speizer, E. Rimm, A. Krolewski, Physical activity and incidence of non-insulin-dependent diabetes mellitus in women, The Lancet, 338 (1991) 774-778.

[113] W. Kerr, E. Williams, L. Li, C. Lui, Y. Ye, T. Greenfield, E. Lown, Alcohol use patterns and risk of diabetes onset in the 1979 National Longitudinal Survey of Youth Cohort, Preventive Medicine, 109 (2018) 22-27.

[114] I. Wakabayashi, Chapter 16 - Relationships of Alcohol Consumption With Risks for Type 2 Diabetes Mellitus and Cardiovascular Disease in Men and Women A2 - Watson, Ronald Ross, in: S. Zibadi (Ed.) Lifestyle in Heart Health and Disease, Academic Press (2018) 213-221.

[115] R. Fagard, P. Nilsson, Smoking and diabetes—The double health hazard, Primary Care Diabetes, 3 (2009) 205-209.

[116] J. Maddatu, E. Anderson-Baucum, C. Evans-Molina, Smoking and the risk of type 2 diabetes, Translational Research, 184 (2017) 101-107.

[117] J. Wang, R. Liu, M. Hawkins, N. Barzilial, L. Rossetti, A nutrient-sensing pathway regulates leptin gene expression in muscle and fat, Nature, 393 (1998) 684-688.

[118] M. Patti, A. Virkamäki, E. Landaker, C. Kahn, H. Yki-Järvinen, Activation of the hexosamine pathway by glucosamine in vivo induces insulin resistance of early post-receptor insulin signaling events in skeletal muscle, Diabetes, 48 (1999) 1562-1571.

[119] W. Jin, M. Patti, Genetic determinants and molecular pathways in the pathogenesis of Type 2 diabetes, Clinical Science, 116 (2009) 99-111.

[120] O. Maddocks, C. Labuschagne, P. Adams, K. Vousden, Serine metabolism supports the methionine cycle and DNA/RNA methylation through De Novo ATP synthesis in cancer cells, Molecular Cell, 61 (2016) 210-221.

[121] W. Srimahaprom, A. Flood, Crystal growth rates and optical resolution of dl-methionine hydrochloride by preferential crystallization from aqueous solution, Journal of Crystal Growth, 362 (2013) 88-92.

[122] P. Garlick, Toxicity of methionine in humans, The Journal of nutrition, 136 (2006) 1722S-1725S.

[123] H. Jinnah, R. Sabina, G. Van Den Berghe, Metabolic disorders of purine metabolism affecting the nervous system, Handbook of clinical neurology, 113 (2013) 1827-1836.

[124] A. Chico, A. Pérez, A. Córdoba, R. Arcelús, G. Carreras, A. de Leiva, F. González-Sastre, F. Blanco-Vaca, Plasma homocysteine is related to albumin excretion rate in patients with diabetes mellitus: a new link between diabetic nephropathy and cardiovascular disease, Diabetologia, 41 (1998) 684-693.

[125] E. Hoogeveen, P. Kostense, P. Beks, A. Mackaay, C. Jakobs, L. Bouter, R. Heine, C. Stehouwer, Hyperhomocysteinemia is associated with an increased risk of cardiovascular disease, especially in non–insulin-dependent diabetes mellitus, Arteriosclerosis, Thrombosis, and Vascular Biology, 18 (1998) 133-138.

[126] P. Tessari, A. Coracina, E. Kiwanuka, M. Vedovato, M. Vettore, A. Valerio, M. Zaramella, G. Garibotto, Effects of insulin on methionine and homocysteine kinetics in type 2 diabetes with nephropathy, Diabetes, 54 (2005) 2968-2976.

[127] M. Malinow, A. Bostom, R. Krauss, Homocysteine, Diet, and Cardiovascular Diseases, A Statement for Healthcare Professionals From the Nutrition Committee, American Heart Association, 99 (1999) 178-182.

[128] L. Sweetman, W.. Nyhan, Excretion of hypoxanthine and xanthine in a genetic disease of purine metabolism, Nature, 215 (1967) 859-860.

[129] M. Alderman, K. Aiyer, Uric acid: Role in cardiovascular disease and effects of losartan, Current Medical Research and Opinion, 20 (2004) 369-379.

[130] E. Liberopoulos, D. Christides, M. Elisaf, Comparative effects of losartan and irbesartan on serum uric acid in hypertensive patients with hyperuricemia and gout, Journal of Hypertension, 20 (2002) 347.

[131] R. Johnson, D. Kang, D. Feig, S. Kivlighn, J. Kanellis, S. Watanabe, K. Tuttle, B. Rodriguez-Iturbe, J. Herrera-Acosta, M. Mazzali, Is there a pathogenetic role for uric acid in hypertension and cardiovascular and renal disease?, Hypertension, 41 (2003) 1183-1190.

[132] W. Waring, D. Webb, S. Maxwell, Uric acid as a risk factor for cardiovascular disease, Quarterly Journal of Medicine (QJM) - Monthly Journal of the Association of Physicians, 93 (2000) 707-713.

[133] P. Klemp, S. Stansfield, B. Castle, M. Robertson, Gout is on the increase in New Zealand, Annals of the Rheumatic Diseases, 56 (1997) 22-26.

[134] D. Lakshmi, M.. Whitcombe, F. Davis, P. Sharma, B. Prasad, Electrochemical detection of uric acid in mixed and clinical samples: A Review, Electroanalysis, 23 (2011) 305-320.

[135] I. Hisatome, M. Tsuboi, C. Shigemasa, Renal hypouricemia, Nippon Rinsho. Japanese Journal of Clinical Medicine, 54 (1996) 3337-3342.

[136] V. Sharma, F. Jelen, L. Trnkova, Functionalized solid electrodes for electrochemical biosensing of purine nucleobases and their analogs: A review, Sensors (Switzerland), 15 (2015) 1564-1600.

[137] D. Butterfield, A. Bush, Alzheimer's amyloid β-peptide (1-42): Involvement of methionine residue 35 in the oxidative stress and neurotoxicity properties of this peptide, Neurobiology of Aging, 25 (2004) 563-568.

[138] D. Butterfield, J. Kanski, Methionine residue 35 is critical for the oxidative stress and neurotoxic properties of Alzheimer's amyloid β-peptide 1-42, Peptides, 23 (2002) 1299-1309.

[139] C. Schöneich, Redox processes of methionine relevant to β-amyloid oxidation and Alzheimer's disease, Archives of Biochemistry and Biophysics, 397 (2002) 370-376.

[140] C. Glaser, G. Yamin, V. Uversky, A. Fink, Methionine oxidation, α-synuclein and Parkinson's disease, Biochimica et Biophysica Acta (BBA) - Proteins and Proteomics, 1703 (2005) 157-169.

[141] W. Zhou, C. Long, S. Reaney, D. Di Monte, A. Fink, V. Uversky, Methionine oxidation stabilizes non-toxic oligomers of α-synuclein through strengthening the auto-inhibitory intra-molecular long-range interactions, Biochimica et Biophysica Acta (BBA) - Molecular Basis of Disease, 1802 (2010) 322-330.

[142] L. Nesti, A. Natali, Metformin effects on the heart and the cardiovascular system: A review of experimental and clinical data, Nutrition, Metabolism and Cardiovascular Diseases, 27 (2017) 657-669.

[143] M. Maiorino, G. Bellastella, D. Giugliano, K. Esposito, Can diet prevent diabetes?, Journal of Diabetes and its Complications, 31 (2017) 288-290.

[144] M. Siomos, M. Andreoni, S. Buchholz, K. Dickins, A Guide to Physical Activity for Individuals With Diabetes, The Journal for Nurse Practitioners, 13 (2017) 82-88.

[145] P. Cavuoto, M. Fenech, A review of methionine dependency and the role of methionine restriction in cancer growth control and life-span extension, Cancer Treatment Reviews, 38 (2012) 726-736.

[146] E. Cellarier, X. Durando, M. Vasson, M. Farges, A. Demiden, J. Maurizis, J. Madelmont, P. Chollet, Methionine dependency and cancer treatment, Cancer Treatment Reviews, 29 (2003) 489-499.

[147] K. Borowczyk, G. Chwatko, P. Kubalczyk, H. Jakubowski, J. Kubalska, R. Głowacki, Simultaneous Determination of Methionine and Homocysteine by on-column derivatization with o-phtaldialdehyde, Talanta, 161 (2016) 917-924.

[148] Y. Jiang, B. Mistretta, S. Elsea, Q. Sun, Simultaneous determination of plasma total homocysteine and methionine by liquid chromatography-tandem mass spectrometry, Clinica Chimica Acta, 464 (2017) 93-97.

[149] Z. Deáková, Z. Ďuračková, D. Armstrong, J. Lehotay, Two-dimensional high-performance liquid chromatography for determination of homocysteine,

methionine and cysteine enantiomers in human serum, Journal of Chromatography A, 1408 (2015) 118-124.

[150] L. Kuang, L. Zhang, A. Xu, Z. Li, R. Liang, J. Qiu, Bio-dots assembly-induced aggregation of gold nanoparticles for highly sensitive and selective colorimetric detection of methionine, Sensors and Actuators B: Chemical, 244 (2017) 1031-1036.

[151] M. Zhou, A. Wang, C. Li, X. Luo, Y. Ma, Flow-based determination of methionine in pharmaceutical formulations exploiting TGA-capped CdTe quantum dots for enhancing the luminol-KIO4 chemiluminescence, Journal of Luminescence, 183 (2017) 206-211.

[152] M. Murugavelu, B. Karthikeyan, Synthesis, characterization of Ag-Au core-shell bimetal nanoparticles and its application for electrocatalytic oxidation/sensing of l-methionine, Materials Science and Engineering: C, 70 (2017) 656-664.

[153] D. Zhang, C. Xu, S. Li, R. Zhang, H. Yan, H. Miao, Y. Fan, B. Yuan, Electrochemically controlling oxygen functional groups in graphene oxide for the optimization in the electrocatalytic oxidation of dihydroxybenzene isomers and L-methionine, Journal of Electroanalytical Chemistry, 717-718 (2014) 219-224.

[154] B. Prasad, I. Pandey, A. Srivastava, D. Kumar, M. Tiwari, Multiwalled carbon nanotubes-based pencil graphite electrode modified with an electrosynthesized molecularly imprinted nanofilm for electrochemical sensing of methionine enantiomers, Sensors and Actuators, B: Chemical, 176 (2013) 863-874.

[155] F. Chekin, S. Bagheri, S. Abd Hamid, Synthesis of Pt-doped TiO_2 nanoparticles: Characterization and application for electrocatalytic oxidation of l-methionine, Sensors and Actuators, B: Chemical, 177 (2013) 898-903.

[156] A. Jeevagan, S. John, Electrochemical determination of l-methionine using the electropolymerized film of non-peripheral amine substituted Cu(II) phthalocyanine on glassy carbon electrode, Bioelectrochemistry, 85 (2012) 50-55.

[157] K.. Stone, D. Wanders, M. Orgeron, C. Cortez, T. Gettys, Mechanisms of increased in vivo insulin sensitivity by dietary methionine restriction in mice, Diabetes, 63 (2014) 3721-3733.

[158] G. Ables, J. Johnson, Pleiotropic responses to methionine restriction, Experimental Gerontology, 94 (2017) 83-88.

[159] K. Stone, D. Wanders, L. Calderon, S. Spurgin, P. Scherer, T. Gettys, Compromised responses to dietary methionine restriction in adipose tissue but not liver of ob/ob mice, Obesity (Silver Spring, Md.), 23 (2015) 1836-1844.

[160] R. Theuer, Effect of essential amino acid restriction on the growth of female C57BL mice and their implanted BW10232 adenocarcinomas, Journal of Nutrition, 101 (1971) 223-232.

[161] T. Hoshi, S. Heinemann, Regulation of cell function by methionine oxidation and reduction, The Journal of Physiology, 531 (2001) 1-11.

[162] P. Huang, N. Gao, J. Li, F. Wu, Colorimetric detection of methionine based on anti-aggregation of gold nanoparticles in the presence of melamine, Sensors and Actuators B: Chemical, 255 (2018) 2779-2784.

[163] I. Shakir, N. Turkey, R. Hassan, Determination of methionine via chemiluminescence-continuous flow injection analysis, Kerbala Journal of Pharmaceutical Science, 4 (2012) 191-204.

[164] Y. Wang, S. Liu, Z. Liu, J. Yang, X. Hu, A l-tryptophan-Cu(II) based fluorescence turn-on probe for detection of methionine, Journal of Luminescence, 147 (2014) 107-110.

[165] Y. Jiang, R. Shen, G. Wei, Y. Cheng, B. Wang, A New fluorescent probe based on rhodamine derivative for detection of both Cu^{2+} and l-Methionine and living cells imaging, Tetrahedron, 72 (2016) 2354-2358.

[166] A. Zinellu, S. Sotgia, M. Usai, E. Zinellu, A. Posadino, L. Gaspa, R. Chessa, A. Pinna, F. Carta, L. Deiana, C. Carru, Plasma methionine determination by capillary electrophoresis–UV assay: Application on patients affected by retinal venous occlusive disease, Analytical Biochemistry, 363 (2007) 91-96.

[167] J. Bártl, P. Chrastina, J. Krijt, J. Hodík, K. Pešková, V. Kožich, Simultaneous determination of cystathionine, total homocysteine, and methionine in dried blood spots by liquid chromatography/tandem mass spectrometry and its utility for the management of patients with homocystinuria, Clinica Chimica Acta, 437 (2014) 211-217.

[168] R. Mashima, T. Nakanishi-Ueda, Y. Yamamoto, Simultaneous determination of methionine sulfoxide and methionine in blood plasma using gas chromatography-mass spectrometry, Analytical Biochemistry, 313 (2003) 28-33.

[169] J. Wang, Electrochemical glucose biosensors, Chemical Reviews, 108 (2008) 814-825.

[170] J. Liu, C. Guo, C. Li, Y. Li, Q. Chi, X. Huang, L. Liao, T. Yu, Carbon-decorated ZnO nanowire array: A novel platform for direct electrochemistry of enzymes and biosensing applications, Electrochemistry Communications, 11 (2009) 202-205.

[171] Y. Xiao, F. Patolsky, E. Katz, J. Hainfeld, I. Willner, Plugging into enzymes: Nanowiring of redox enzymes by a gold nanoparticle, Science, 299 (2003) 1877-1881.

[172] M. Beluomini, J. da Silva, G. Sedenho, N. Stradiotto, D-mannitol sensor based on molecularly imprinted polymer on electrode modified with reduced graphene oxide decorated with gold nanoparticles, Talanta, 165 (2017) 231-239.

[173] N. Ismail, Q. Le, H. Yoshikawa, M. Saito, E. Tamiya, Development of Non-enzymatic electrochemical glucose sensor based on graphene oxide nanoribbon – gold nanoparticle hybrid, Electrochimica Acta, 146 (2014) 98-105.

[174] A. Kawde, M. Aziz, M. El-Zohri, N. Baig, N. Odewunmi, Cathodized Gold Nanoparticle-Modified Graphite Pencil Electrode for Non-Enzymatic Sensitive Voltammetric Detection of Glucose, Electroanalysis, 29 (2017) 1214-1221.

[175] S. Pourbeyram, K. Mehdizadeh, Nonenzymatic glucose sensor based on disposable pencil graphite electrode modified by copper nanoparticles, Journal of Food and Drug Analysis, 24 (2016) 894-902.

[176] Y. Zhao, J. Zhao, D. Ma, Y. Li, X. Hao, L. Li, C. Yu, L. Zhang, Y. Lu, Z. Wang, Synthesis, growth mechanism of different Cu nanostructures and their application for non-enzymatic glucose sensing, Colloids and Surfaces A: Physicochemical and Engineering Aspects, 409 (2012) 105-111.

[177] Y. Zhong, T. Shi, Z. Liu, S. Cheng, Y. Huang, X. Tao, G. Liao, Z. Tang, Ultrasensitive non-enzymatic glucose sensors based on different copper oxide nanostructures by in-situ growth, Sensors and Actuators B: Chemical, 236 (2016) 326-333.

[178] N. Baig, A. Kawde, A cost-effective disposable graphene-modified electrode decorated with alternating layers of Au NPs for the simultaneous detection of dopamine and uric acid in human urine, RSC Advances, 6 (2016) 80756-80765.

[179] A. Kawde, M. Aziz, N. Baig, Y. Temerk, A facile fabrication of platinum nanoparticle-modified graphite pencil electrode for highly sensitive detection of hydrogen peroxide, Journal of Electroanalytical Chemistry, 740 (2015) 68-74.

[180] M. Aziz, A. Kawde, Gold nanoparticle-modified graphite pencil electrode for the high-sensitivity detection of hydrazine, Talanta, 115 (2013) 214-221.

[181] A. Kawde, M. Aziz, Porous Copper-Modified Graphite Pencil Electrode for the Amperometric Detection of 4-Nitrophenol, Electroanalysis, 26 (2014) 2484-2490.

[182] M. Akanda, M. Sohail, M. Aziz, A. Kawde, Recent Advances in Nanomaterial-Modified Pencil Graphite Electrodes for Electroanalysis, Electroanalysis, 28 (2015) 408-424.

[183] J. Wang, A. Kawde, Pencil-based renewable biosensor for label-free electrochemical detection of DNA hybridization, Analytica Chimica Acta, 431 (2001) 219-224.

[184] C. Giacomelli, F. Giacomelli, A. Santana, V. Schmidt, A. Pires, J. Bertolino, A. Spinelli, Interaction of poly(4-vinylpyridine) with copper surfaces:

electrochemical, thermal and spectroscopic studies, Journal of the Brazilian Chemical Society, 15 (2004) 818-824.

[185] R. Gonçalves, A. Lucho, Electrochemical studies of copper in N-N, dimethylformamide in the presence of water, ethanol and acetic acid as additives, Journal of the Brazilian Chemical Society, 11 (2000) 486-490.

[186] Y. Liu, Z. Wang, X. He, M. Shao, M. Li, One unexpected mixed-valence Cu(I,II)-cyanide coordination polymer in situ originating from the cleavage of acetonitrile, Inorganic Chemistry Communications, 80 (2017) 46-48.

[187] K. Tang, X. Wang, W. Yan, J. Yu, R. Xu, Fabrication of superhydrophilic Cu_2O and CuO membranes, Journal of Membrane Science, 286 (2006) 279-284.

[188] B.V. Crist, Handbooks of monochromatic XPS spectra, the element and native oxides, XPS International incorporation LLC, mountain view, California USA (1999) 313-362.

[189] D. Dhar, W. Tolman, Hydrogen Atom Abstraction from Hydrocarbons by a Copper(III)-hydroxide complex, Journal of the American Chemical Society, 137 (2015) 1322-1329.

[190] M. Taki, H. Kumei, S. Itoh, S. Fukuzumi, Hydrogen atom abstraction by Cu(II)- and Zn(II)-phenoxyl radical complexes, models for the active form of galactose oxidase, Journal of Inorganic Biochemistry, 78 (2000) 1-5.

[191] J. Yang, W. Zhang, S. Gunasekaran, An amperometric non-enzymatic glucose sensor by electrodepositing copper nanocubes onto vertically well-aligned multi-walled carbon nanotube arrays, Biosensors and Bioelectronics, 26 (2010) 279-284.

[192] H. Wu, W. Cao, Y. Li, G. Liu, Y. Wen, H. Yang, S. Yang, In situ growth of copper nanoparticles on multiwalled carbon nanotubes and their application as non-enzymatic glucose sensor materials, Electrochimica Acta, 55 (2010) 3734-3740.

[193] J. Luo, H. Zhang, S. Jiang, J. Jiang, X. Liu, Facile one-step electrochemical fabrication of a non-enzymatic glucose-selective glassy carbon electrode modified with copper nanoparticles and graphene, Microchimica Acta, 177 (2012) 485-490.

[194] Y. Zhang, L. Su, D. Manuzzi, H. de los Monteros, W. Jia, D. Huo, C. Hou, Y. Lei, Ultrasensitive and selective non-enzymatic glucose detection using copper nanowires, Biosensors and Bioelectronics, 31 (2012) 426-432.

[195] Z. Zhuang, X. Su, H. Yuan, Q. Sun, D. Xiao, M. Choi, An improved sensitivity non-enzymatic glucose sensor based on a CuO nanowire modified Cu electrode, Analyst, 133 (2008) 126-132.

[196] Z. Wu, L. Xie, Y. Xiao, D. Wang, Silver wrapped MoS_2 hybrid electrode materials for high-performance supercapacitor, Journal of Alloys and Compounds, 708 (2017) 763-768.

[197] K. Devarayan, J. Park, H. Kim, B. Kim, Facile green synthesis of silver nanodendrite/cellulose acetate thin film electrodes for flexible supercapacitors, Carbohydrate Polymers, 163 (2017) 153-161.

[198] M. Mirzaeian, A. Ogwu, H. Jirandehi, S. Aidarova, Z. Ospanova, N. Tsendzughul, Surface characteristics of silver oxide thin film electrodes for supercapacitor applications, Colloids and Surfaces A: Physicochemical and Engineering Aspects, 519 (2017) 223-230.

[199] K. Aoshima, S. Arai, K. Fukuhara, T. Yamada, T. Hasegawa, Surface modification of printed silver electrodes for efficient carrier injection in organic thin-film transistors, Organic Electronics, 41 (2017) 137-142.

[200] E. Jung, C. Kim, M. Kim, H. Chae, J. Cho, S. Cho, Roll-to-roll preparation of silver-nanowire transparent electrode and its application to large-area organic light-emitting diodes, Organic Electronics, 41 (2017) 190-197.

[201] Y. Lee, M. Suh, K. Kim, H. Kim, D. Kim, H. Chang, D. Lee, Y. Kim, S. Kim, D. Jeon, Conjugated polyelectrolyte-assisted vacuum-free transfer-printing of silver nanowire network for top electrode of polymer light-emitting diodes, Organic Electronics, 43 (2017) 64-69.

[202] S. Ghasemi, S. Hosseini, F. Mousavi, Electrophoretic deposition of graphene nanosheets: A suitable method for fabrication of silver-graphene counter electrode for dye-sensitized solar cell, Colloids and Surfaces A: Physicochemical and Engineering Aspects, 520 (2017) 477-487.

[203] F. Quan, M. Xiong, F. Jia, L. Zhang, Efficient electroreduction of CO_2 on bulk silver electrode in aqueous solution via the inhibition of hydrogen evolution, Applied Surface Science, 399 (2017) 48-54.

[204] Y. Feng, H. Liu, P. Wang, F. Ye, Q. Tan, J. Yang, Enhancing the electrocatalytic property of hollow structured platinum nanoparticles for methanol oxidation through a hybrid construction, Scientific Reports, 4 (2014) 6204-6210.

[205] K. Promsuwan, P. Thavarungkul, P. Kanatharana, W. Limbut, Flow injection amperometric nitrite sensor based on silver microcubics-poly (acrylic acid)/poly

(vinyl alcohol) modified screen-printed carbon electrode, Electrochimica Acta, 232 (2017) 357-369.

[206] O. Vajdle, V. Guzsvány, D. Škorić, J. Csanádi, M. Petković, M. Avramov-Ivić, Z. Kónya, S. Petrović, A. Bobrowski, Voltammetric behavior and determination of the macrolide antibiotics azithromycin, clarithromycin and roxithromycin at a renewable silver – amalgam film electrode, Electrochimica Acta, 229 (2017) 334-344.

[207] P. Arul, S.. John, Silver nanoparticles built-in zinc metal-organic framework modified electrode for the selective non-enzymatic determination of H_2O_2, Electrochimica Acta, 235 (2017) 680-689.

[208] S. Lee, H. Lim, I. Ibrahim, A. Jamil, A. Pandikumar, N. Huang, Horseradish peroxidase-labeled silver/reduced graphene oxide thin film-modified screen-printed electrode for detection of carcinoembryonic antigen, Biosensors and Bioelectronics, 89 (2017) 673-680.

[209] K. Rawat, S. Kailasa, 4-Amino nicotinic acid-mediated synthesis of gold nanoparticles for visual detection of arginine, histidine, methionine and tryptophan, Sensors and Actuators, B: Chemical, 222 (2016) 780-789.

[210] E. Molaakbari, A. Mostafavi, H. Beitollahi, Simultaneous electrochemical determination of dopamine, melatonin, methionine and caffeine, Sensors and Actuators, B: Chemical, 208 (2015) 195-203.

[211] A. Salimi, M. Roushani, Electrocatalytic oxidation of sulfur-containing amino acids at renewable Ni-powder doped carbon ceramic electrode: Application to

amperometric detection l-cystine, l-cysteine and l-methionine, Electroanalysis, 18 (2006) 2129-2136.

[212] Y. Wan, X. Wang, S. Liu, Y. Li, H. Sun, Q. Wang, Effect of electrochemical factors on formation and reduction of silver oxides, International Journal of Electrochemical Science, 8 (2013) 12837-12850.

[213] K. Hiller, B. Masloch, M. Göbl, K. Asmus, Mechanism of the OH· radical-induced oxidation of methionine in aqueous solution, Journal of the American Chemical Society, 103 (1981) 2734-2743.

[214] K. Hiller, K. Asmus, Tl^{2+} and Ag^{2+} metal-ion-induced oxidation of methionine in aqueous solution. A pulse radiolysis study, International Journal of Radiation Biology and Related Studies in Physics, Chemistry and Medicine, 40 (1981) 597-604.

[215] G. Hoflund, Z. Hazos, G. Salaita, Surface characterization study of Ag, AgO, and Ag_2O using X-ray photoelectron spectroscopy and electron energy-loss spectroscopy, Physical Review B, 62 (2000) 11126-11133.

[216] R. Rebelo, S. Calderon, R. Fangueiro, M. Henriques, S. Carvalho, Influence of oxygen content on the antibacterial effect of Ag-O coatings deposited by magnetron sputtering, Surface and Coatings Technology, 305 (2016) 1-10.

[217] S. Holmstrom, J. Cox, Electrocatalysis at a conducting composite electrode doped with a ruthenium(II) metallodendrimer, Analytical Chemistry, 72 (2000) 3191-3195.

[218] L. Agüí, J. Manso, P. Yáñez-Sedeño, J. Pingarrón, Colloidal-gold cysteamine-modified carbon paste electrodes as suitable electrode materials for the

electrochemical determination of sulphur-containing compounds: Application to the determination of methionine, Talanta, 64 (2004) 1041-1047.

[219] W. Tan, J. Goh, Electrochemical oxidation of methionine mediated by a fullerene-C 60 modified gold electrode, Electroanalysis, 20 (2008) 2447-2453.

[220] M. Gómez-Mingot, J. Iniesta, V. Montiel, R. Kadara, C. Banks, Direct oxidation of methionine at screen printed graphite microelectrodes: Towards rapid sensing platforms, Sensors and Actuators, B: Chemical, 155 (2011) 831-836.

[221] O. Baturina, Q. Lu, F. Xu, A. Purdy, B. Dyatkin, X. Sang, R. Unocic, T. Brintlinger, Y. Gogotsi, Effect of nanostructured carbon support on copper electrocatalytic activity toward CO_2 electroreduction to hydrocarbon fuels, Catalysis Today, 288 (2017) 2-10.

[222] Z. Xiong, B. Yan, K. Zhang, C. Wang, S. Li, H. Xu, Y. Du, C. Zhai, A facile synthesis of 3D network PdCu nanostructure with enhanced electrocatalytic activity towards ethanol oxidation, Journal of the Taiwan Institute of Chemical Engineers, 75 (2017) 12-17.

[223] G. Karim-Nezhad, P. Seyed Dorraji, Copper chloride modified copper electrode: Application to electrocatalytic oxidation of methanol, Electrochimica Acta, 55 (2010) 3414-3420.

[224] G. Karim-Nezhad, B. Dizajdizi, P. Dorraji, Electrocatalytic oxidation of ethanol at copper bromide modified copper electrode in comparison to bare and copper chloride modified copper electrodes, Catalysis Communications, 12 (2011) 906-909.

[225] R. Abbasi, K. Farhadi, S. Banisaeid, N. Pesyan, A. Jamali, F. Rahmani, Electrosynthesized polytyramine-copper oxalate nanocomposite on copper electrode for electrocatalytic oxidation of methanol in alkaline medium, Chinese Journal of Catalysis, 35 (2014) 1098-1104.

[226] M. Sun, C. Zhai, J. Hu, M. Zhu, J. Pan, Plasmon-enhanced electrocatalytic oxidation of ethanol and organic contaminants on gold/copper iodide composites under visible light irradiation, Journal of Colloid and Interface Science, 511 (2018) 110-118.

[227] A. Ourari, B. Ketfi, S. Malha, A. Amine, Electrocatalytic reduction of nitrite and bromate and their highly sensitive determination on carbon paste electrode modified with new copper Schiff base complex, Journal of Electroanalytical Chemistry, 797 (2017) 31-36.

[228] B. Dinesh, R. Saraswathi, Electrochemical synthesis of nanostructured copper-curcumin complex and its electrocatalytic application towards reduction of 4-nitrophenol, Sensors and Actuators B: Chemical, 253 (2017) 502-512.

[229] M. Farsak, E. Telli, F. Tezcan, F. Akgül, A. Yüce, G. Kardaş, The electrocatalytic properties of lithium copper composite in the oxygen reduction reaction, Electrochimica Acta, 148 (2014) 276-282.

[230] K. Liu, Y. Song, S. Chen, Electrocatalytic activities of alkyne-functionalized copper nanoparticles in oxygen reduction in alkaline media, Journal of Power Sources, 268 (2014) 469-475.

[231] S. Hosseini, S. Ghasemi, S. Ghasemi, Effect of surfactants on electrocatalytic performance of copper nanoparticles for hydrogen evolution reaction, Journal of Molecular Liquids, 222 (2016) 1068-1075.

[232] P. Mayuri, N. Saravanan, A. Senthil Kumar, A bioinspired copper 2,2-bipyridyl complex immobilized MWCNT modified electrode prepared by a new strategy for elegant electrocatalytic reduction and sensing of hydrogen peroxide, Electrochimica Acta, 240 (2017) 522-533.

[233] A. Brzózka, D. Szeliga, E. Kurowska-Tabor, G. Sulka, Synthesis of copper nanocone array electrodes and its electrocatalytic properties toward hydrogen peroxide reduction, Materials Letters, 174 (2016) 66-70.

[234] M. Thorseth, C. Letko, E. Tse, T. Rauchfuss, A. Gewirth, Ligand effects on the overpotential for dioxygen reduction by tris(2-pyridylmethyl)amine derivatives, Inorganic Chemistry, 52 (2013) 628-634.

[235] M. Asahi, S. Yamazaki, S. Itoh, T. Ioroi, Electrochemical reduction of dioxygen by copper complexes with pyridylalkylamine ligands dissolved in aqueous buffer solution: The relationship between activity and redox potential, Dalton Transactions, 43 (2014) 10705-10709.

[236] P. Gayathri, A. Senthil Kumar, Electrochemical behavior of the 1,10-phenanthroline ligand on a multiwalled carbon nanotube surface and its relevant electrochemistry for selective recognition of copper ion and hydrogen peroxide sensing, Langmuir, 30 (2014) 10513-10521.

[237] S. Baskar, J. Chang, J. Zen, Extremely stable copper-polymelamine composite material for amperometric hydrogen peroxide sensing, Journal of Polymer Science, Part B: Polymer Physics, 51 (2013) 1639-1646.

[238] Y. Xi, P. Wei, R. Wang, J. Liu, Bio-inspired multinuclear copper complexes covalently immobilized on reduced graphene oxide as efficient electrocatalysts for the oxygen reduction reaction, Chemical Communications, 51 (2015) 7455-7458.

[239] B. Luo, X. Li, J. Yang, L. Xue, J. Gu, M. Wang, L. Jiang, Non-enzymatic electrochemical sensors for the detection of hydrogen peroxide based on Cu2O/Cu nanocomposites, Analytical Methods, 6 (2014) 1114-1120.

[240] X. Wang, B. Chen, H. Lin, H. Hu, J. Li, Synthesis, structure, electrochemistry and electrocatalysis of a new copper(II) complex: $[Cu_2(bpp)(\mu\text{-}CH_3COO)_4] \cdot 2H_2O$ [bpp = 1,3-bis(4-pyridyl)propane], Transition Metal Chemistry, 34 (2009) 307-312.

[241] J. Zhang, F. Anson, Complexes of Cu(II) with electroactive chelating ligands adsorbed on graphite electrodes: Surface coordination chemistry and electrocatalysis, Journal of Electroanalytical Chemistry, 348 (1993) 81-97.

[242] J. Zhang, F. Anson, Electrocatalysts for the reduction of O_2 and H_2O_2 based on complexes of Cu(II) with the strongly adsorbing 2,9-dimethyl-1,10-phenanthroline ligand, Electrochimica Acta, 38 (1993) 2423-2429.

[243] L. Zhang, H. Li, Y. Ni, J. Li, K. Liao, G. Zhao, Porous cuprous oxide microcubes for non-enzymatic amperometric hydrogen peroxide and glucose sensing, Electrochemistry Communications, 11 (2009) 812-815.

[244] Q. Xu, Y. Zhao, J. Xu, J. Zhu, Preparation of functionalized copper nanoparticles and fabrication of a glucose sensor, Sensors and Actuators, B: Chemical, 114 (2006) 379-386.

[245] A. Korshunov, M. Heyrovský, Electrochemical behavior of copper metal core/oxide shell ultra-fine particles on mercury electrodes in aqueous dispersions, Journal of Electroanalytical Chemistry, 629 (2009) 23-29.

[246] S. Annamalai, B. Palani, K. Chandrasekara Pillai, Highly stable and redox active nano copper species stabilized functionalized-multiwalled carbon nanotube/chitosan modified electrode for efficient hydrogen peroxide detection, Colloids and Surfaces A: Physicochemical and Engineering Aspects, 395 (2012) 207-216.

[247] E. Caussé, A. Pradelles, B. Dirat, A. Negre-Salvayre, R. Salvayre, F. Couderc, Simultaneous determination of allantoin, hypoxanthine, xanthine, and uric acid in serum/plasma by Capillary electrophoresis, Electrophoresis, 28 (2007) 381-387.

[248] N. Cooper, R. Khosravan, C. Erdmann, J. Fiene, J. Lee, Quantification of uric acid, xanthine and hypoxanthine in human serum by HPLC for pharmacodynamic studies, Journal of Chromatography B: Analytical Technologies in the Biomedical and Life Sciences, 837 (2006) 1-10.

[249] Z. Wang, X. Dong, J. Li, An inlaying ultra-thin carbon paste electrode modified with functional single-wall carbon nanotubes for simultaneous determination of three purine derivatives, Sensors and Actuators, B: Chemical, 131 (2008) 411-416.

[250] R. Ojani, A. Alinezhad, Z. Abedi, A highly sensitive electrochemical sensor for simultaneous detection of uric acid, xanthine and hypoxanthine based on poly(l-

methionine) modified glassy carbon electrode, Sensors and Actuators B: Chemical, 188 (2013) 621-630.

[251] R. Thangaraj, A. Kumar, Graphitized mesoporous carbon modified glassy carbon electrode for selective sensing of xanthine, hypoxanthine and uric acid, Analytical Methods, 4 (2012) 2162-2171.

[252] Y. Wang, L. Tong, Electrochemical sensor for simultaneous determination of uric acid, xanthine and hypoxanthine based on poly (bromocresol purple) modified glassy carbon electrode, Sensors and Actuators B: Chemical, 150 (2010) 43-49.

[253] J. Zen, Y. Lai, H. Yang, A. Senthil Kumar, Multianalyte sensor for the simultaneous determination of hypoxanthine, xanthine and uric acid based on a preanodized nontronite-coated screen-printed electrode, Sensors and Actuators B: Chemical, 84 (2002) 237-244.

[254] F. Zhang, Z. Wang, Y. Zhang, Z. Zheng, C. Wang, Y. Du, W. Ye, Simultaneous electrochemical determination of uric acid, xanthine and hypoxanthine based on poly(l-arginine)/graphene composite film modified electrode, Talanta, 93 (2012) 320-325.

[255] Y. Wang, Simultaneous determination of uric acid, xanthine and hypoxanthine at poly(pyrocatechol violet)/functionalized multi-walled carbon nanotubes composite film modified electrode, Colloids and Surfaces B: Biointerfaces, 88 (2011) 614-621.

[256] X. Liu, X. Ou, Q. Lu, J. Zhang, S. Chen, S. Wei, Electrochemical sensor based on overoxidized dopamine polymer and 3,4,9,10-perylenetetracarboxylic acid for

simultaneous determination of ascorbic acid, dopamine, uric acid, xanthine and hypoxanthine, RSC Advances, 4 (2014) 42632-42637.

[257] D. Lan, L. Zhang, Electrochemical synthesis of a novel purine-based polymer and its use for the simultaneous determination of dopamine, uric acid, xanthine and hypoxanthine, Journal of Electroanalytical Chemistry, 757 (2015) 107-115.

[258] A. Luo, Q. Lian, Z. An, Z. Li, Y. Guo, D. Zhang, Z. Xue, X. Zhou, X. Lu, Simultaneous determination of uric acid, xanthine and hypoxanthine based on sulfonic groups functionalized nitrogen-doped graphene, Journal of Electroanalytical Chemistry, 756 (2015) 22-29.

[259] N. Lavanya, C. Sekar, R. Murugan, G. Ravi, An ultrasensitive electrochemical sensor for simultaneous determination of xanthine, hypoxanthine and uric acid based on Co-doped CeO_2 nanoparticles, Materials Science and Engineering: C, 65 (2016) 278-286.

[260] M. Raj, S. John, Simultaneous determination of uric acid, xanthine, hypoxanthine and caffeine in human blood serum and urine samples using electrochemically reduced graphene oxide modified electrode, Analytica Chimica Acta, 771 (2013) 14-20.

[261] M. Frisch, G. Trucks, H. Schlegel, G. Scuseria, M. Robb, J. Cheeseman, G. Scalmani, V. Barone, B. Mennucci, G. Petersson, H. Nakatsuji, M. Caricato, X. Li, H. Hratchian, A. Izmaylov, J. Bloino, G. Zheng, J. Sonnenberg, M. Hada, M. Ehara, K. Toyota, R. Fukuda, J. Hasegawa, M. Ishida, T. Nakajima, Y. Honda, O. Kitao, H. Nakai, T. Vreven, J.. Montgomery Jr., J. Peralta, F. Ogliaro, M. Bearpark, J. Heyd, E. Brothers, K. Kudin, V. Staroverov, R. Kobayashi, J.

Normand, K. Raghavachari, A. Rendell, J. Burant, S. Iyengar, J. Tomasi, M. Cossi, N. Rega, J. Millam, M. Klene, J. Knox, J. Cross, V. Bakken, C. Adamo, J. Jaramillo, R. Gomperts, R. Stratmann, O. Yazyev, A. Austin, R. Cammi, C. Pomelli, J. Ochterski, R. Martin, K. Morokuma, V. Zakrzewski, G. Voth, P. Salvador, J. Dannenberg, S. Dapprich, A. Daniels, O. Farkas, J. Foresman, J. Ortiz, J. Cioslowski, D. Fox, Gaussian 09, Revision A.1, (2009).

[262] D. Brownson, C. Banks, Interpreting Electrochemistry, in: The handbook of graphene electrochemistry, Springer London, London (2014) 23-77.

[263] J. Yang, N. Hu, Direct electron transfer for hemoglobin in biomembrane-like dimyristoyl phosphatidylcholine films on pyrolytic graphite electrodes, Bioelectrochemistry and Bioenergetics, 48 (1999) 117-127.

[264] R. Wopschall, I. Shain, Effects of adsorption of electroactive species in stationary electrode polarography, Analytical Chemistry, 39 (1967) 1514-1527.

[265] S. Rebelo, A. Guedes, M. Szefczyk, A. Pereira, J. Araujo, C. Freire, Progress in the Raman spectra analysis of covalently functionalized multiwalled carbon nanotubes: unraveling disorder in graphitic materials, Physical Chemistry Chemical Physics, 18 (2016) 12784-12796.

[266] G. Rantitsch, W. Lämmerer, E. Fisslthaler, S. Mitsche, H. Kaltenböck, On the discrimination of semi-graphite and graphite by Raman spectroscopy, International Journal of Coal Geology, 159 (2016) 48-56.

[267] L. Tjioe, T. Joshi, B. Graham, L. Spiccia, Synthesis and phosphate ester cleavage properties of copper(II) complexes of guanidinium-bridged bis(1,4,7-triazacyclononane) ligands, Polyhedron, 120 (2016) 11-17.

[268] R. Frost, P. Williams, W. Martens, J. Kloprogge, P. Leverett, Raman spectroscopy of the basic copper phosphate minerals cornetite, libethenite, pseudomalachite, reichenbachite and ludjibaite, Journal of Raman Spectroscopy, 33 (2002) 260-263.

[269] L. Passauer, H. Bender, Functional group analysis of starches reacted with urea-phosphoric acid-correlation of wet chemical measures with FT Raman spectroscopy, Carbohydrate Polymers, 168 (2017) 356-364.

[270] J. Maiuolo, F. Oppedisano, S. Gratteri, C. Muscoli, V. Mollace, Regulation of uric acid metabolism and excretion, International Journal of Cardiology, 213 (2016) 8-14.

[271] L.. Moreira, L. Silveira, A. da Silva, A. Fernandes, M. Pacheco, D. Rocco, Raman spectroscopy applied to identify metabolites in urine of physically active subjects, Journal of Photochemistry and Photobiology B: Biology, 176 (2017) 92-99.

[272] J. Liao, C. Chen, J. Fang, A novel phosphate chemosensor utilizing anion-induced fluorescence change, Organic Letters, 4 (2002) 561-564.

[273] L. Huang, T. Song, S. Shi, Z. Tian, L. Wang, L. Zhang, Hydrothermal synthesis, characterization and fluorescence property of a novel layered fluorinated gallium phosphite with heptameric building unit, Journal of Solid State Chemistry, 181 (2008) 1279-1284.

[274] H. Lee, K. Swamy, S. Kim, J. Kwon, Y. Kim, S. Kim, Y. Yoon, J. Yoon, Simple but Effective Way to sense pyrophosphate and inorganic phosphate by fluorescence changes, Organic Letters, 9 (2007) 243-246.

[275] T. Sakamoto, A. Ojida, I. Hamachi, Molecular recognition, fluorescence sensing, and biological assay of phosphate anion derivatives using artificial Zn(ii)-Dpa complexes, Chemical Communications, (2009) 141-152.

[276] B. Bastakoti, Y. Hsu, S. Liao, K. Wu, M. Inoue, S. Yusa, K. Nakashima, Y. Yamauchi, Inorganic-organic hybrid nanoparticles with biocompatible calcium phosphate thin shells for fluorescence enhancement, Chemistry-An Asian Journal, 8 (2013) 1301-1305.

[277] K. Sowoidnich, H.-D. Kronfeldt, Fluorescence Rejection by Shifted Excitation Raman Difference Spectroscopy at Multiple Wavelengths for the Investigation of Biological Samples, International Scholarly Research Network (ISRN) Spectroscopy, 2012 (2012) 1-11.

[278] T. Hasegawa, J. Nishijo, J. Umemura, Separation of Raman spectra from fluorescence emission background by principal component analysis, Chemical Physics Letters, 317 (2000) 642-646.

[279] G. Niaura, A. Gaigalas, V. Vilker, Surface-Enhanced Raman Spectroscopy of Phosphate Anions: Adsorption on silver, gold, and copper electrodes, The Journal of Physical Chemistry B, 101 (1997) 9250-9262.

[280] K. Haruna, T. Saleh, J. Al Thagfi, A. Al-Saadi, Structural properties, vibrational spectra and surface-enhanced Raman scattering of 2,4,6-trichloro- and tribromoanilines: A comparative study, Journal of Molecular Structure, 1121 (2016) 7-15.

[281] Q. Zhu, J. Bao, D. Huo, M. Yang, C. Hou, J. Guo, M. Chen, H. Fa, X. Luo, Y. Ma, 3D graphene hydrogel – gold nanoparticles nanocomposite modified glassy carbon

electrode for the simultaneous determination of ascorbic acid, dopamine and uric acid, Sensors and Actuators B: Chemical, 238 (2017) 1316-1323.

[282] S. Padayatty, A. Katz, Y. Wang, P. Eck, O. Kwon, J. Lee, S. Chen, C. Corpe, M. Levine, A. Dutta, S. Dutta, Vitamin C as an antioxidant: Evaluation of its role in disease prevention, Journal of the American College of Nutrition, 22 (2003) 18-35.

[283] M. Zhang, K. Liu, L. Xiang, Y. Lin, L. Su, L. Mao, Carbon nanotube-modified carbon fiber microelectrodes for in vivo voltammetric measurement of ascorbic acid in rat brain, Analytical Chemistry, 79 (2007) 6559-6565.

[284] H. Liu, C. Gu, C. Hou, Z. Yin, K. Fan, M. Zhang, Plasma-assisted synthesis of carbon fibers/ZnO core-shell hybrids on carbon fiber templates for detection of ascorbic acid and uric acid, Sensors and Actuators B: Chemical, 224 (2016) 857-862.

[285] A. Abellán-Llobregat, L. Vidal, R. Rodríguez-Amaro, Á. Berenguer-Murcia, A. Canals, E. Morallón, Au-IDA microelectrodes modified with Au-doped graphene oxide for the simultaneous determination of uric acid and ascorbic acid in urine samples, Electrochimica Acta, 227 (2017) 275-284.

[286] H. Zare, N. Nasirizadeh, M. Mazloum Ardakani, Electrochemical properties of a tetrabromo-p-benzoquinone modified carbon paste electrode. Application to the simultaneous determination of ascorbic acid, dopamine and uric acid, Journal of Electroanalytical Chemistry, 577 (2005) 25-33.

[287] L. Zhang, J. Feng, K. Chou, L. Su, X. Hou, Simultaneously electrochemical detection of uric acid and ascorbic acid using glassy carbon electrode modified

with chrysanthemum-like titanium nitride, Journal of Electroanalytical Chemistry, 803 (2017) 11-18.

[288] A. Abellán-Llobregat, M. Ayán-Varela, L. Vidal, J. Paredes, S. Villar-Rodil, A. Canals, E. Morallón, Flavin mononucleotide-exfoliated graphene flakes as electrodes for the electrochemical determination of uric acid in the presence of ascorbic acid, Journal of Electroanalytical Chemistry, 783 (2016) 41-48.

[289] E. Ergün, Ş. Kart, D. Zeybek, B. Zeybek, Simultaneous electrochemical determination of ascorbic acid and uric acid using poly(glyoxal-bis(2-hydroxyanil)) modified glassy carbon electrode, Sensors and Actuators B: Chemical, 224 (2016) 55-64.

[290] D. Zhang, L. Li, W. Ma, X. Chen, Y. Zhang, Electrodeposited reduced graphene oxide incorporating polymerization of l-lysine on electrode surface and its application in simultaneous electrochemical determination of ascorbic acid, dopamine and uric acid, Materials Science and Engineering: C, 70, (2017) 241-249.

[291] Y. Xie, J. Yuan, H. Ye, P. Song, S. Hu, Facile ultrasonic synthesis of graphene/SnO2 nanocomposite and its application to the simultaneous electrochemical determination of dopamine, ascorbic acid, and uric acid, Journal of Electroanalytical Chemistry, 749 (2015) 26-30.

[292] Q. Qin, X. Bai, Z. Hua, Electropolymerization of a conductive β-cyclodextrin polymer on reduced graphene oxide modified screen-printed electrode for simultaneous determination of ascorbic acid, dopamine and uric acid, Journal of Electroanalytical Chemistry, 782 (2016) 50-58.

[293] W. He, Y. Ding, W. Zhang, L. Ji, X. Zhang, F. Yang, A highly sensitive sensor for simultaneous determination of ascorbic acid, dopamine and uric acid based on ultra-small Ni nanoparticles, Journal of Electroanalytical Chemistry, 775 (2016) 205-211.

[294] A. Granero, G. Pierini, S. Robledo, M. Di Nezio, H. Fernández, M. Zon, Simultaneous determination of ascorbic and uric acids and dopamine in human serum samples using three-way calibration with data from square wave voltammetry, Microchemical Journal, 129 (2016) 205-212.

[295] X. Zhang, Y. Zhang, L. Ma, One-pot facile fabrication of graphene-zinc oxide composite and its enhanced sensitivity for simultaneous electrochemical detection of ascorbic acid, dopamine and uric acid, Sensors and Actuators B: Chemical, 227 (2016) 488-496.

[296] S. Qi, B. Zhao, H. Tang, X. Jiang, Determination of ascorbic acid, dopamine, and uric acid by a novel electrochemical sensor based on pristine graphene, Electrochimica Acta, 161 (2015) 395-402.

[297] N. Lavanya, E. Fazio, F. Neri, A. Bonavita, S. Leonardi, G. Neri, C. Sekar, Simultaneous electrochemical determination of epinephrine and uric acid in the presence of ascorbic acid using SnO_2/graphene nanocomposite modified glassy carbon electrode, Sensors and Actuators B: Chemical, 221 (2015) 1412-1422.

[298] N. Lavanya, E. Fazio, F. Neri, A. Bonavita, S. Leonardi, G. Neri, C. Sekar, Electrochemical sensor for simultaneous determination of ascorbic acid, uric acid and folic acid based on Mn-SnO_2 nanoparticles modified glassy carbon electrode, Journal of Electroanalytical Chemistry, 770 (2016) 23-32.

[299] X. Liu, L. Zhang, S. Wei, S. Chen, X. Ou, Q. Lu, Overoxidized polyimidazole/graphene oxide copolymer modified electrode for the simultaneous determination of ascorbic acid, dopamine, uric acid, guanine and adenine, Biosensors and Bioelectronics, 57 (2014) 232-238.

[300] J. Kariuki, An electrochemical and spectroscopic characterization of pencil graphite electrodes, Journal of the Electrochemical Society, 159 (2012) H747-H751.

[301] I.G. David, D.-E. Popa, M. Buleandra, Pencil Graphite Electrodes: A Versatile Tool in Electroanalysis, Journal of Analytical Methods in Chemistry, 2017 (2017) 1-22.

[302] S. Chehreh Chelgani, M. Rudolph, R. Kratzsch, D. Sandmann, J. Gutzmer, A review of graphite beneficiation techniques, Mineral Processing and Extractive Metallurgy Review, 37 (2016) 58-68.

[303] R. Krishna, J. Wade, A. Jones, M. Lasithiotakis, P. Mummery, B. Marsden, An understanding of lattice strain, defects and disorder in nuclear graphite, Carbon, 124 (2017) 314-333.

[304] J. Li, C. Zheng, L. Qi, M. Yoshio, H. Wang, Storage behavior of isomeric quaternary alkyl ammonium cations in graphite electrodes for graphite/activated carbon capacitors, Electrochimica Acta, 248 (2017) 342-348.

[305] A. Rosehr, D. Griebe, G. Luinstra, Graphite nanosheets - polypropylene composites from in toluene delaminated graphite using atactic polypropylene as dispersant, Composites Science and Technology, 156 (2018) 28-38.

[306] J. An, E. Lee, I. Hong, Preparation of the spheroidized graphite-derived multi-layered graphene via GIC (graphite intercalation compound) method, Journal of Industrial and Engineering Chemistry, 47 (2017) 56-61.

[307] A. Ferrari, Raman spectroscopy of graphene and graphite: Disorder, electron-phonon coupling, doping and nonadiabatic effects, Solid State Communications, 143 (2007) 47-57.

[308] L. Luo, A. Zhang, M. Janik, K. Li, C. Song, X. Guo, Facile fabrication of ordered mesoporous graphitic carbon nitride for RhB photocatalytic degradation, Applied Surface Science, 396 (2017) 78-84.

Vitae

Name	:Nurudeen Adewale Odewunmi
Nationality	:Nigerian
Date of Birth	:5/8/1977
Email	:mailwale32@yahoo.com, mailwale32@gmail.com
Address	:6, Akinola Street, Shasha, Ajako, Alimosho LGA, Lagos, Nigeria
Academic Background	:Doctor of Philosophy (Ph.D) in Chemistry, King Fahd University of Petroleum & Minerals (2014 – 2018), Master of Science (Msc) in Chemistry, King Fahd University of Petroleum & Minerals (2010 – 2012) and Bachelor of Technology in Industrial Chemistry (B. Tech), Federal University of Technology Akure. Ondo State Nigeria (2000 – 2005).